Climatic Mass Balance and Meltwater Routing of Glacierized area of Kongsfjord basin, northwest Svalbard

Ankit Pramanik

Norwegian Polar Institute

Department of Geosciences

Faculty of Mathematics and Natural Sciences
University of Oslo

National Centre for Polar and Ocean Research

A thesis submitted for the degree of
Philosophiae Doctor (PhD)

September 2018

Series of dissertations submitted to the
Faculty of Mathematics and Natural Sciences, University of Oslo
No. 2070

ISSN 1501-7710

Cover: Hanne Baadsgaard Utigard.
Print production: Reprosentralen, University of Oslo.

Calving front of Kronebreen ending in Kongsfjord, northwest Svalbard

Abstract

The Arctic is experiencing a higher rate of warming than any other part of the world, through a feedback mechanism known as the "Arctic Amplifications". The Arctic region contains approximately 3 million km^3 of land ice, which, if melted, has the potential to rise sea level by 8 m. Although, most of this ice is stored in the Greenland ice sheet, the smaller glaciers and ice caps have been most affected by the recent warming climate, and represent a major contributor to sea level rise over the last century. The high Arctic archipelago of Svalbard has a glacierized area of 34,000 km^2, which, if melted, would lead to 17-26 mm of eustatic sea-level rise. Svalbard is situated at the end of the Gulf-stream through which warm Atlantic water is advected northwards. This relatively warm water keeps the western fjords of Svalbard largely ice free year-round, but the eastern side of the archipelago is dominated by cold Arctic Ocean currents, and there is as a result more sea ice there. There is also contrasting behavior in the atmospheric circulation, with southerly flow bringing warm and moist air, and cold and dry air coming from north-east. This oceanic and atmospheric pattern combined with the fluctuating Arctic Ocean sea ice edge leads to substantial variability in temperature and precipitation across the archipelago, which is often referred to as one of the most climate-sensitive region in the world.

In northwest Svalbard, the Kongsfjord basin is a hotspot for interdisciplinary studies. The fjord is surrounded by glaciers of different shapes and sizes; glaciers on the south sides of the fjord are all small land-terminating glaciers, whereas the glaciers on the east and north side of the fjord are mostly tidewater glaciers, fed by large ice fields. Runoff from tidewater glaciers emerges beneath glacier ice to create buoyant freshwater plumes. The strong upward current that is induced by the upwelling plume brings nutrients to the fjord surface, creating a fertile feeding ground for marine life. Glacier freshwater mixes with the salt water of the outer fjord at different vertical depths, thereby affecting the large scale fjord circulation. Freshwater from land-terminating glaciers mixes with the fjord at the surface and controls the physical and chemical environment of the fjord. To understand how these glaciers are responding to the changing climate, evaluation of long-

term mass balance evolution is necessary, by understanding the processes occurring at the glacier-atmosphere boundary.

The main goals of this thesis is to quantify the spatial and temporal distribution of freshwater discharge at the outlet points of the subbasins around Kongsfjord, and to investigate long-term mass balance evolution of the entire glacierized area of Kongsfjord basin. To achieve these goals, an energy balance model coupled with a subsurface snow model is used to simulate the mass balance of entire glacierized area, seasonal snow development at the non-glacierized area, and spatial distribution of runoff from glacierized and non-glacierized area of the basin.

The mass balance model requires appropriate precipitation forcing, else it may lead to significant biases compared to the actual mass balance measurements. Precipitation forcing comes either from climate models or is extrapolated from nearby meteorological stations. To evaluate the precipitation forcing, snow depth data from two Automatic Weather Stations (AWS) on two glaciers is investigated to categorize precipitation and accumulation events, comparing them with measurements at the nearby meteorological station in Ny-Ålesund, and with large-scale meteorological reanalysis data in the form of ERA-Interim precipitation.

There is a significant difference in precipitation and accumulation between two glacier AWS sites, and ERA-Interim precipitation events coincide better with the AWS sites than do the Ny-Ålesund precipitation events. Therefore, we use ERA-Interim precipitation as precipitation forcing in the energy balance model used to simulate mass balance and seasonal snow development over the period 1980-2016. The mass balance of entire glacierized area is +0.23 m w.e. a^{-1} over the simulation period. However, there is significant spatial variation in mass balance; glaciers in the south show strong negative mass balance (-0.43 m w.e. a^{-1}), glaciers in the east show weak negative mass balance (-0.08 m w.e. a^{-1}), and glaciers in the north snow positive mass balance (+0.61 m w.e. a^{-1}). The total runoff comprises 16% from the seasonal snow cover in the non-glacierized area, and 84% from glacier discharge. No significant trend is observed in the mass balance time-series; however, the runoff time-series from the entire basin shows that there is a significant increasing trend (6.83×10^6 m^3 a^{-1}) over the simulation period.

Subglacial hydrological analysis of the tidewater glaciers shows that there is likely substantial water piracy between two adjacent glaciers of the basin which is supported by observations. Tidewater glaciers contribute most of the freshwater to the fjord, with the maximum contribution coming from Kronebreen, on the east side of the fjord. The land-terminating glaciers altogether contribute 10% of the total runoff to the fjord. Dis-

charge hydrographs derived by simple routing model and by physically based HydroFlow show good agreement for both land-terminating glaciers and for tidewater glaciers. The runoff delay during peak discharge events is typically 17-30 hours for bigger glaciers like Kronebreen.

Sammendrag

Oppvarmingen i Arktis skjer raskere enn i andre deler av kloden, den såkalte "Arctic Amplification". Den Arktiske regionen inneholder omlag 3 mill. kubikk-kilometer is på land. Dette utgjør en potensiell havnivåstigning på ca. 8 m om all is skulle smelte. Det meste av dette isvolumet er lagret i Grønlandsisen, men de mindre breene og iskappene i Arktis er sårbar for små endringer i temperaturen og smeltingen av disse bremassene har gitt et betydelig bidrag til havnivåstigning de siste hundre år. Øygruppen Svalbard har et bredekt areal på c. 34000 km^2 med et volum tilsvarende en midlere global havnivåstigning på 17-26 mm. Svalbard påvirkes klimatisk av Golfstrømmen som fører varme vannmasser nordover. Disse relativt varme vannstrømmene holder fjordene i de vestlige deler av Svalbard stort sett isfrie året rundt mens de østlige deler påvirkes mer av kaldere arktiske havstrømmer som resulterer i mer havis om vinteren her. Tilsvarende er det også store variasjoner i den atmosfæriske sirkulasjonen med sørlige og sørvestlige luftstrømmer som bringer inn varm og fuktig luft mens kald og tørr luft kommer inn fra nord-øst. Disse sirkulasjonsmønstrene fører til store variasjoner i både temperatur og nedbør over øygruppen. Svalbard refereres ofte til som en av de mest klimafølsomme regioner på kloden.

Kongsfjorden og Ny-Ålesundområdet i nord-vestlige Svalbard er et forskningsområde med stort fokus på interdisiplinære studier. Mange breer drenerer ned mot Kongsfjorden, breene på sørsiden av fjorden er små dalbreer som ender på land, mens breene i nord og øst er tidevannsbreer med store dreneringsarealer. Avrenningen fra tidevannsbreene kommer ut under breen og under havnivå og gir oppdriftsstrømmer av ferskvann i fjorden. Disse sterke strømmene bringer næringsstoff opp til overflaten og gir et næringsrikt område for marint liv. Ferskvannet fra de marine breene blander seg med det salte vannet i fjordene i ulike vertikale dybder og påvirker dermed den storskala vannsirkulasjonen. Ferskvannet fra breene som ender på land blander seg med fjorden i overflata og påvirker det fysiske og kjemiske miljøet i fjorden. For å forstå hvordan disse breene responderer på klimaendringer er det nødvendig med analyser av utviklingen i massebalansen over lang tid og å forstå prosessene i grenselaget bre/atmosfære. Hovedmålet med denne avhandlingen er å kvantifisere de romlige og tidsmessige ferskvannsfluksene fra de ulike dreneringsfel-

tene ut i Kongsfjorden samt å evaluere lang-tids utviklingen av massebalansen til hele det bredekte området i Kongsfjorden. Til disse analysene er det brukt en energibalansemodell koblet til en modell av utviklingen i snøpakken for å simulere massebalansen i de bredekte områdene, utviklingen av snødekket i de brefrie områdene og den romlige fordelingen av avrenningen fra bredekte og brefrie områder i hele Kongsfjordbassenget. Massebalansemodellen krever en presis input av nedbøren, som uten det kan gi store avvik sammenlignet med faktiske massebalansemålinger. Nedbørsdataene kommer fra klimamodeller eller som ekstrapolerte data fra nærliggende meteorologiske målestasjoner. Nedbørsdataene blir validert og testet ved hjelp snømålinger og nedbørshendelser ved to automatiske værstasjoner (AWS) på to av breene og sammenlignet med nedbørsdata fra den permanente meteorologiske stasjonen i Ny-Ålesund og med storskala re-analyserte meteorologiske data (ERA-Interim).

Det er en signifikant forskjell mellom nedbør og snøakkumulasjon fra de to værstasjonene på breene. ERA-Interim nedbørsdata korrelerer bedre med AWS-dataene enn nedbørsdata fra den meteorologiske stasjonen i Ny-Ålesund. Av den grunn er ERA-Interim nedbørsdata brukt som input data i energibalansemodellen til å simulere massebalansen og snøens sesongvariasjoner over perioden 1980 til 2016. Den midlere massebalansen over hele perioden for hele det bredekte arealet i Kongsfjorden er + 0.23 m w.e. a^{-1}. Det er imidlertid signifikante romlige variasjoner i massebalansen; breene på sørsiden av fjorden viser sterk negativ massebalanse med en middelverdi på -0.43 m w.e. a^{-1}, breene i øst har en svak negativ balanse med -0.08 m w.e. a^{-1}, og breene i nord viser en positiv massebalanse på + 0.61 m w.e. a^{-1}. Den samlede avrenningen viser at 16% kommer fra snøsmelting i brefrie områder og 84% fra snø og issmelting på breene. De små landbaserte breene bidrar med omlag 10% av den samlede avrenningen. Det er ikke observert noen signifikant trend i de lange tidsseriene av massebalansen. Imidlertid viser avrenningsdataene fra hele bassenget en økning med 6.83×10^6 m^3 a^{-1} over hele simuleringsperioden. Tidevannsbreene bidrar naturlig nok mest til ferskvannsfluksen ut i fjorden siden de er betydelig større enn breene som ender på land. Den største avrenningen kommer fra Kronebreen innerst i fjorden. Avrenningsmønsteret modellert med enkle hydrologiske modeller viser samme mønster fra landbaserte og marine breer. Ved kraftige smeltehendelser er det en forsinkelse i toppvannføringen på 17-30 timer for de store breene slik som Kronebreen.

Acknowledgements

This work would not have been possible without the support and guidance of my supervisors and colleagues at Norwegian Polar Institute (NPI), University of Oslo and National Centre for Polar and Ocean Research (NCPOR). I am especially thankful to my supervisors: Jack Kohler, Thomas V. Schuler, Jon Ove Hagen and Thamban Meloth. Jack has always been very supportive both at the field and at the office. I was lucky having a supervisor like him, so kind, supportive and patient. He opened up glaciology to me from our very first meeting at Ny-Ålesund in 2014. I owe much of my field knowledge to him. He was very patient with my writing skill and made me better with his analytical corrections in the manuscripts. His office door was always open for me for discussions, and even after I left Tromsø, he was always there for discussions over skype. Thomas always guided me whenever needed in course of PhD. I learned a lot about scientific writing from his discerning comments in the manuscripts. Jon Ove and Thamban Meloth helped me in official work whenever needed, and made things easier for me. Ward, although not my official supervisor, but guided me from the very first day of my work as a supervisor and was always there to help. Much of this thesis work would not be possible without his assistance. I learned a lot about modeling from him. A big thanks to Ward!

I am grateful to Ministry of Earth Sciences (MoES), Govt. of India and National Centre for Polar and Ocean Research for having been given me the opportunity and the funding to pursue PhD at Norwegian Polar Institute. I would like to thank the director of NCPOR, Dr. M. Ravichandran, for providing me office space at NCPOR and facilitating the completion of my PhD work. The three and half years in Tromsø was phenomenal for my life. I met many nice people, especially my housemates and colleagues, spent good time with them, participated in various local events and outdoor activities, and all these made me feel Tromsø a home away from home. Thanks to them who helped me to learn skiing, ice skating, and kayaking after moving to Tromsø, and these outdoor activities gave me a relief when I was stressed with work at the office. Tusen takk!

I must acknowledge numerous colleagues and friends at Norwegian Polar Institute and at University of Oslo, especially the colleagues of glaciology group at NPI; Elisabeth,

Geir, JC, Vikram, Jelte, Alistair, Katrin, Alex, Anja, Rob, Ioanna, George. Thanks for your support, all those discussions and occasional cakes. Thanks to Elisabeth for being so kind and supportive and to JC, Ioanna, and Alex for all those in between work squash matches. I was happy having two nice colleagues at my office, Vikram and Jelte. Discussion with these two guys helped me immensely, especially, when I was stuck with some problems. Vikram is a technophile, and I learned about various technological stuffs from him. Vikram was always ready for any kind of scientific discussions which were always fruitful. Thanks to Remi and Ruben for helping me in coding and convincing me to switch to Linux, George for his occasional help in QGIS, and Fred for resolving the computer problems in time.

A big thanks to all my Ny-Ålesund field buddies/colleagues. All four fieldworks are unforgettable to me and I always want to go back there. It was difficult sometimes in the field with cold, high wind, bad weather, driving over the sastrugi, struck snowmobile in the snow, but above all it was fun, and I always enjoyed being there on glaciers. All the funny and interesting discussions over breakfast, dinner, and coffee made my stay at Ny-Ålesund a memorable one, and all these along with adventurous trips to the glaciers made month-long fieldworks seem less. Jack, Chris, Ward, Elizabeth, Kenneth, JC, Thomas, Torbjørn, Mats, Katrin, Alex, Lana, Ceaser; thanks for the nice time that I spend with you all during the fieldwork at Ny-Ålesund. I wish I will get the opportunity to be there again. I would also like to thank all the personnel of Sverdrup stations for being helpful.

I am thankful to Glen Liston for providing the HydroFlow code and helping me to understand it. I would also like to thank Fred Wenger for providing the Bayelva discharge data, NPI mapping section for providing the DEM, Penny How for providing the Plume data.

A special thank goes to Ritwik for helping me in finally converting this thesis to LaTeX , and for all the funny and interesting conversations we used to have over Skype. Thanks to the bachelor group in Tromsø; Vikram, Sunny, Raju, Mukesh, Arpit, Nishant, Visheh, Hari, Amitap, for occasional gatherings and all those delicious Indian food. I would also like to thank my NCPOR colleagues for their support toward the end of my PhD.

Finally, I would like to thank my parents for being so supportive throughout, letting me do what I wanted, and encouraging to complete my PhD, and Tanaya, for being by my side even in difficult times.

Himansh Station, July 2018 Ankit Pramanik

Contents

Part I

Overview

1 Introduction

1.1 Motivation

Glaciers and ice sheets represent the largest reservoir of freshwater on the planet (Gleick and White, 1993). Apart from their contribution to sea level rise (Church et al., 2011, Leclercq et al., 2011), they play a crucial role on the ecosystem and on human life. Glaciers are susceptible to the increasing global temperature, and hence are a good indicator of climate change. Glacier changes will affect the water resources, eco-system, and hydropower production on a large scale. Glaciers affect human activities in mountain regions as well as downstream as glacier meltwater is a source of drinking and irrigation water (Jones, 1999). Many rivers (e.g. in Himalaya, Hindu-Kush, Tibetian Plateau, Andes) originate from glaciers, and millions of peoples' livelihood are dependent on these rivers (Sharma et al., 2000, Bolch et al., 2012, Immerzeel et al., 2013). In the polar regions, freshwater from glaciers affects large scale-ocean circulations, and on a smaller scale, the local ecosystem, especially at the front of tidewater glaciers. Meltwater from tidewater glaciers enters the fjord from beneath the glacier to create buoyant plumes (Carroll et al., 2015, Mankoff et al., 2016, Slater et al., 2017), which bring nutrients to the surface of the fjord, creating a foraging hotspot for marine mammals and birds (Lydersen et al., 2014, Urbanski et al., 2017). In the future warming climate, freshwater flux from glaciers to the fjord/ocean will supposedly increase substantially, which would cause more rapid vertical mixing of freshwater with the fjord water, which will further impact the fjord/ocean circulation (Björk et al., 2001, Cottier et al., 2005, Shchepetkin and McWilliams, 2005) and affect the foraging habits of different species. Freshwater from land-terminating glaciers and from the seasonal snow of non-glacierized area mixes with the fjord at the surface and impacts the physical and chemical environment of the fjord (Nash and Moum, 2005, Nowak and Hodson, 2013, 2014, 2015). Thus, quantifying freshwater influx from glaciers and seasonal snow of non-glacierized area to the fjord/ocean is important, to investigate sea-level rise, on a broader scale, and on a smaller scale, to understand fjord/ocean circulation and fjord ecosystem.

1 Introduction

Glaciers gain mass through precipitation and lose mass mainly due to melting and calving. Glacier mass balance affects glacier geometry, e.g. glacier length (Nye, 1960), and varies with climate perturbations. Systematic measurements of glacier length around the world are available sporadically before the 1960s (Leclercq and Oerlemans, 2012), but have been better monitored in recent decades. Glacier volume and temperature for different regions of the world have been reconstructed from glacier length fluctuations (Oerlemans, 2005, Lüthi et al., 2010). Due to logistical expenses, systematic glacier mass-balance measurements are limited to certain glaciers around the world, although recent developments in satellite remote sensing help to monitor glaciers and their changes through a wide range of different sensors.

Long-term mass balance measurements help to understand the impact of changing climate on glaciers. Mass balance of glaciers can be measured in several ways. Direct mass balance measurements are conducted seasonally or annually by measuring stakes drilled into the ice/firn surface along the glacier centerline or distributed around the glacier in a network. Changes in exposed stake height multiplied by the density of snow/ice yields the mass change at a certain point. These point measurements are extrapolated over the entire glacier using area-altitude distribution (hypsometry).

The geodetic mass balance uses elevation data from satellites or photogrammetry (Cox and March, 2004, Kohler et al., 2007), or radar altimetry (Moholdt et al., 2010b, Nuth et al., 2010). Glaciers lose mass from surface melting, basal melting, and through dynamic loss, by calving. The basal mass loss is difficult to estimate, and is of lesser importance for glaciers and ice sheets, but more significant for ice shelves (Rignot, 2002, Depoorter et al., 2013). The dynamic mass loss is a major mass loss term for fast-flowing tidewater glaciers, but surface mass loss dominates for land-terminating glaciers. In the context of recent global warming, surface mass loss has increased on all glaciers and ice shelves around the world (Rignot, 2002, Parkinson, 2006, Shekhar et al., 2017).

The Arctic region is experiencing greater warming than the global average through a feedback caused by sea ice retreat, surface reflectivity, and air temperature, in a process known as "Arctic Amplification" (Serreze and Francis, 2006, Serreze et al., 2009). The High Arctic archipelago Svalbard has experienced 0.5 °C decade^{-1} of warming since 1960, the strongest measured in Europe (Nordli et al., 2014). Svalbard has a glacierized area of 34,000 km^2 (Nuth et al., 2013) which, if melted, would lead to 17-26 mm of eustatic sea level rise (Radić and Hock, 2010, Huss and Farinotti, 2012, Martín-Español et al., 2015). In spite of being small in size compared to Greenland and Antarctica, Svalbard glaciers have some similarities to these large ice sheets.

In the northwest of Svalbard, Kongsfjord is an important site for scientific research, with many interdisciplinary investigations underway. Kongsfjord is open to the sea to the west and surrounded by glaciers on the other three sides. These glaciers are of different shapes and sizes and show varying dynamic behavior (Hagen et al., 1993). The glaciers on the southwest side of the fjord are land-terminating whereas those to the north and east of the fjord are mostly tidewater glaciers. The proximity to the research town of Ny-Ålesund and its ready logistical accessibility makes this area ideal for field studies. Long-term monitoring of glaciers in Kongsfjord started in 1967 by Norwegian Polar Institute (NPI).

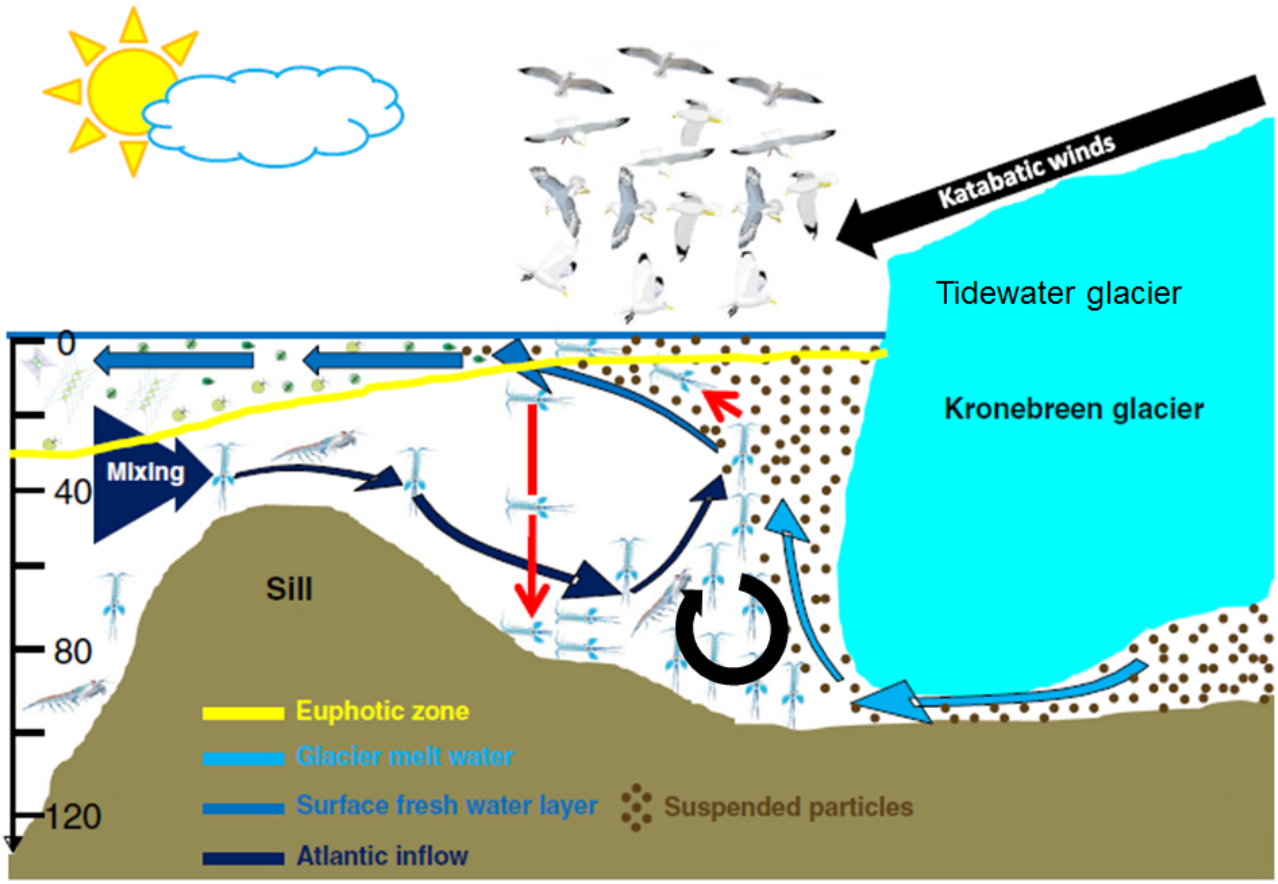

Figure 1.1: Schematic of tidewater glacier front in summer. Discharge from tidewater glaciers underneath glacier ice mixes with fjord water and creates plumes. Plumes bring phytoplankton and zooplankton to the fjord surface to make a feeding ground for birds and marine mammals. Picture modified from Lydersen et al. (2014).

1.2 Objectives

Glaciers lose mass in two ways; static mass loss and dynamic mass loss. As glaciers move downslope under their own weight, different areas experiences different rates of inflow and outflow of ice. Dynamic loss from a certain region occurs when outflow exceeds the inflow. With high spatial and temporal resolution of satellite data, geodetic mass loss over a wide region can be calculated (Schutz et al., 2005, Zwally et al., 2002, Moholdt et al., 2010a). Static mass loss is more challenging to account for, because it involves surface and subsurface processes. Surface mass balance measured in situ is relatively restricted spatially. Extrapolation of point measurements can be done analytically or empirically, by modeling climatic mass balance components (Hock, 2003, Arnold et al., 2006, Sicart et al., 2008). Mass balance models can be used to calculate the static mass balance of glaciers on daily or even sub-daily scales. There are several model approaches, ranging in complexity from conceptual temperature index-models to more physically-based energy balance models. Mass balance models simulate different mass fluxes (positive and negative) by considering the physical processes through which the glacier interacts with the atmosphere. The parameters of the model are calibrated with observational data. Surface mass balance is calculated as the sum of all positive and negative mass fluxes over a certain period. It requires climate forcing from either meteorological station or from reanalysis data.

Surface mass balance models are able to produce mass balance estimates over short time scales (days to hours) but their applicability is often limited by the climate forcing. Precipitation data are especially crucial for estimating mass balance (Machguth et al., 2008), a local phenomenon controlled to a large degree by topography and wind. Inaccurate precipitation estimation can lead to substantial biases in modeled mass balance, relative to that measured. Obtaining distributed precipitation data in the field requires a dense measurement network and frequent monitoring, which is challenging for remote areas (Braaten, 2000, Fountain et al., 2010, Knuth et al., 2010). Nevertheless, automatic weather stations (AWSs) with snow height sensors can provide important information about the spatial and temporal distribution of snow accumulation and precipitation. With the help of a few distributed AWSs in a region, spatial and temporal accumulation and snowfall variability could be inferred. Also, in situ measurement can be used for validation of weather models. This information combined with reanalysis data e.g. ERA-40, ERA-Interim, NORA10 can constrain estimates of the precipitation field for mass balance modeling.

Distributed mass balance models can be used to calculate melt and runoff over large areas. Runoff is transported through the glacier hydrologic system to the exit points, either via portals on land-terminating glaciers or at the base of calving fronts on tidewater glaciers. However, there can be substantial delays involved in the transport of meltwater between where it is produced and where runoff exits the glacier (Bartholomew et al., 2012, Chandler et al., 2013, Cowton et al., 2013). The delay varies temporally due to the evolution of the hydrological system over a season. Quantifying time-varying discharge is important for ocean modeling (Sundfjord et al., 2017) and for investigating the time-varying behavior of foraging species at tidewater glacier fronts (Lydersen et al., 2014). Hydrological models are required to account for different water transport processes inside glaciers, models which take into account formation and evolution of channel system beneath the glacier over time (Walder and Fowler, 1994, Fountain and Walder, 1998, Hewitt, 2011, Hewitt et al., 2012). Simple runoff routing models can also be used to reproduce discharge hydrographs (Slater et al., 2017); these are computationally less expensive, and often serve the purpose of glaciologists, biologists, oceanographers who are interested in discharge hydrographs at daily or sub-daily timescales.

This thesis combines both analyses of observational data and modeling in order to better estimate the mass balance of glaciers and the temporally varying input of freshwater into the fjord of the Kongsfjord basin, in northwest Svalbard. The basic questions I seek to address in the thesis are:

1. What is the spatial and temporal variability in precipitation and accumulation between two glaciers? How does observational accumulation data correlate to nearby meteorological data at Ny-Ålesund and to reanalysis data?

2. How has the long-term mass balance of the glaciers around Kongsfjord evolved? What is the spatial variability of melt and runoff throughout the glacierized and non-glacierized part of this region?

3. What is the temporal variability of the freshwater flux to the fjord at different outlet points around Kongsfjord?

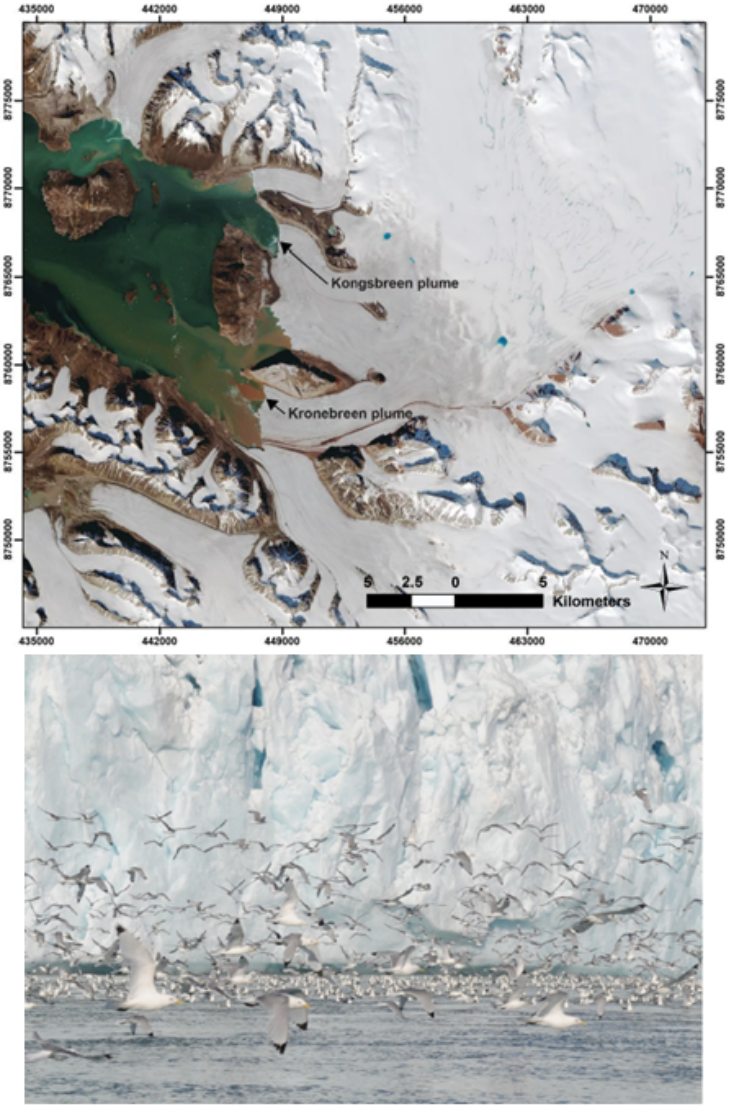

Figure 1.2: Plumes at tidewater glacier fronts (upper panel) (Sentinel image of 10 July 2016). These glacier fronts are foraging hotspot for marine mammals and seabirds. Here kittiwakes foraging at the Kronebreen glacier front (lower panel) (Picture is taken from Lydersen et al. (2014))

1.3 Outline

I seek to answer the research questions stated in the previous section in the following papers.

- PAPER I focuses on the spatial and temporal variability of accumulation and precipitation analyzed from automatic weather station data situated on two of the larger glaciers in the Kongsfjord basin. I also compare the accumulation measured at the glacier sites with nearby meteorological station data from Ny-Ålesund and to downscaled ERA-Interim precipitation. Through this study, I seek to evaluate precipitation data used in the papers on mass balance modeling.
- PAPER II focuses on modeling the long-term mass balance evolution and runoff of glaciers in the Kongsfjord basin, as well as runoff from the non-glacierized region. I use a surface energy balance model coupled to a subsurface snow/firn model to simulate mass balance, refreezing and runoff of glaciers. A subsurface soil model has been incorporated into the energy balance model to simulate seasonal snow development and runoff from the non-glacierized area.
- PAPER III focuses on meltwater routing for the Kongsfjord glaciers. A simple routing model is implemented to calculate discharge hydrographs at the outlets of the glaciers. The model is calibrated and validated with different observational data.

There are in addition three papers where the model data are used in different contexts.

- PAPER IV investigates subglacial discharge revealed by CTD-instrumented ringed seals. Runoff data from Paper III is used in a plume model to derive plumes which shows good correlation with the foraging of ringed seals at the outlet of Kronebreen glaciers in Kongsfjord basin. PAPER V investigates the influence of different factors (subglacial discharge, fjord circulation, and free convection) on calving rates at Kongsbreen North glacier, where runoff data is used to derive subglacial discharge and its effect on calving. Paper VI investigates the effect of discharge from tidewater glaciers and bedrock characteristics on the local primary production in Kongsfjord. Runoff data from five tidewater glaciers are used in a plume model to estimate the volume of upwelling driven by subglacial discharge plume. Papers IV, V, and VI are not discussed in detail, only the abstract of these papers are provided.

In this thesis, Chapter 2 focuses on the scientific background of the mass balance model and the simple delay model, the core of paper II and paper III. Chapter 3 gives an

introduction to the study area, to the climate and glaciers of the Kongsfjord basin and Chapter 4 discusses the data used in this study. Observational data have been used for analyses in paper I and for model calibration and validation in paper II and paper III. The papers that constitute this thesis are summarized in Chapter 5. Thesis outcome, limitations of the study, and future outlook are discussed in Chapter 6. A flowchart of the goals, methods used and findings are shown with a schematic in Figure 1.3.

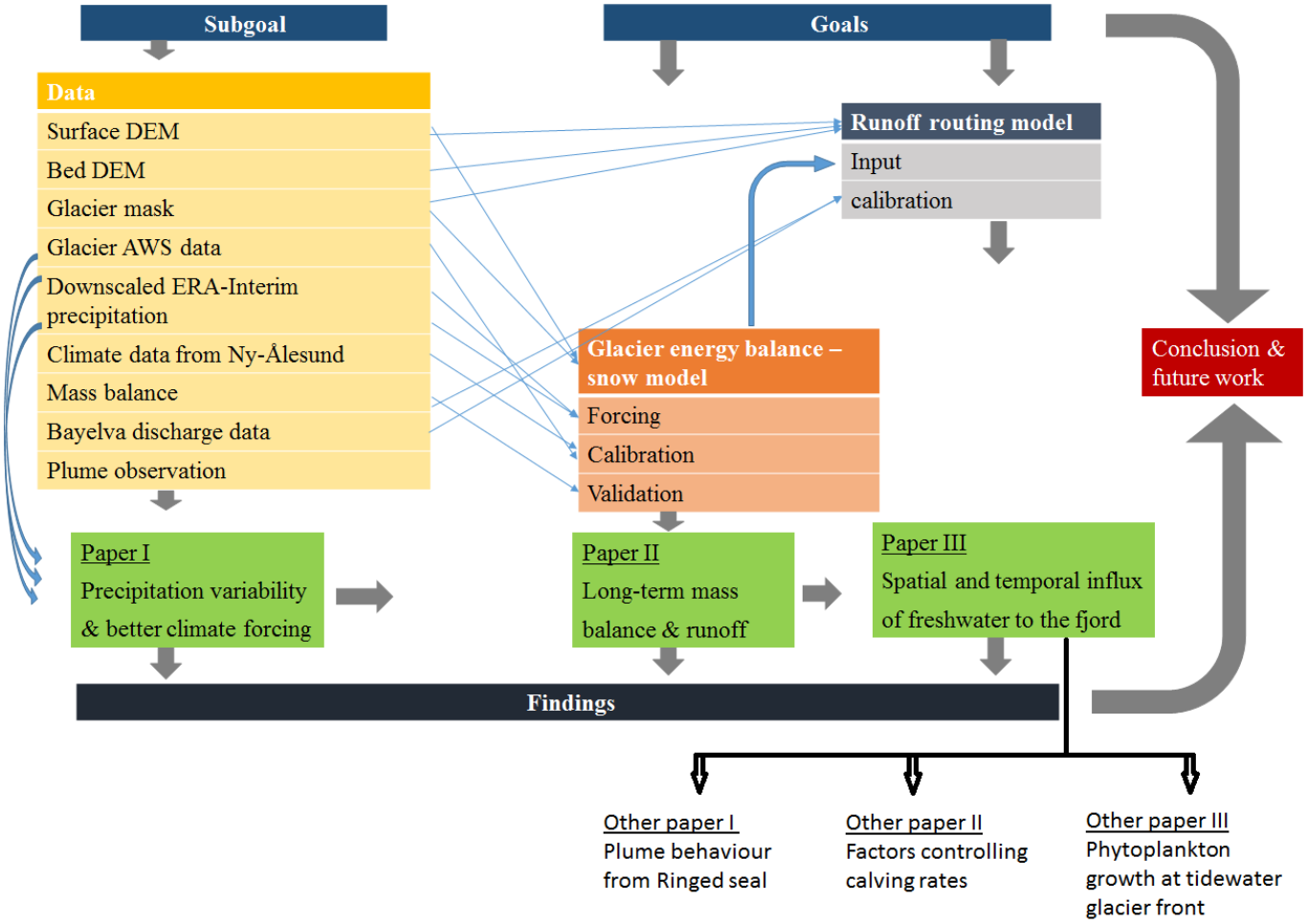

Figure 1.3: Flowchart showing the connection between papers, methodology used, data associated with the work, and outlook.

2 Scientific Background

The intention of this section is to briefly introduce the concepts and underlying physics that form the basis of the thesis. Each paper describes the method and interpretation of result in greater detail. Section 2.1 describes direct mass balance measurements, section 2.2 discusses glacier mass balance modelling, and section 2.3 introduces two runoff routing models.

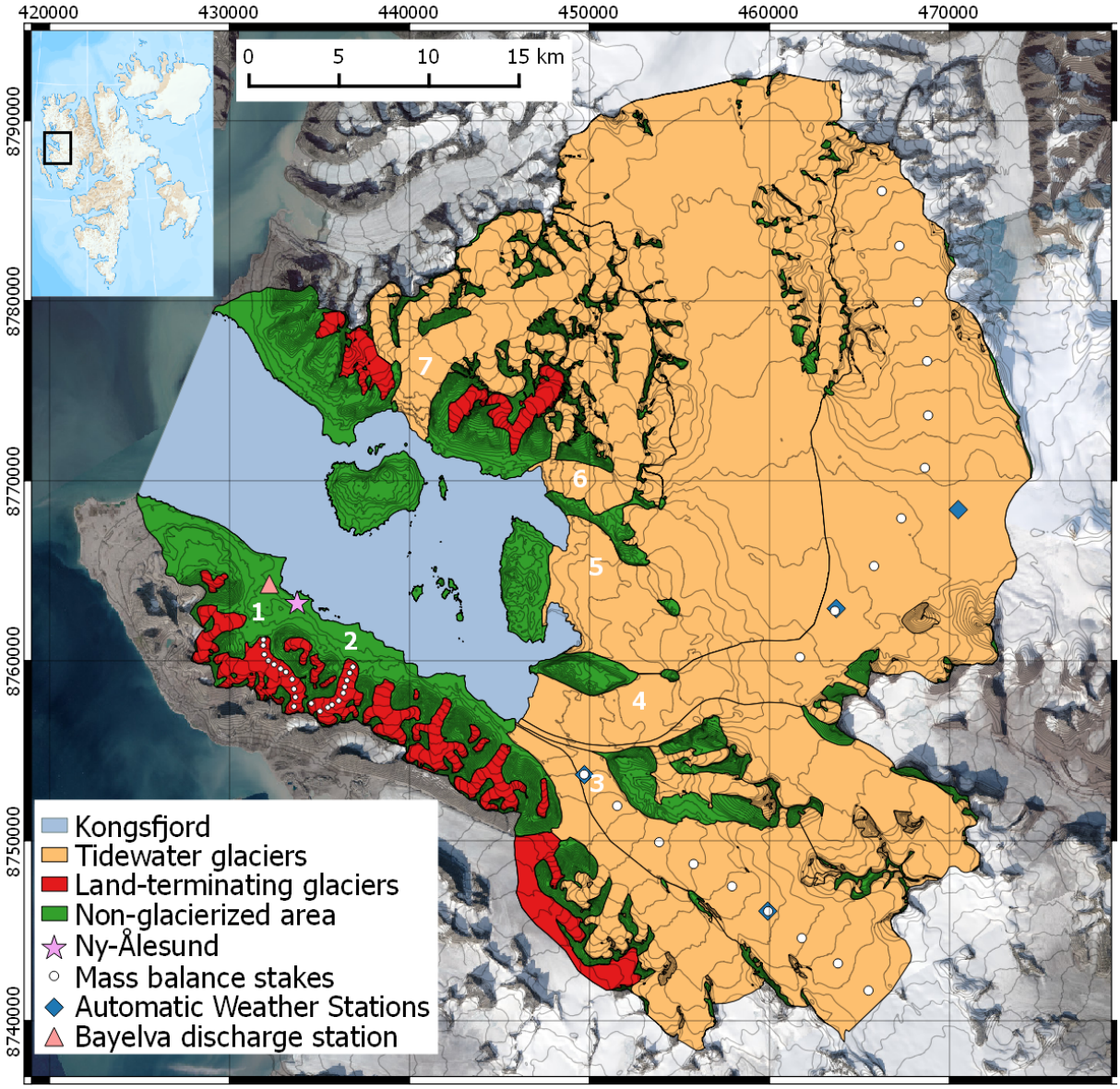

Figure 2.1: Kongsfjord basin: Orange indicates tidewater glaciers, red indicates land-terminating glaciers. White circles show mass balance stake locations, blue diamonds show the locations of the four automatic weather stations, orange triangle shows the location of the Bayelva discharge measurement site, and the magenta star indicates the location of Ny-Ålesund. The background is a Landsat image.

2.1 Direct mass balance observations

This section describes the surface mass balance measurements as measured on four glaciers in the Kongsfjord basin. Glacier surface mass balance is measured along the centerline of the glaciers, which is assumed to be representative of the entire area. Surface mass balance is measured twice a year; the winter mass balance is measured in spring (April-May) and the summer balance is measured in early autumn (September). Direct mass balance measurements are acquired by drilling stakes into ice or firn, along the centerline of the glacier, with stakes covering uniform elevation intervals. Even with little transverse mass balance variability, as few as 5 stakes can be used to characterize the balance as a function of elevation (Fountain and Vecchia, 1999). A larger number of stakes can capture both elevation and any lateral dependence of the surface mass balance (Krimmel, 1999, Jansson and Pettersson, 2007). Stakes are replaced ideally just before they melt out (ablation zone) or become buried under snow (accumulation zone). Surface mass balance is calculated by multiplying changes in the exposed stake heights by the density of the material (snow/ice) gained or lost. In spring, snow density is measured by taking vertical density profiles in snow pits or in ice cores. A compilation of 196 snow pit bulk density measurements made between 2000 and 2016 at four glaciers in Kongsfjord basin yields a mean bulk density of 0.37 g cm^{-3}, with a standard deviation of 0.04 g cm^{-3} (Nuth, 2011). The bulk density is used to convert winter snow depth to water equivalent whereas a combination of snow and ice density (0.9 g cm^{-3}) is used to convert the summer stake changes to water equivalent. If the equilibrium line altitude of a glacier increases, stakes in the firn area must use firn density to convert to water equivalent mass change. While firn density is reported in the literature to vary between 0.4 to 0.8 g cm^{-3} (Paterson, 1993), firn density profiles available from various ice core measurement (Pinglot et al., 1999, Isaksson et al., 2001, Pohjola et al., 2002, Sjögren et al., 2007) around Svalbard, as well as unpublished data (Jon Ove Hagen, personal communications) yield an average of 0.55 g cm^{-3} for Svalbard glaciers.

Meltwater produced at the surface enters the snowpack where it refreezes or is stored as irreducible water. During later autumn or early winter, residual percolated water may refreeze at the subsurface interface between snow or firn to ice, and form an ice layer when cooling occurs from below or above. These ice layers, forming above the previous year's summer surface is known as Superimposed Ice (SI) (Figure 2.4). The mass balance of Arctic glaciers must account for SI formation (König et al., 2002, Brandt et al., 2008). SI formation constitutes a substantial component of winter mass balance. SI cores are

Figure 2.2: Snow density measurement at glacier Midtre Lovénbreen. Photo by Ankit Pramanik.

taken at stake locations in spring to account for the winter SI contribution. In summer, glacier melts predominantly at the surface, with water percolating through the snowpack either to be stored in the pore space or to refreeze, depending upon the condition of the snowpack. Refreezing or storage of meltwater acts as a buffer to mass loss which is not reflected in the surface measurement. In the accumulation zone, percolated meltwater may penetrate deeper into snow/firn and refreezing can occur below the previous year's summer surface, referred to as "Internal Accumulation" (IA). Unlike SI, it is difficult to measure internal accumulation, which acts as an additional source of positive mass.

Glacier wide surface mass balance B is determined by extrapolating discrete mass balance measurement utilizing the glacier hypsometry.

$$B = \sum_{1}^{z} [b(z)A(z)] \tag{2.1}$$

where $b(z)$ is the winter, summer and/or net surface mass balance as a function of elevation z or averaged within an elevation bin, and $A(z)$ is the hypsometry of glacier. On glaciers with dense stake measurement network, kriging could be applied (Hock and Jensen, 1999, Jansson and Pettersson, 2007). Ideally, for glaciers undergoing change, the hypsometry is updated often, although in practice this is not usually possible. Typically using two digital elevation models from different years, hypsometry can be interpolated, assuming linear transformation between two maps.

Errors in surface mass balance measurements include stake measurement errors, density conversion errors, and sampling errors. Jansson (1999) find a stochastic error of ±0.1 m from the sparse distribution of stakes for mass balance measurement in Storglaciären but the mass balance was not sensitive to density and sampling error. Other studies have shown specific measurement errors ranging from 0.2 m to 0.4 m (Cogley and Adams, 1998, Cox and March, 2004), or even larger errors by combining all stochastic and systematic errors (Thibert et al., 2008, Zemp et al., 2010). Systematic errors e.g. from shrinking stakes in firn area (Østrem and Brugman, 1991) or unaccounted internal accumulation in accumulation zone are difficult to account for.

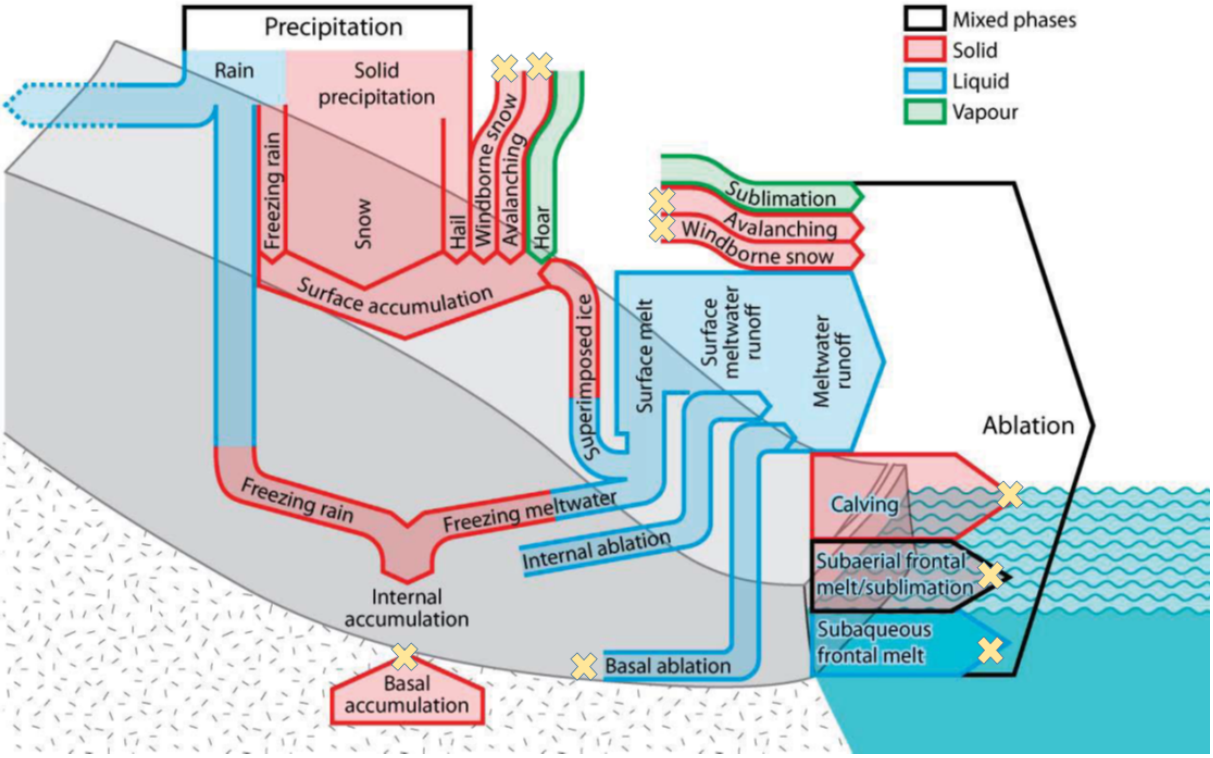

Figure 2.3: Glacier processes that control glacier mass balance. Processes that are not considered in this study are marked with a cross. Figure modified from Cogley et al. (2011).

2.2 Glacier mass balance modelling

While mass balance can be measured with in situ measurements on one or several glaciers, remote sensing and modeling are the tools needed to estimate mass balance on a regional

scale. Mass balance models have the further advantage that they can be used to estimate mass gain or mass loss over shorter timescales than can be obtained in the field.

Mass balance models not only compute mass changes over a certain period but also provide information about factors controlling the glacier behavior, for example, climate sensitivity, and thus help to understand the implications of future climate scenarios. With the recent advancement of remote sensing technology, geodetic mass balance can be measured quite accurately; however, the subsurface processes remain unknown in this method.

The term climatic mass balance (CMB) includes all the climate-related processes relevant to mass balance and takes into account internal accumulation/ablation. The total glacier mass balance is the sum of CMB, frontal ablation due to calving at the glacier front, and mass loss at the base (Figure 2.3). The latter two processes are not considered in this study; despite their importance, it is beyond the scope of this study to consider them. However, there is ample scope to further extend this study by coupling glacier dynamic models with the mass balance model.

Models for calculating climatic mass balance range from simplified degree-day model to more complex energy balance models. Degree-day model uses only temperature for melt calculation, a meteorological parameter that is relatively easy to obtain. Distributed models are forced with meteorological measurements from a weather station located on the glacier or nearby. With the recent availability of climate models and reanalysis data, gridded climate data at the appropriate scale has enabled full surface energy balance simulations over glaciers without in-situ meteorological data, since relevant data are embedded in the climate model land-surface schemes (van de Berg et al., 2006, Lang et al., 2015, Fettweis et al., 2017).

In this study, a surface energy balance model coupled to a subsurface snow/firn model developed by Van Pelt et al. (2012) is modified (Paper II of this thesis) by Pramanik et al. (2018) for the entire Kongsfjord basin. The subsurface model is based on SOMARS (Simulation Of glacier surface Mass balance and Related Subsurface processes), which was first used in Greenland (Greuell and Konzelmann, 1994). The two models are coupled, with meltwater production at the surface due to the exchange of energy serving as input to the multilayered subsurface model, which simulates storage and refreezing of percolated water. The following sections give a detailed description of the model.

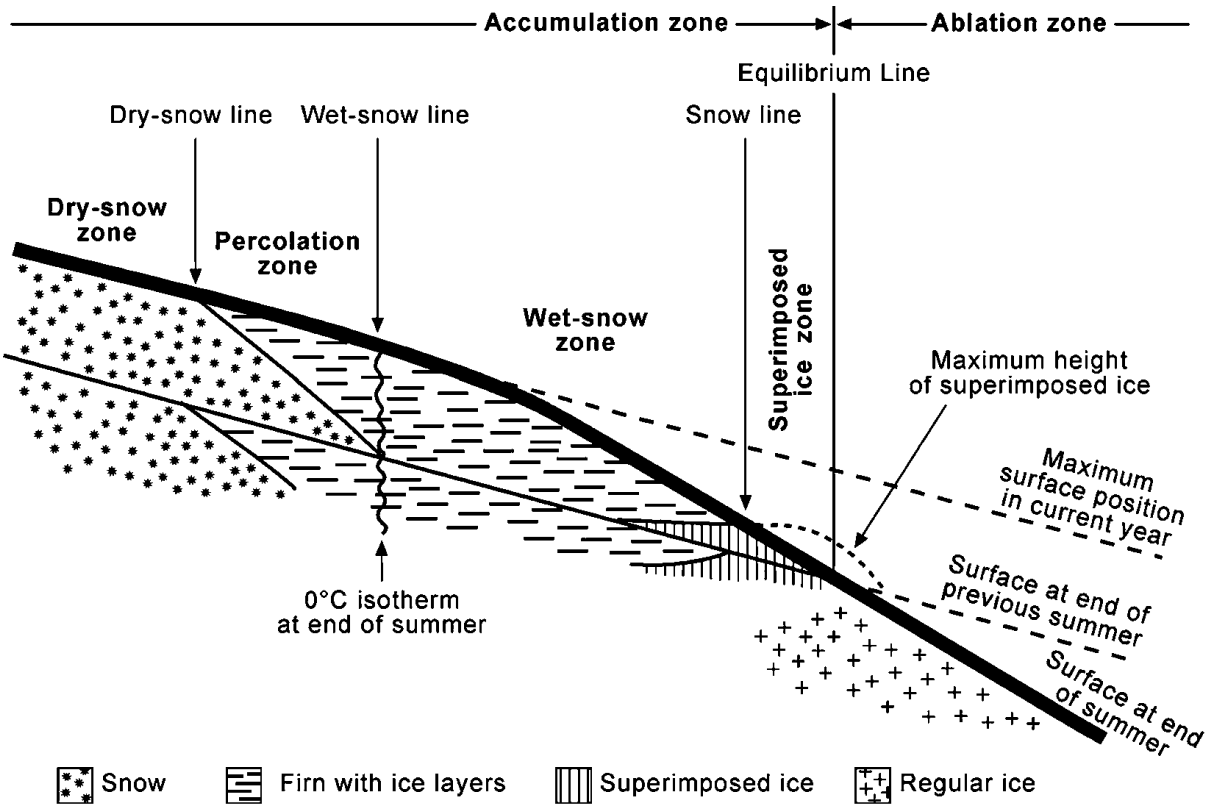

Figure 2.4: Glacier facies. The figure is taken from Cuffey and Paterson (2010).

2.2.1 Surface energy balance model

The surface energy balance model calculates all the energy fluxes interacting with the glacier surface (Figure 2.5). The sum of the energy fluxes is equal to the energy available for melting:

$$Q_{melt} = SW_{net} + LW_{net} + Q_{sens} + Q_{lat} + Q_{rain} + Q_{sub} \ , \tag{2.2}$$

where SW_{net} is the net shortwave radiation, LW_{net} is the net longwave radiation, Q_{sens} and Q_{lat} are the turbulent sensible and latent heat fluxes, Q_{rain} is the heat production by rainfall, and Q_{sub} is the glacier subsurface heat flux.

In each time step, the surface energy balance model iteratively computes the surface temperature from the net energy. If the surface temperature is above the melting point, it is set to the melting point and the excess energy is used to melt the surface and warm the snowpack.

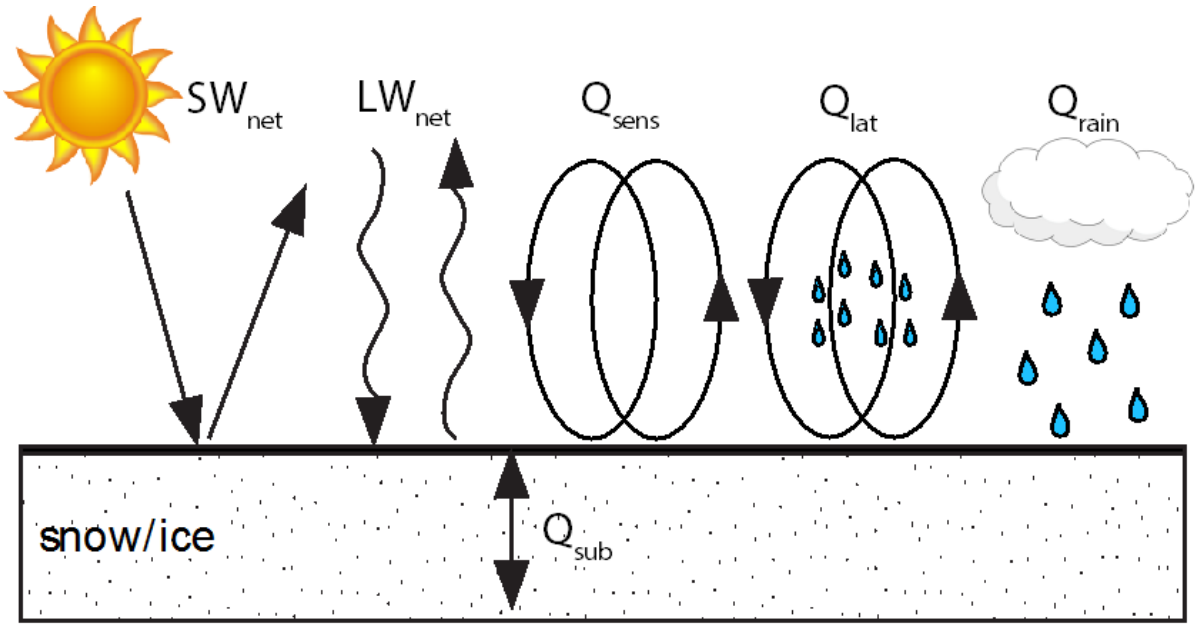

Figure 2.5: Schematic diagram of energy fluxes interact with glacier surface. The figure is taken from Van Pelt et al. (2013).

Radiation fluxes

There are four radiation fluxes; incoming and outgoing shortwave, and incoming and out-going longwave. The net radiation flux is determined by

$$Q_{rad} = SW_{in} + SW_{out} + LW_{in} + LW_{out} \ , \tag{2.3}$$

where SW_{in} is the incoming shortwave radiation, SW_{out} is the outgoing shortwave radiation, LW_{in} is the incoming longwave radiation and LW_{out} is the outgoing longwave radiation.

The amount of solar radiation which impinges on the surface grid cells as incoming shortwave radiation depends on several factors. These are the top-of-the-atmosphere radiation, the transmissivity of the atmosphere, shading by surrounding terrain, the slope aspect and gradient of grid cell, reflectivity of the surrounding grid cell and the diffusivity of the sky. Cloud cover, air pressure and specific humidity are used to compute atmospheric transmissivity due to Rayleigh scattering and gaseous absorption (Kondratyev, 1972), water vapor absorption (McDonald, 1960) and attenuation by aerosols and clouds (Houghton, 1954) and, thereby direct, diffuse and reflected solar radiation from surround-

ing grid cells are computed. Shading by surrounding topography is determined using the digital elevation model (DEM) and solar angle.

Outgoing shortwave radiation is computed using

$$SW_{out} = -\alpha SW_{in} \ , \tag{2.4}$$

Where α is the reflection coefficient for shortwave radiation known as albedo. Albedo is derived from a parameterization by Oerlemans and Knap (1998), in which albedo is a function of the snow depth and the timing of the last snowfall.

As a result, the net shortwave radiation is given by:

$$SW_{net} = SW_{in} + SW_{out} = SW_{in}(1 - \alpha) \ , \tag{2.5}$$

Incoming longwave radiation flux from the sky is computed as:

$$LW_{in} = \epsilon \sigma T_{air}^4 \ , \tag{2.6}$$

where the emissivity ϵ is a function of specific humidity and cloud cover, σ is the Stefan-Boltzmann constant, and T_{air} is the air temperature.

The Stefan-Boltzmann law of blackbody emission is used to compute both incoming and outgoing longwave radiation:

$$LW_{out} = \sigma T_s^4 \ , \tag{2.7}$$

where T_s is the temperature of the glacier surface.

Turbulent heat fluxes

The turbulent sensible heat flux (Q_{sens}), and latent heat flux (Q_{lat}) are calculated following Oerlemans and Grisogono (2002):

$$Q_{sens} = -\rho_{air} C_p K_{kat} (T_{air} - T_{surf}) \ , \tag{2.8}$$

where ρ_{air} is the air density, C_p is the specific heat of dry air, T_{air} is the air temperature, T_{surf} is the surface temperature, and K_{kat} is the katabatic bulk exchange coefficient. The latter is defined as

$$K_{kat} = -k_1 C(\frac{g}{T_o \gamma P_r})^{1/2} \tag{2.9}$$

where k_1 is empirical constants, C is the temperature deficit at the glacier surface, γ is background potential temperature lapse rate, P_r is Prandtl number.

Equation 2.9 is used to calculate latent heat flux (Oerlemans and Grisogono, 2002) which is based on Prandtl model (Prandtl, 1942, Van den Broeke et al., 1994) via:

$$Q_{lat} = 0.622 \rho_{air} L_s K_{kat}(e_{air} - e_{surf}) \ , \tag{2.10}$$

where L_s is the latent heat of sublimation, e_{air} is the vapour pressure at the atmosphere, e_{surf} is the vapour pressure at the surface.

In contrast to Monin-Obukhov theory (Foken, 2006, Pelliccioni et al., 2012), the above theory does not take into account the near-surface temperature, humidity, and wind characteristics, which is strongly influenced by the ice surface.

Sensible heat from rain

Energy supplied by rain is calculated from

$$Q_{rain} = C_w R_{rain}(T_{rain} - T_{surf}) \ , \tag{2.11}$$

where T_{rain} is the temperature of the rain, T_{surf} is the surface temperature, C_w is the specific heat capacity of water and R_{rain} is the rate of rainfall. The temperatures in the above equation are simplified by assuming that $T_{rain} = T_{air}$ and $T_{surf} = 273$ K.

Subsurface heat flux

The glacier heat flux depends on the conductivity of the medium and the vertical temperature gradient between the subsurface layers:

$$Q_{sub} = G(T_{sub} - T_{surf}) \ , \tag{2.12}$$

Where G is a function of the conductivity of the subsequent layers.

2.2.2 Subsurface Model

Temperature

Subsurface temperature evolution is calculated by solving the thermodynamic equation:

$$\rho c(T)\frac{dT}{dt} = \frac{d(\xi(\rho)\frac{dT}{dz})}{dz} + \frac{RL}{\Delta z} \tag{2.13}$$

where ρ is the layer density, T is the layer temperature, $c(T)$ is the heat capacity of the layer, z is the vertical coordinate, $\xi(\rho)$ is the effective conductivity, R is the refreezing rate, L is the latent heat of melting and z is the layer thickness. Expressions for $\xi(\rho)$ and $c(T)$ come from Sturm et al. (1997) and Yen (1981) respectively:

$$\xi(\rho) = 0.138 - 1.01 \times 10^{-3}\rho + 3.23 \times 10^{-6}\rho^2 \ , \tag{2.14}$$

$$c(T) = 152.2 + 7.122 \times \Delta T \ . \tag{2.15}$$

Vertical diffusive heat flux is represented by the first term on the right-hand side of Equation 2.13, whereas the second term of Equation 2.13 represents heat production by refreezing of water within a layer.

Refreezing

The energy associated with positive temperatures is used for melting. The energy per time step is:

$$Q_M = m_i c_i \Delta T \ , \tag{2.16}$$

where m_i is the mass of the current layer, c_i is the specific heat capacity of ice, and T is the temperature above freezing point. This available energy is used to melt the ice mass via

$$m_{melt} = m_i c_i \frac{\Delta T}{L_f} \ , \tag{2.17}$$

where L_f is the latent heat of fusion.

If liquid water is present in the snow with subzero temperatures, water will start to refreeze. Refreezing in a layer is restricted by the mass of the available water and by the temperatures. When refreezing occurs in a layer, the temperature of the layer increases, by virtue of latent heat release. Temperature increase due to refreezing can be expressed as:

$$\Delta T = \frac{m_{frozen} L_f}{m_{melt} c_{melt}} \tag{2.18}$$

Densification

Densification occurs in wet snow and firn relatively rapidly due to melt-refreeze metamorphism, while in dry snowpacks the process is slower, and caused by sintering and compaction. The time evolution of subsurface density is described by:

$$\frac{d\rho}{dt} = K_g(\rho, T) + \frac{R}{\Delta z} \ . \tag{2.19}$$

Here K_g represents gravitational densification which was derived by Arthern et al. (2010) based on in situ measurements of Antarctic snow compaction and later modified by Ligtenberg et al. (2011):

$$K_g(\rho, T) = c(b) b g (\rho_{ice} - \rho) \exp(-\frac{E_c}{R_d T} + \frac{E_g}{R_d T_{avg}}) \ , \tag{2.20}$$

where b is the accumulation rate (in mm a^{-1}), g is the gravitational acceleration (9.81 m s^{-2}), ρ_{ice} is the density of ice (917 kg m^{-3}), R_d is the universal gas constant, and E_c (60 kJ mol^{-1}) and E_g (42.4 kJ mol^{-1}) are the activation energy associated with creep by lattice diffusion and grain growth respectively. T_{avg} is the mean subsurface temperature and is

computed by taking the mean subsurface temperature of the preceding year. Ligtenberg et al. (2011) described the dependence of *c(b)* on accumulation rate as:

$$c(b) = \begin{cases} 0.0991 - 0.0103\log(b), \text{ if} & \rho < 500 \text{ kg m}^{-3} \\ 0.0701 - 0.0086\log(b), \text{ if} & \rho \geq 500 \text{ kg m}^{-3} \end{cases} \tag{2.21}$$

Percolation and water contect

Meltwater percolates down through the subsurface layers until it refreezes. If all available water does not refreeze in a layer, a small amount of water will be held between snow grains by capillary forces; this is known as irreducible water. The residual percolates to the next layer. An empirical relationship, following Schneider and Jansson (2004) is used to compute the maximum irreducible water content Θ_{mi} of a layer via:

$$\Theta_{mi} = 0.0143\exp(3.3\phi) \tag{2.22}$$

where ϕ is the layer porosity

Slush water

If the total availability of water exceeds the slush water content, water starts to accumulate on top of impermeable ice, where it may form a slush layer. Slush water runs off gradually, resulting in an exponential decay of slush water content S in time:

$$S(t) = S(t - t^*)exp(-\frac{\Delta t}{t^*}) \ , \tag{2.23}$$

where Δt is the model time-step, and the time-scale t^* determines the estimated runoff from a grid cell. The latter is expressed as a function of surface slope following Zuo and Oerlemans (1996):

$$t^* = C1 + C2exp(-C3\tan\tau) \ , \tag{2.24}$$

where *C1*, *C2*, and *C3* are constants given values 0.5, 200 and 133 respectively (Reijmer and Hock, 2008), and τ is the surface slope. On a horizontal surface, runoff occurs when the slush water level exceeds the snowpack height or when bare ice is exposed at the

surface.

2.2.3 Climatic Mass Balance

Finally, the climatic mass balance (B_{clim}) of a certain grid cell over one time-step is calculated as

$$B_{clim} = P_s + P_l + R - \frac{Q_m}{L_f} \pm \frac{Q_l}{L_s} \ , \tag{2.25}$$

where P_s is the solid precipitation rate, P_l is the liquid precipitation, R is the refreezing calculated in the subsurface model, Q_m is the melt flux and Q_l is the negative latent heat flux, and L_f= 3.340x$\times 10^5$ K J kg^{-1} and L_s = 2.849$\times 10^6$ K J kg^{-1} are the latent energy of fusion and sublimation respectively.

2.2.4 Model Set-up

Model Grid

We used a 250×250 m horizontal resolution model grid in the surface energy balance model. The subsurface model consists of a vertically moving grid with 100 layers of varying thickness. The uppermost layer has a variable depth which shifts upward or downward as the layer thickness decreases or increases. Layer thickness is increased at depths from the surface by merging the 15$^{\text{th}}$, 30$^{\text{th}}$, 45$^{\text{th}}$ layers and reaches up to 0.8 m.

Calibration

Calibration is used to deduce appropriate values for a number of parameters which are often poorly constrained. Van Pelt and Kohler (2015) calibrated parameters associated with short and long wave radiation using automatic weather station data.

Here we calibrated the temperature lapse rate using summer balance data from the four NPI monitored glaciers. We considered a linear decrease of temperature with elevation using:

$$T_{nya}(Z,t) = T_{nya}(t) + 273.15 - C_T(Z - Z_{nya}) \ , \tag{2.26}$$

where $T_{nya}(t)$ is the Ny-Ålesund temperature time series, Z is the elevation of the grid point, and Z_{nya} is the elevation of Ny-Ålesund, and C_T is a temperature lapse rate, which is adjusted by running the model at the stake locations on the four glaciers until the model data match the observed summer balance values.

2.3 Runoff Routing

2.3.1 Simple Routing Model

Water which makes it to the bottom of the subsurface layer model defines the spatial production of meltwater and runoff from each grid cell, which then is transported through different channels to the fjord (Figure 2.6). There can be a significant delay between meltwater production and runoff to the fjord (Chandler et al., 2013), a delay which depends on several factors and varies through time with the evolution of the different channelized systems as melt season progresses (Hewitt et al., 2012, Liston and Mernild, 2012, Schoof et al., 2014, Lindbäck et al., 2015, Banwell et al., 2016, Schild et al., 2016, van As et al., 2017). The subglacial hydrology system controls water movement underneath the glacier, as well as influences the glacier ice flow speed (Zwally et al., 2002). A number of studies have addressed the evolution of subglacial hydrology through time (Walder and Fowler, 1994, Fountain and Walder, 1998), and models have been developed which are capable of calculating water flow with high temporal resolution (Hewitt et al., 2012, Schoof et al., 2012, Werder et al., 2013), but which require a number of assumptions about the drainage system.

Here we are interested in the discharge at the major outlet points of the Kongsfjord tidewater glaciers at sub-daily intervals. Complex hydrological models require high computational power and are highly parameterized; here we use a simple routing model to calculate the drainage basin and hydrographs at outlet points. We only considered topographically controlled flow and used different uniform wave speeds to simulate the time it takes runoff to reach the outlet points. Outlet points are determined using the Matlab Topotoolbox package (Schwanghart and Scherler, 2014) which calculates drainage basins, flow paths, and outlet points.

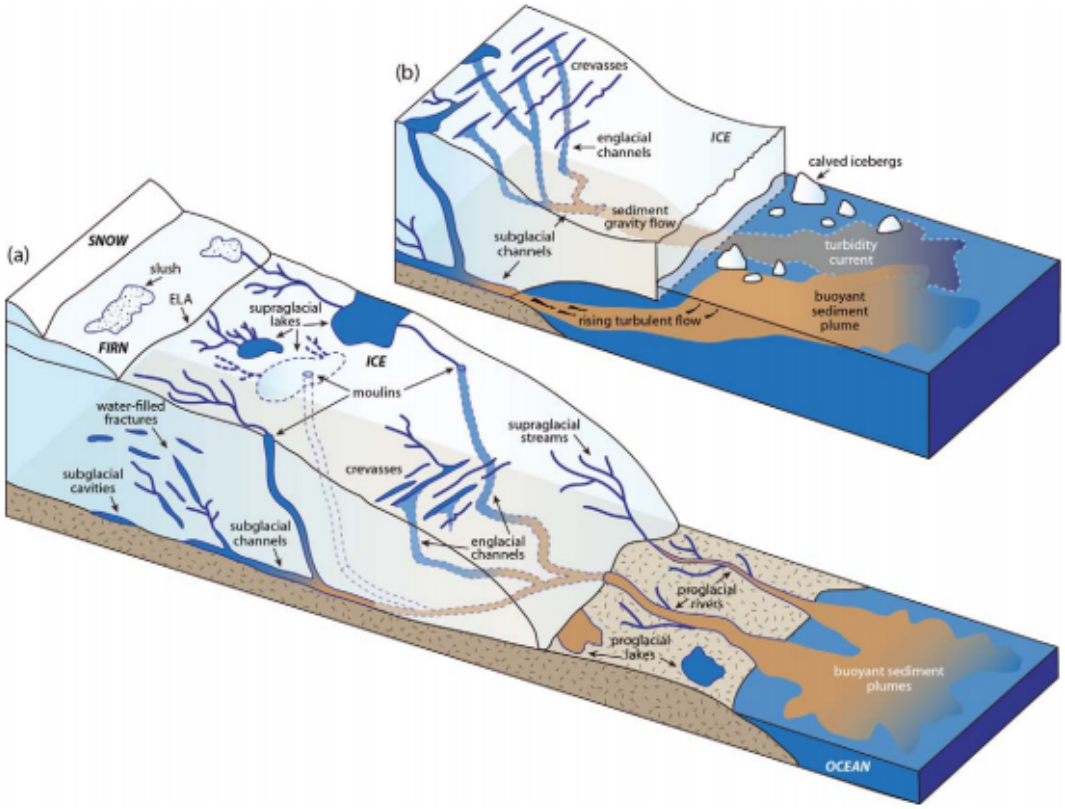

Figure 2.6: Elements of a hydrologic system for a) ice sheet and land-terminating glacier, b) marine-terminating glaciers. The figure is taken from Chu (2013).

We computed the hydraulic potential of tidewater glaciers and used hydraulic head gradient to control the water flow (Lindbäck et al., 2015, Everett et al., 2016). Hydraulic potential is the sum of the potential of ice overburden pressure and elevation potential, and is a steady-state proxy for the effect of subglacial hydrology on the flow system. The hydraulic potential is calculated as:

$$\Phi = P_i + P_e = \psi \rho_i g H + \rho_w g (Z_i - H) \tag{2.27}$$

where ρ_i is the density of ice (916 kg m^{-3}), ρ_w is the density of water at 0°C (1000 kg m^{-3}), g is the gravitational acceleration, H is the ice thickness (Lindbäck et al., 2018), and Z_i is the ice surface elevation (Shreve, 1972).

The hydraulic potential can be expressed in terms of hydraulic head via:

$$h = \psi \frac{\rho_i}{\rho_w} H + (Z_i - H) \ , \tag{2.28}$$

where the value of the parameter ψ determines the fraction of ice overburden pressure contributing to the subglacial water in the drainage system. When ψ equals 1, the subglacial water flow pressure is equivalent to the ice overburden pressure, a situation we normally expect in winter. If ψ equals 0, the subglacial water pressure is at atmospheric pressure and moves according to the bed topography alone. Any intermediate ψ value leads to water flow along the steepest slope of hydraulic head gradient. To calculate hydraulic potential we assume uniform ψ over the entire glacier and route water accordingly. The assumption of uniform ψ is not accurate as ψ varies in space and time; however, this gives a first-order estimate of subglacial water routing on spatial scales where the main control of drainage is the geometry of the glacier.

We use hydraulic potential to derive flow paths and derive the distance of each grid cell to its basin outlet point. Flow paths are derived according the steepest slope of the hydraulic head around each grid cell (Schwanghart and Scherler, 2014). We assign a uniform wave speed i.e., the velocity of water to calculate a time delay associated with each grid cell, summing the delayed runoff from all the grid points in a basin to derive the discharge hydrograph at the outlet points. We test different wave speeds in the range [0.05—1 m s^{-1}] to consider the effect of slower or faster flow of water, and use observational plume and discharge data to determine an optimal wave speed.

2.3.2 HydroFlow Model

We compare the simple routing approach to a somewhat more physical model, the physically based topographically controlled model HydroFlow (Liston and Mernild, 2012). HydroFlow is a linear reservoir model which considers snow thickness to calculate time-varying time coefficient associated with each model grid cell. Although HydroFlow is a physically based model and has been tested in different glaciated and river catchments (Mernild et al., 2017), it does not consider any subglacial hydrology in its flow routine. For land-terminating glaciers, supraglacial channels play a major role to transport water whereas, for tidewater glaciers, subglacial hydrology is quite important. Nevertheless, the model can derive the discharge hydrograph on sub-daily timescale with a relatively simple parameterization of complex processes as a series of linked linear reservoirs.

HydroFlow model was developed and first tested in Mittivakkat glacier catchment basin in southeast Greenland by Liston and Mernild (2012). The physics of the model is described by Liston and Mernild (2012), but briefly, each grid cell acts as a liner reservoir which transfers water from itself and upslope to the downward cell. It consists of four different submodels. First, the model calculates topographically controlled flow networks from the DEM. Second, it calculates the individual watersheds inside the domain of interest. Third, it assumes that there are two different transfer components (transfer functions) associated with each grid: a slow-response flow and a fast-response flow. These transfer functions are associated with different time-scales and represent different physical processes. The slow time-scale accounts for the time it takes to runoff from each grid cell produced from snow/ice melt, rain, whereas fast time-scale represents water transport through channelized systems such as supraglacial, subglacial, en-glacial flow. These two parameters are tuned with observational data.

The slow time-scale storage is defined as

$$\frac{dS_s}{dt} = Q_m - Q_s \tag{2.29}$$

where S_s is slow time-scale storage, Q_m is melt-generated runoff and Q_s is slow-response outflow.

The fast time-scale storage is defined as

$$\frac{dS_f}{dt} = I_{fi} + Q_s - Q_f \tag{2.30}$$

where S_f is the fast time-scale storage, I_{fi} is the fast time-scale inflow from the adjacent cells and Q_f is fast-response outflow.

To solve these equations a relationship between storage and outflow is required. The model assumes each grid cell is linear storage reservoir (i.e., storage is proportional to outflow), and thus represented by

$$S(t) = k(t)Q(t) \ , \tag{2.31}$$

where S is the total storage, Q is the outflow and k is the residence time coefficient.

Water flow at an arbitrary point in the grid domain is governed by

$$\frac{dS}{dt} = I - Q \ , \tag{2.32}$$

where I is the inflow from neighboring grid cells and from the runoff simulated in energy balance-subsurface model

The general solution to the equation has the form

$$Q = Q_{t-1} exp(-\frac{\Delta t}{k}) + I_t[1 - exp(-\frac{\Delta t}{k})] \ , \tag{2.33}$$

where I_t represents inflow contribution from grid cell runoff, slow storage and/or flow network, *dt* is the model time increment and *t* and *t-1* are the current and previous time steps respectively. Two different solutions are derived for the two (fast and slow) flow systems:

$$Q_{f,t} = Q_{f,t-1} exp(-\frac{\Delta t}{k_f}) + (Q_{f,i} + Q_{s,t})[1 - exp(-\frac{\Delta t}{k_f})] \ , \tag{2.34}$$

$$Q_{s,t} = Q_{s,t-1} exp(-\frac{\Delta t}{k_s}) + Q_{m,t}[1 - exp(-\frac{\Delta t}{k_s})] \ . \tag{2.35}$$

To solve the equation, a resident time-coefficient value k must be defined. This k value for land, glaciers, ice sheet could be formulated in such a way that it could be a function of surface slope, density of surface depression storage, distance traveled, deviations from straight path, snow, ice, soil porosity, cold content, density of supraglacial and englacial moulins, channel dimension and roughness, hydraulic potential, water pressure (Liston and Mernild, 2012).

Here the most basic form of k is considered:

$$k = \frac{D}{V} \ , \tag{2.36}$$

where D is the distance or average length dimension of grid cells and V is the velocity. This V value for slow response time V_s has been calibrated using field measurement. The model considers four different V_s values for four different cases; snow-covered ice, snow-free ice, snow-covered land, snow-free land.

The fast velocity is defined as

$$V_f = \beta V_s \Gamma \ , \tag{2.37}$$

where β is a scaling parameter that is used to control the flow speed and Γ is the surface slope.

3 Study area: Svalbard and Kongsfjord basin

The Svalbard archipelago is located between 75-81° North and 10-34° East, and was first discovered by the Dutch explorer Willem Barentsz in 1596. The archipelago comprises the main islands Spitsbergen, Nordaustlandet, Edgeøya, Barentsøya, and Kvitøya. Spitsbergen is the largest island, and the location of Svalbard's largest settlement, Longyearbyen. Initially, whalers and hunters mostly visited the archipelago, with increasing numbers of scientific expeditions in the 19th and early 20th centuries. Svalbard has extensive coal deposits, which were discovered in the early 1900s. In the last decades, tourism and research have become the main focus of Svalbard.

Research is localized around the main settlement in Longyearbyen and around the research town Ny-Ålesund, located in the Kongsfjord basin, northwestern Svalbard (Figure 2.1). Initially, Ny-Ålesund was a coal mining town. Following the closing of the mines in the 1960s, research became the primary focus, with a large number of studies in glaciology, biology, ecology and oceanography. The total glacierized area of Kongsfjord basin is around 1150 km^2, with the total non-glacierized area comprising only 20 percent of the total basin area. Kongsfjord is open to the Arctic Ocean in the west and surrounded by glaciers on the other three sides. The glaciers on the southwest side of the fjord are land-terminating whereas those on the east and north side of the fjord are mostly tidewater glaciers. Two ice fields in this area, Holtedahlfonna and Isachsenfonna, drain to Kongsfjord through the outlet glaciers Kronebreen and Kongsbreen, respectively. These two are among the fastest flowing glaciers in Svalbard. Land-terminating glaciers in this area are relatively slow and are experiencing rapid thinning; most have small accumulation areas.

3.1 Climate

Svalbard glaciers are susceptible to changing climate (Lang et al., 2014, Aas et al., 2015, Van Pelt and Kohler, 2015). As they respond rapidly to changing climate, frequent monitoring is necessary to understand their response. Svalbard is situated at the northern end of the Gulf Stream. Advection of warm Atlantic water through the Norwegian current keeps the fjord of the western side of Svalbard mostly ice-free year-round (Walczowski and Piechura, 2011), whereas eastern Svalbard is dominated by Arctic ocean currents (Loeng, 1991). Similarly, warm and moist air associated with the southerly flow and colder and drier air masses originating from the north (Käsmacher and Schneider, 2011) influence Svalbard with contrasting atmospheric regimes. The oceanic and atmospheric circulation pattern along with sea ice retreat leads to large spatiotemporal gradients of temperature and precipitation across the archipelago (Hisdal, 1998). The sea ice cover around the archipelago has declined substantially in recent decades, and there has been an increase in the length of the ice-free season (Rodrigues, 2008). The ongoing decrease of the sea ice extent strongly modulates the air-ocean exchanges of heat and moisture and has led to an amplified temperature increase through albedo effect (Hanssen-Bauer and Førland, 1998, Serreze and Francis, 2006, Serreze et al., 2009).

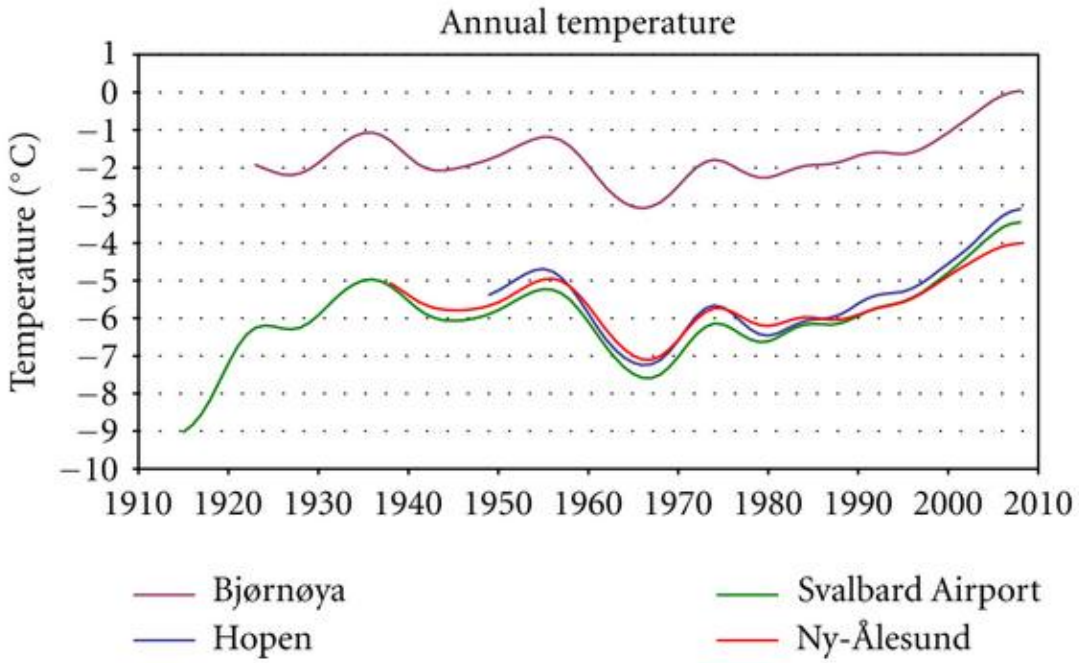

Figure 3.1: Time-series of annual temperature at multiple sites in Svalbard. Figure is taken from Førland et al. (2011).

Overall, Svalbard has experienced 0.5°C decade^{-1} of warming since 1960, the strongest measured in Europe (Nordli et al., 2014). The recent warming is more pronounced in winter/spring compared to summer/autumn, and is expected to continue into the 21st century. Climate model experiments project large regional gradients of temperature for Svalbard, with increases of 3°C in the southwest and 8°C in the northeast between 1961-1900 and 2071-2100 (Nakićenović, 2000, Førland et al., 2011).

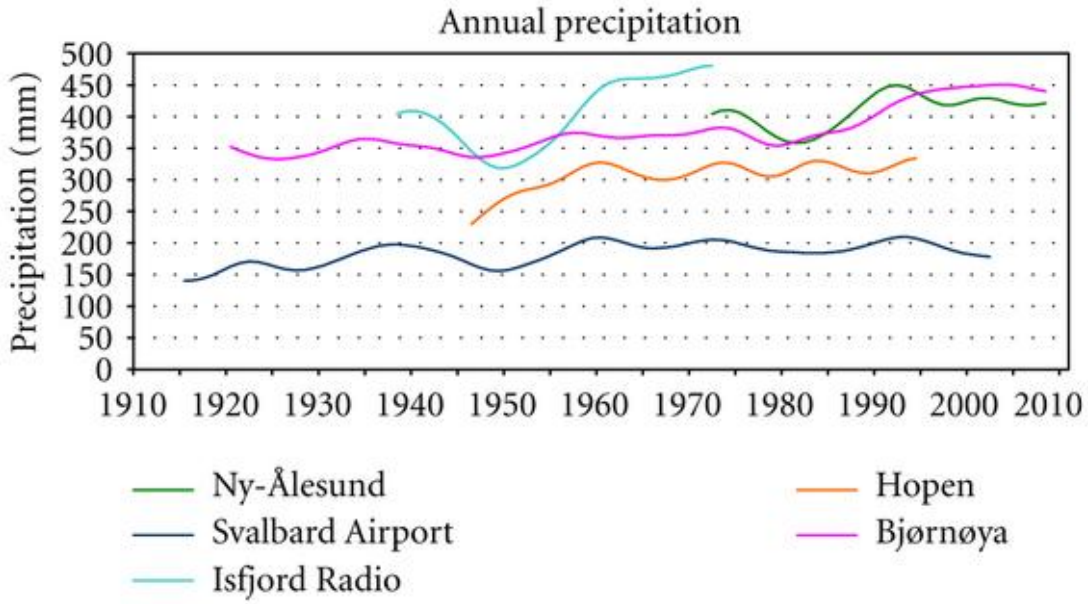

Figure 3.2: Time-series of annual precipitation at multiple sites in Svalbard. Figure is taken from Førland et al. (2011).

Simultaneously, precipitation in the archipelago has increased by 1.7% decade^{-1} (Førland and Hanssen-Bauer, 2000, Førland et al., 2011), which has been ascribed to changes in atmospheric circulation (Hanssen-Bauer and Førland, 1998). However, precipitation measurements are highly uncertain due to the effect of wind at measurement sites. For example, Førland and Hanssen-Bauer (2003) report up to 50% undercatch in precipitation gauges in Svalbard. Future projections indicate a further increase of precipitation. Førland et al. (2011) project increase ranging from a few percents in southwest of Svalbard to 40% in the northeast, comparing the periods 1981-1990 to 2071-2100 (Førland et al., 2011). This is in line with IPCC (2007), which projects a precipitation increase of <5% over the northern Atlantic and between 30 and 40% over the Arctic Ocean.

Large precipitation variability is observed across Svalbard, with a significant precipitation gradient from west to east and from north to south. Sand et al. (2003) reported twice as high snow accumulation on glaciers in the south, compared to those in the north, over

the period 1997-99. Central Spitsbergen experiences less precipitation and less interannual variability compared to the east and west coasts (Winther et al., 2003), with about 40% higher accumulation in the east compared to the west and 50% increase moving from north to south; the mean accumulation gradient was measured to be 97 mm per 100 m elevation.

3.2 Glaciers

Svalbard has a glacierized area of around 34,000 km^2 (Nuth et al., 2013) which is equivalent to 4% of the world's land-ice mass outside of the Greenland and Antarctica ice sheets (Aas et al., 2015). Sixty percent of Svalbard is glacier-covered (Hagen et al., 2003a), which, if melted, could potentially contribute 17-26 mm of sea level rise (Radić and Hock, 2010, Huss and Farinotti, 2012, Martín-Español et al., 2015). Glaciers in Svalbard show different dynamic behavior. Small cirque and valley type glaciers are mostly present in central Spitsbergen, whereas interconnected glaciers and ice caps are found to the northwest and in the eastern islands of the archipelago (Hagen et al., 1993).

Here I give a brief overview of the mass balance and dynamics of glaciers around Kongsfjord basin.

3.2.1 Mass Balance

Mass balance is the difference in mass gain and mass loss over a specific time period, usually over a year. Mass is gained mainly through precipitation, and secondarily through riming. Avalanches also may add significant mass to the glaciers. Mass loss occurs through melting, calving, and sublimation (Cogley et al., 2011). The part of the glacier where the net mass change is negative over a year is the ablation area, while the area with net mass gain is known as the accumulation area. The altitude where the net mass balance is zero is called the equilibrium line altitude (ELA), which nominally separates the accumulation and ablation areas, although in reality there is no one single elevation for which the mass balance is zero.

3.2.2 Dynamics

Glacier ice flows downslope under the influence of gravity, deforming internally under its own weight, and sliding over its bed as well as through deformation of till substratum, when present. Steady glacier geometry is achieved when ice dynamics compensate for

mass loss and mass gain at the surface. Błaszczyk et al. (2009) estimated roughly 7 km^3 a^{-1} mass loss is due to calving from entire Svalbard.

Svalbard has many surge-type glaciers (Lefauconnier and Hagen, 1992, Jiskoot et al., 1998). Surging has been linked to switch in basal thermal regime or to the hydrological system (Murray et al., 2000, Fowler et al., 2001, Murray et al., 2003, Flowers et al., 2011, Dunse et al., 2015, Sevestre et al., 2015). Surges of Svalbard glaciers last between 3-15 years (Dowdeswell et al., Sund et al., 2009), while the surge recurrence period estimated to be from 10s to 100s of years. Surges of marine-terminating glaciers can lead to significant mass loss by calving over limited timespans (Bartholomaus et al., 2015, McNabb et al., 2016, Medrzycka et al., 2016).

Figure 3.3: Velocity measurement with differential GPS. Photo by Ankit Pramanik.

3.2.3 Monitoring

A number of glaciers in and around Kongsfjord are being monitored by different international institutions (Figure 3.4.). Mass balance monitoring in the Kongsfjord area is mostly restricted to glaciers in southwest and east side of the fjord. Altogether nine glaciers in this area are currently monitored, four of them by the Norwegian Polar Insti-

tute. Mass balance monitoring in Kongsfjord basin started with the monitoring of Austre Brøggerbreen in 1967, and Midtre Lovénbreen the following year. Monitoring of tidewater glaciers started in 1987 with Kongsvegen, and then with Holtedahlfonna-Kronebreen in 2003, (WGMS, 2017).

Svalbard glaciers have had a mostly negative mass balance in the years since measurement started. Hagen et al. (2003b) estimated the total Svalbard mass balance to be -0.1 m w.e. a^{-1} over the period 1979-2000 from extrapolating stake mass balance gradients, accumulation rate from ice cores and snowline from aerial photographs. Geodetic mass balance estimate from aerial photography for the period 1960-1990 to 2003-2007 for southern and western Spitsbergen glaciers reveal mass loss of -0.30 m w.e. a^{-1} (Nuth et al., 2013). Mass loss even increased over the period 1961-2005 (James et al., 2012, Nuth et al., 2012). James et al. (2012) found enhanced thinning (-0.76 m a^{-1}) of six glaciers since 1990.

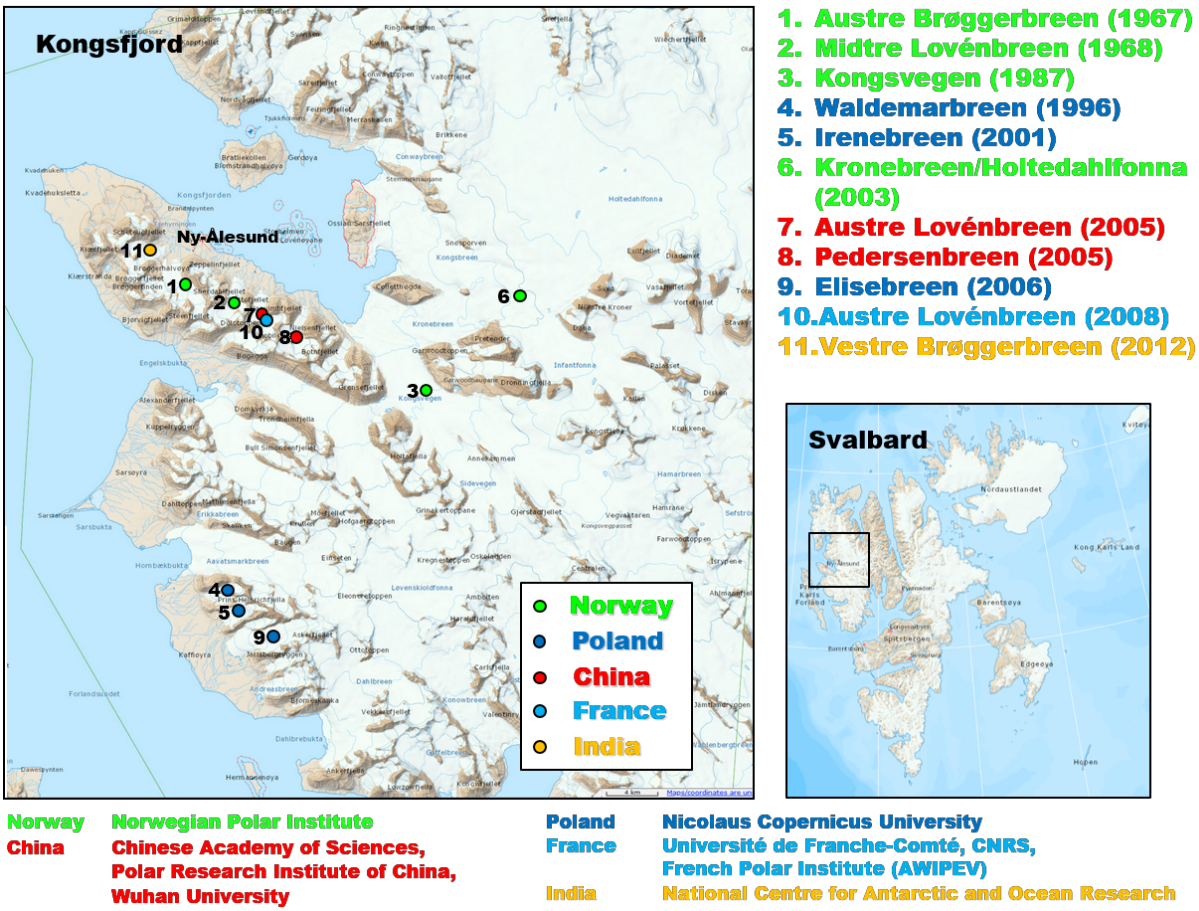

Figure 3.4: Glacier mass balance monitoring in Svalbard with responsible institutes. The year indicate the starting year. Figure: Jack Kohler / Norwegian Polar Institute.

Mass balance of the monitored glaciers in Kongsfjord show a steady negative trend, both from in situ measurements and from models. Bruland and Hagen (2002) used a precipitation-runoff model for Austre Brøggerbreen to find an average mass balance of -0.69 m w.e. a^{-1} for the year period 1971-1999. Nuth et al. (2012) used a degree-day model on the glaciers KNG and HDF to find a weakly negative net surface mass balance of -0.04 and -0.02 m w.e. a^{-1} between 1969 and 2007. Lefauconnier et al. (1994) found a slightly negative mass balance of (-0.11 m w.e. a^{-1}) for Kongsvegen over the period 1967-90. Van Pelt and Kohler (2015) found a slightly positive mass balance (0.08 m w.e. a^{-1}) for the glaciers Kongsvegen and Holtedahlfonna over the period 1961-2012 using a distributed energy balance model.

Kongsvegen is a surge-type glacier which is currently in its quiescent phase and flowing with low velocities (2-8 m a^{-1}) and experiencing surface steepening (Hagen et al., 1993, Kohler et al., 2007, Nuth et al., 2012). Kongsvegen last surged in 1948 (Melvold and Hagen, 1998). Kronebreen, which is fed by Holtedahlfonna and shares its terminus with Kongsvegen, is the fastest flowing tidewater glacier (300-800 m a^{-1}) (Kääb et al., 2005) in this area. It has experienced two periods of rapid frontal retreat of ∼3 km between 1966 and 1980, and ∼1 km between 2011 and 2013 (Nuth et al., 2012, 2013).

Three other tidewater glaciers exist in the north of Kongsfjord: Blomstrandbreen, Conwaybreen, and Kongsbreen. Blomstrandbreen is a surge-type glacier (Burton et al., 2016), which last surged in 2007 (Sund and Eiken, 2010, Mansell et al., 2012). Kongsbreen, which is connected to Isachsenfonna ice cap was observed to move at around 2.7 m d^{-1} speed at its front in summer 2012 (Schellenberger et al., 2015). Land-terminating glaciers in this area are relatively slow moving. Austre Brøggerbreen and Midtre Lovénbreen are moving at speeds of up to 3 m a^{-1} and 7 m a^{-1}, respectively, as measured by differential GPS on the mass balance stakes (Jack Kohler, personal communication).

4 Data

This chapter presents the data used in this study. Paper I analyzes sonic ranger data of snow surface height along with temperature, wind speed and direction data from Automatic Weather Stations. Meteorological data from Ny-Ålesund have been used as forcing for the energy balance model in Paper II. Stake mass balance data, discharge and plume data are used to calibrate and validate models in Paper II and Paper III.

4.1 Surface DEM, Glacier mask and Bed DEM

I use a digital elevation model (DEM) with a 5 m horizontal resolution, constructed by the Norwegian Polar Institute from aerial surveys in 2009 and 2010 (NPI, 2014), elevations are resampled onto a 250 × 250 m model grid. A recent glacier mask (König et al., 2014) is used throughout the study period. Radar surveys have been conducted from 2009-2015 using helicopter over the tidewater glaciers in Kongsfjord to determine ice thicknesses (Lindbäck et al., 2018). We use the resultant bed DEM to analyze subglacial water routing in Paper III.

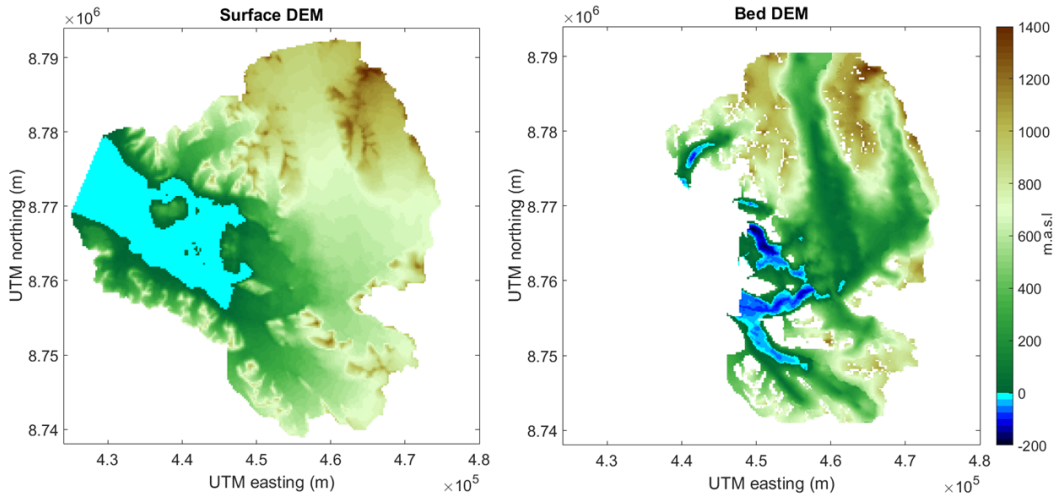

Figure 4.1: Surface elevation of entire Kongsfjord basin and Bed elevation of the glacierized area east and north of Kongsfjord basin.

4.2 Glacier AWS data

Holtedahlfonna and Kongsvegen have two automatic weather stations each; one in the ablation area and another close to equilibrium line altitude. I use sonic ranger data along with temperature, radiation, relative humidity, wind speed and wind direction from two automatic weather stations on Holtedahlfonna and Kongsvegen to analyze the spatial and temporal variability of accumulation and precipitation between two sites of these glaciers. The weather stations in the ablation zone have a number of periods with missing snow surface height data and are not used in the analysis. Only data from two weather stations close to the ELA have been used for the evaluation of precipitation forcing. These two weather stations have been operational since 2000 (Kongsvegen) and 2008 (Holtedahlfonna). Data were limited to the years 2012-2014 and 2015-16. Incoming and outgoing shortwave radiation, longwave radiation and temperature data from all four weather stations are used to calibrate the mass balance model (Van Pelt and Kohler, 2015), which is the core of Paper II.

4.3 Climate data from Ny-Ålesund

The energy balance model requires precipitation, air temperature, air pressure, relative humidity and cloud cover data as forcing for the model. This forcing comes either from regional climate model data or from nearby meteorological stations. The precipitation forcing for the energy balance model comes from ERA-Interim reanalyses precipitation forcing, discussed in section 4.4. I use meteorological data from the nearby meteorological site at Ny-Ålesund, extrapolating these data to the model grid by deducing a lapse rate to force the model. While temperature, relative humidity, and cloud cover are extrapolated linearly with elevation, air pressure is extrapolated exponentially with elevation. Precipitation data from Ny-Ålesund has been used in paper I to investigate the synchronicity of precipitation and accumulation events at glacier sites with the measured precipitation at Ny-Ålesund.

Table 4.1: Specifications of the sensors used in this study

Variable	Instrument	Measurement range	Accuracy
Snow (ice) surface height	Campbell SR 50A	0.5m to 10m	0.01m or 0.4%
Temperature	Vaisala HMP45C	-40°C to +60°C	0.3°C
Wind speed	Young 05103	1 to 60 ms^{-1}	0.3 ms^{-1}
Wind direction	Young 05103	0-360°	3°
Longwave radiation	Kipp and Zonen CNR1	0 to 2000 W m^{-2}	10% of daily total
Relative humidity	Vaisala HMP45C	0 to 100%	±2% (RH< 90%), ±3% (RH>90%)

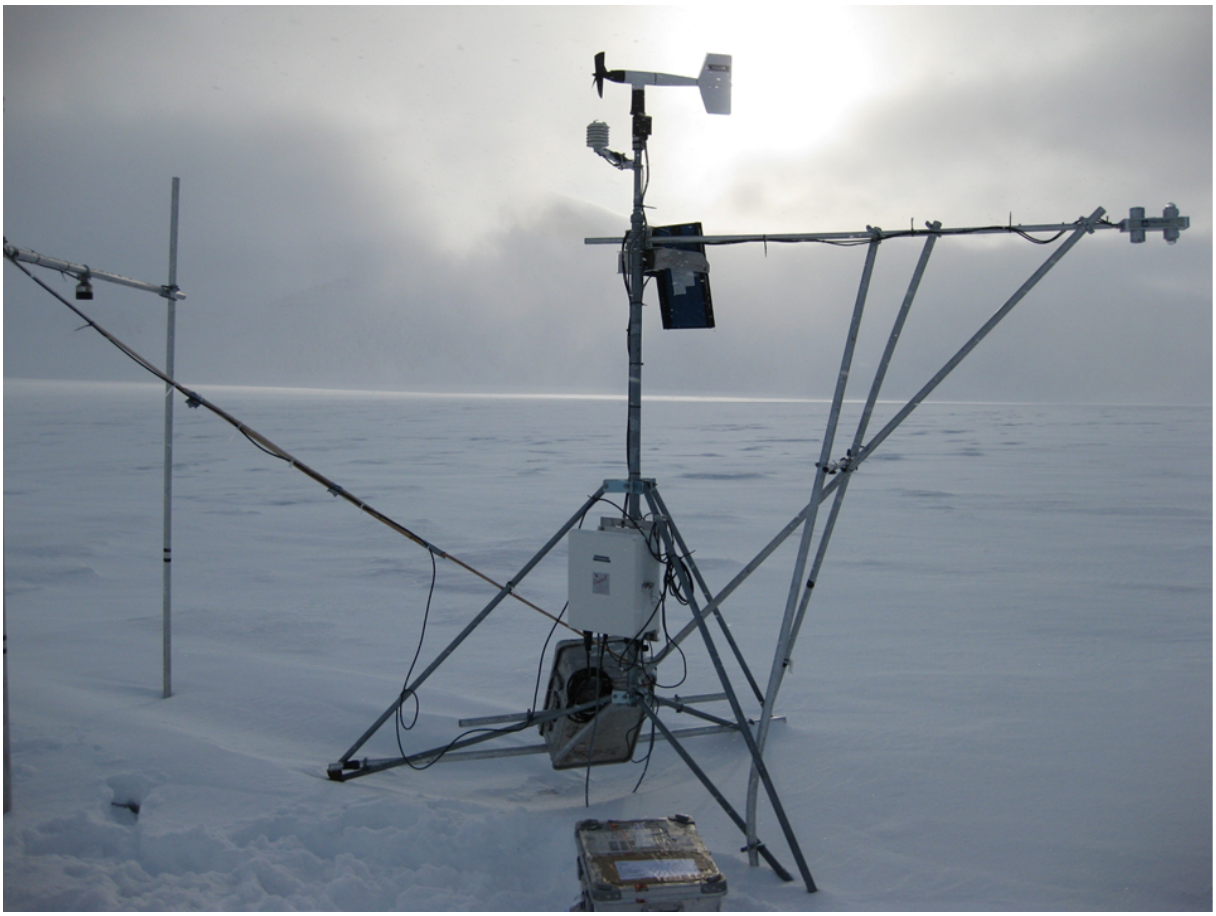

Figure 4.2: Glacier automatic weather station at HDF2. Photo: Jack Kohler.

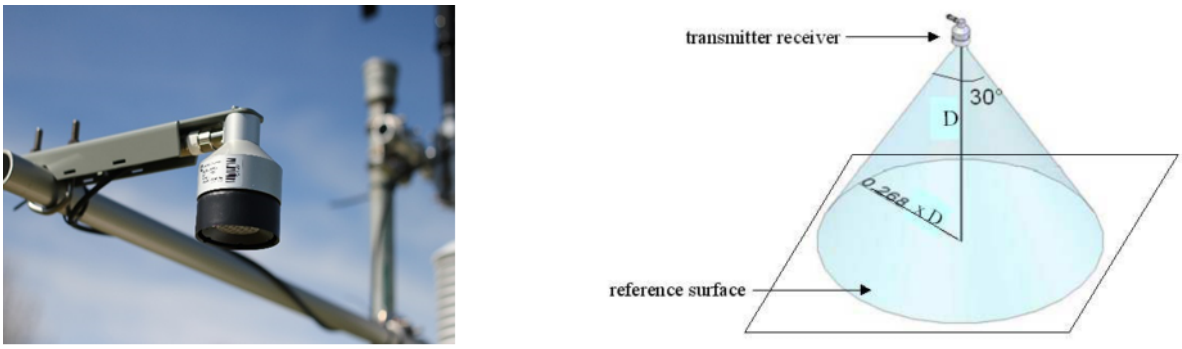

Figure 4.3: Sonic ranger of the automatic weather station.

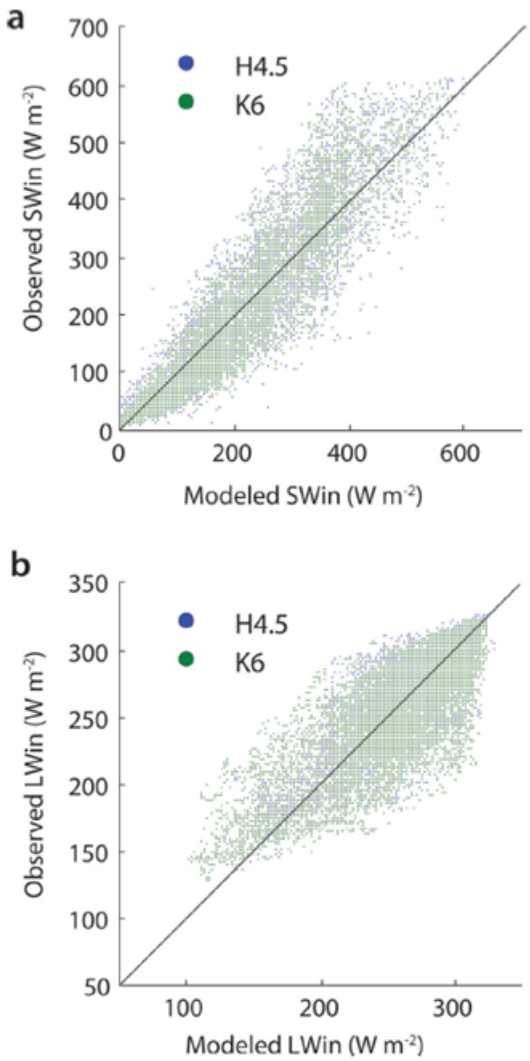

Figure 4.4: Calibration of radiation fluxes with AWS data. Figure is taken from Van Pelt and Kohler (2015).

4.4 Downscaled ERA-Interim precipitation data

The ERA-Interim reanalysis dataset provides meteorological parameters on an 80 km spatial grid and with a 6-hour temporal resolution (Dee et al., 2011). We used precipitation data of ERA-Interim for our analysis in papers I and II, which have been downscaled to 1000 m resolution by Østby et al. (2017). These data are used for comparison with the accumulation measurement from the sonic ranger data at two glacier sites in Paper I, which shows that the downscaled ERA-Interim data are in good agreement with the accumulation measurements at the glacier sites.

In the coarsely resolved reanalysis products, precipitation is highly biased in certain areas (Schuler et al., 2008). Østby et al. (2017) used linear theory (LT) of orographic precipitation (Barstad and Smith, 2005) to scale precipitation for all of Svalbard using winter balance data from selected glaciers of Svalbard, in different parts of the archipelago. These downscaled precipitation data are used as precipitation forcing to the CMB model, after further downscaling to 250 m resolution through linear interpolation. We observe wide variability of precipitation and accumulation around the Kongsfjord basin (Paper I) and hence, a distributed precipitation field is preferable to simply extrapolating precipitation data from the nearby meteorological site.

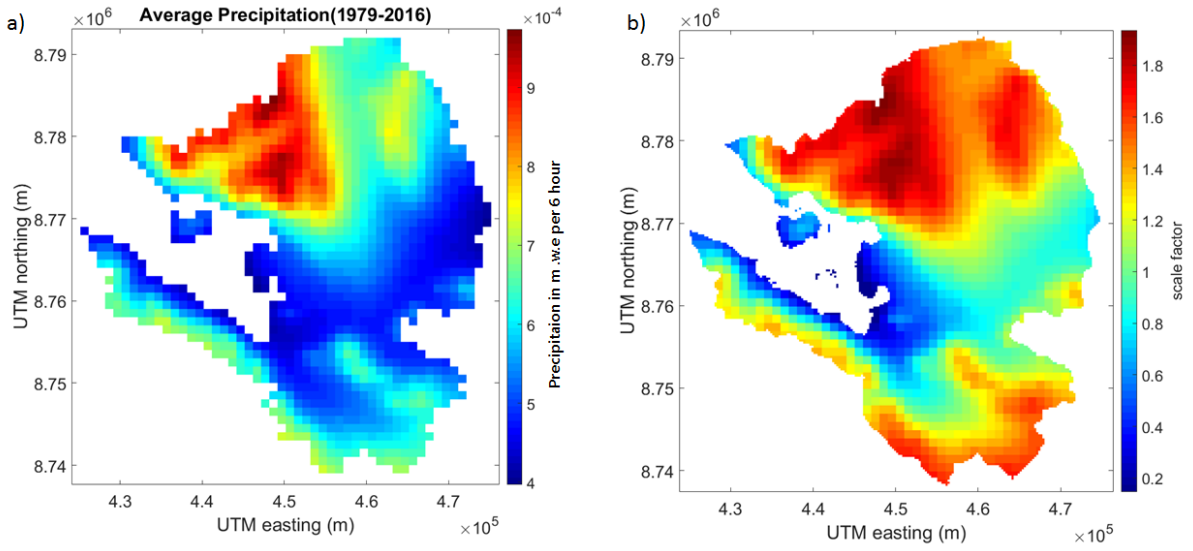

Figure 4.5: a) Average ERA-Interim precipitation over Kongsfjord basin during the period 1979-2016. b) The scale factor used to adjust precipitation. Scaling parameters are calculated using point mass balance measurement (Østby et al., 2017).

4.5 Winter, summer, and net mass balance data of four glaciers

Stake measurements of winter and summer balance data from four glaciers (Austre Brøggerbreen, Midtre Lovénbreen, Kongsvegen, and Holtedahlfonna) are used for calibration and validation of the energy balance model in paper II.

Summer stake balance data are used to calibrate temperatures for the different glaciers, and winter stake balance data to scale precipitation. Winter balance of a year is measured around mid-April whereas summer balance is measured around mid-September of that year. Svalbard glaciers can experience significant superimposed ice formation in the upper ablation area and around the ELA which is not always reflected in the stake measurements and which causes biases in the mass balance measurement. In recent years, superimposed ice cores are taken every year during spring field campaigns to acquire accurate measurement of winter mass balance.

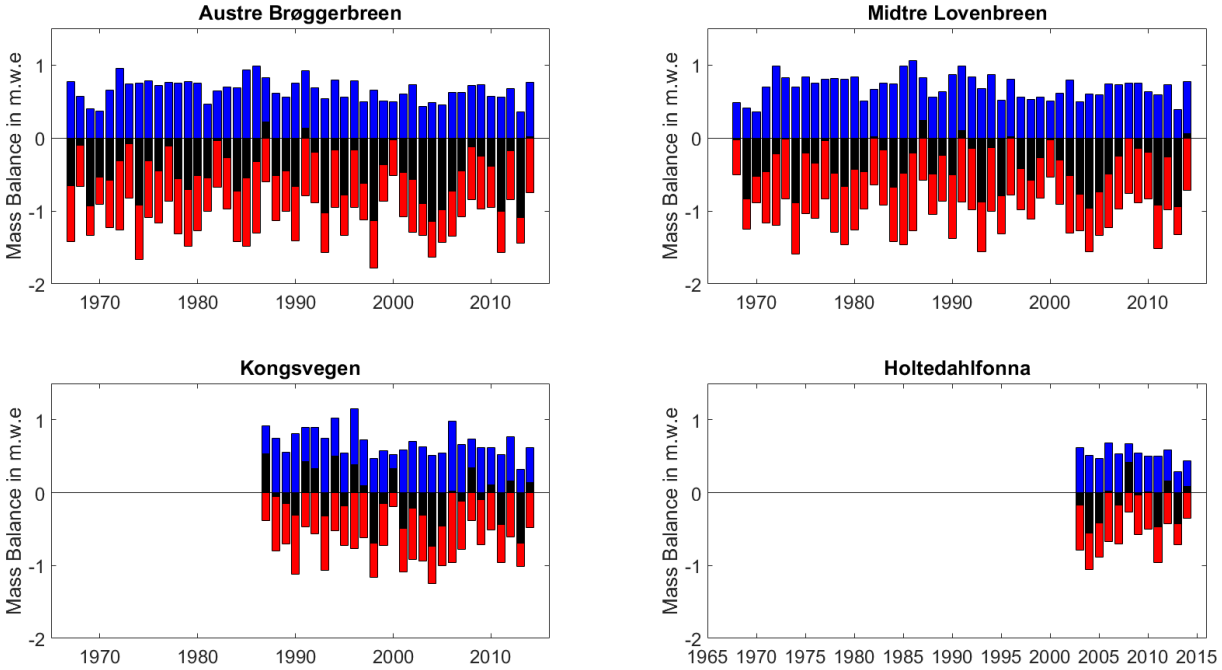

Figure 4.6: Measured winter(blue), summer(red) and net mass(black) balance of four glaciers.

4.6 Discharge measurement Bayelva

I use proglacial discharge data from the river Bayelva to validate the routing models in paper III. Bayelva river is fed by ice-melt from two glaciers Austre Brøggerbreen and

Vestre Brøggerbreen situated on the southwest side of the Kongsfjord basin. The total catchment area of Bayelva is 31 km^2, 61% of which is glacierized. In spring, seasonal snow-melt from the non-glacierized area and snow and ice melt from the glaciers is transported through the river, whereas by late summer, it is mostly meltwater from the glaciers which feeds the river. The discharge measurement site (Figure 2.1) is around 3 km from the glacier snout. This site is maintained by NVE, Norwegian Water Resources and Energy Directorate, and has been operational since 1989. During the period 1989-1999, discharge was measured daily, but since 2000 discharge has been measured hourly (Fred Wenger, personal communication). Sediment and ice build up at the sensor lead to some erroneous data in certain years, but the timing of discharge peaks is mostly not affected.

Figure 4.7: Discharge measurement site of Bayelva. The site is maintained by NVE, Norwegian Water Resources and Energy Directorate. Photo was taken by Ankit Pramanik.

4.7 Plume data

When meltwater from tidewater glacier exits into the fjord, at depths, it generates a freshwater plume. The appearance of the plume at the surface depends on several factors e.g. runoff, wind, outlet shape, terminus depth (Cowton et al., 2015). Unlike tidewater glaciers in Greenland, which have deep fronts or often ice cover at the front, glaciers around Kongsfjord end in relatively shallow ($<$ 100 m) water depth, the fjord water is

ice-free during summers. Penny How at the University of Edinburgh installed time-lapse cameras near the glacier terminus to observe long-term plume dynamics at the outlet of Kronebreen, and calculated the plume area extent over the period 2014-2016 from these time-lapse images (How et al., 2017). Although plume area extent depends on several factors, we believe one major factor which determines the intensity of plume, and hence its extent, is the runoff from the tidewater glacier. We used plume area extent data as a proxy to runoff to calibrate the parameters of the simple routing model. Plume data has been recorded with high temporal resolution for short periods in certain years, but here we use hourly data of plume area extent (Figure 4.8).

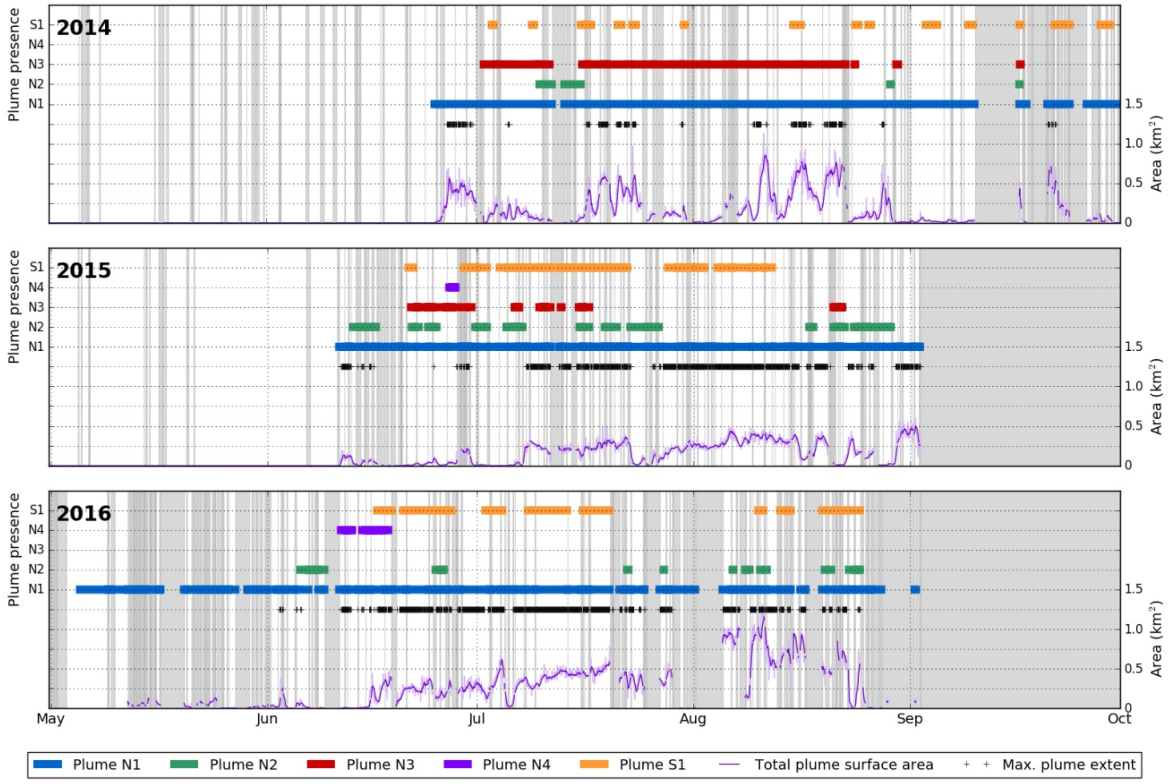

Figure 4.8: Observation plume visibility and surface area extent for the period 2014-2016. Figure provided by Penelope How.

5 Summary of Papers

5.1 Paper I

A major source of mass gain of glaciers is precipitation. Mass balance modelling requires distributed precipitation field for accurate estimate of mass balance, else it leads to biases with actual measurement (Box et al., 2004, van de Berg et al., 2006, Østby et al., 2017). RCMs (Regional Climate Models) or GCMs (General Circulation Models), or reanalysis datasets can provide insight into snow precipitation over large areas, but snowfall also varies substantially at smaller spatial scales induced by topography, which, in turn, is too coarsely represented in large-scale models to resolve these effects. In situ records of snowfall are useful for understanding variability over smaller length scales and may provide valuable means to evaluate the performance of atmospheric models in locations offside of synoptic stations (Fountain et al., 2010, Cohen and Dean, 2013). In this study, we analyzed automatic weather station data from two different glaciers Kongsvegen and Holtedahlfonna in Kongsfjord basin. These respective AWS sites are close to mass balance measurement stakes, and are named KNG6 (Kongsvegen stake 6) and HDF4.5 (Holtedahlfonna stake 4.5). Both sites are in the upper ablation zone of each glacier. Sonic ranger sensors on the AWSs measure snow surface height; we filter these data and conduct an event-based analysis of different snow accumulation events at two different glacier sites. We then compare these events with ERA-Interim precipitation and with Ny-Ålesund precipitation record to evaluate whether a model-derived gridded precipitation data or station measured precipitation data better represent the precipitation events at the glacier sites.

Long-term accurate measurements of snowfall is challenging, with any automated measurement, especially due to the complex effect of wind. Sonic rangers measure snow surface height, and hence, positive changes could be ascribed to the accumulation of snow, however, the cause of the snow accumulation, whether through solid precipitation or advection as wind-driven snow, is unknown (Braaten, 2000). Wind-driven snow redistribution (erosion and deposition) is a significant and ongoing challenge for studying snow

on the ground since the process is complex, and depends on many factors; e.g. snow age, air temperature, snow moisture, local topography, and snow grain size (Li and Pomeroy, 1997, Essery et al., 1999, Dery and Yau, 2001, Lenaerts et al., 2014). Nevertheless, valuable information about snow accumulation and snowfall variability could be derived from the sonic ranger, coupled with additional meteorological measurements.

Due to malfunctioning of the sonic ranger, our analysis is limited to the periods 2012-2014 and 2015-2016. We define a significant increase in snow depth over a certain period as an accumulation event, and categorize these accumulation events by applying thresholds of air temperature and wind speed data from respective AWS sites. We first reduced noise by smoothing the hourly data using 6-hour running-mean filter (e.g. Fountain et al., 2010), and computed snow depth changes for each 12-hour event as a sum of consecutive records of non-zero values of snow surface height increase within a 12 hour period. A threshold change of 0.01 m/12 hour is applied to define event-wise accumulation amounts. Corresponding wind speeds for each 12-hour event has been characterized as a maximum of hourly wind speed over the event duration, whereas the temperature of the event is the average over the event. We then categorized accumulation events as either accumulation with low wind (calm snowfall), or as accumulation with high wind, by applying the temperature and wind speed. We investigate the accumulation events and amounts at two sites with associated wind speed and wind direction data, and evaluate how many of the precipitation and accumulation events at the sites are captured by ERA-Interim and Ny-Ålesund precipitation. Finally, we compare the absolute amount of accumulation/precipitation measured at the site with the precipitation of ERA-Interim and Ny-Ålesund.

Overall, we detected more number of accumulation events at KNG6 than HDF4.5, with most of the events associated with synoptic activity. We find overall wind speeds at KNG6 associated with accumulation are high (median 5.68 m s^{-1}) compared to HDF4.5 (median 4.09 m s^{-1}), but we detected more snowfall events at HDF4.5. The prevailing wind direction at KNG6 associated with accumulation events is in the down-glacier direction, from the south-southeast, which is the predominant wind direction associated with moisture-bearing low-pressure synoptic systems from the south. Hence, we found most accumulation events at KNG6 are associated with drifting and blowing snow. At HDF4.5, the prevailing wind direction associated with snowfall is also is in the down-glacier direction, but from the north-northeast. Winds from the north are in general colder and associated with less precipitation.

Comparison of high wind accumulation and calm snowfall at glacier sites with ERA-Interim and Ny-Ålesund precipitation shows that ERA-Interim captures higher number of events at sites compared to Ny-Ålesund. We used two other different accumulation threshold values, 5 mm/12 hours and 1 mm/12 hours, to investigate the sensitivity of the coincident events. With decreasing accumulation threshold, ERA-Interim captures a higher number of coincident events than Ny-Ålesund, and the percentage of coincident events decreases more for Ny-Ålesund than for ERA-Interim. This suggests the ERA-Interim record provides a reasonable representation of precipitation occurrence on the studied glaciers. Comparing the precipitation amounts of ERA-Interim and Ny-Ålesund with sites for coincident events, relatively better correlation is found for ERA-Interim than Ny-Ålesund for high wind accumulation events, whereas correlation is comparable for calm snowfall events.

In summary, in spite of having limitations in continuous precipitation measurement, the sonic ranger could provide valuable information about accumulation and snowfall variability. This type of analysis also helps to validate the synoptic predictions of weather models. We believe that we are able to distinguish wind-influenced accumulation from snowfall events on sub-daily and seasonal timescales, but to investigate in more detail the processes of erosion, deposition, and precipitation, more sophisticated measurement devices would be required; this is challenging for unmanned AWS sites. To gain more detailed information on the spatial scale of precipitation events, a denser network of snow sensors and more frequent monitoring would be required.

5.2 Paper II

In the presently warming climate, meltwater runoff from glaciers and ice caps are major contributors to current sea level rise (Church et al., 2011). The high Arctic archipelago Svalbard has a glacierized area of 34,000 km^2 (Nuth et al., 2013), which, if melted, would lead to 17-26 mm of eustatic sea level rise (Radić and Hock, 2010, Huss and Farinotti, 2012, Martín-Español et al., 2015). The Arctic is warming rapidly with the retreat of sea ice and changes in atmospheric circulation; a feedback mechanism termed as "Arctic amplification" (Serreze and Francis, 2006, Serreze et al., 2009). Changes in precipitation and temperature in Svalbard have been reported in several studies (Hanssen-Bauer and Førland, 1998, Førland et al., 2011). In northwest Svalbard, Kongsfjord basin is a hotspot for interdisciplinary studies addressing the significance of freshwater from seasonal snow and glacier melt on the physical and biological environment. Kongsfjord is open to the

ocean in the west and surrounded by glaciers in the south, east and north. The ongoing interdisciplinary projects along with long-term mass balance measurement of glaciers in this area make it scientifically interesting region. Four glaciers in this region are being monitored by Norwegian Polar Institute. In this study, we aim to simulate long-term evolution of mass balance of glacierized area, seasonal snow development, and associated freshwater flux of Kongsfjord basin. We use a surface energy balance model coupled with subsurface snow/firn model (Van Pelt et al., 2012, Van Pelt and Kohler, 2015) on the entire Kongsfjord basin, represented as a 250×250 m resolution grid, to simulate mass balance, melt, refreezing, and runoff of glaciers, as well as the subsurface evolution of snow/firn pack. A subsurface soil model (Westermann et al., 2011) is incorporated with the energy balance model to simulate seasonal snow development and runoff from the non-glacierized area. The model is calibrated with the stake measured summer balance data from four glaciers. Meteorological forcing for the model comes from nearby meteorological station at Ny-Ålesund, whereas downscaled precipitation from ERA-Interim reanalyses scaled for Svalbard (Østby et al., 2017) is used as precipitation forcing.

We divided the entire glacierized area into three different regions: south, east and north. The climatic mass balance of glacierized area of three subregions and freshwater flux from glacierized and non-glacierized area of the three subregions is analyzed and presented.

We find the area-average climatic mass balance of the entire glacierized area of Kongsfjord basin over the period 1980-2016 is +0.23 m w.e. a^{-1}. We observed wide variability of mass balance inside this region; glaciers on the south and east sides of the fjord show negative mass balance while glaciers on the north side show positive mass balance. In spite of significant increasing summer temperature, the net mass balance time-series of entire glacierized area and subregions show a non-significant trend; however, the summer balance has a weakly negative but significant trend. The anti-correlation of net mass balance with mean summer temperature is very weak and non-significant for glaciers of north (-0.24, $p<0.15$), whereas the anti-correlation is stronger in the east (-0.37, $p<0.03$) and south (-0.42, $p<0.01$) regions, which indicates that the mass balance of glaciers in the south and east are more sensitive to temperature than in the north. Winter precipitation shows a positive but non-significant trend for the entire region over the simulation period, which compensates the decreasing summer balance trend to a certain extent, and thereby leads to no significant trend in the net climatic mass balance. Glaciers on the north side of fjord get high snowfall, which leads to high refreezing and reduced mass loss for these glaciers. Similarly, melt and runoff rates are also low for these glaciers, compared to rest of the glaciers around the fjord. Average refreezing amounts to 0.24 m w.e. a^{-1}, which

accounts for 17% of the total mass gain from precipitation and moisture deposition, and plays a crucial role for climatic mass balance estimate. Air temperature in this region shows an increasing trend; an average increase of 2 K a^{-1} winter temperature is observed between 1980 and 2016. Precipitation (snowfall and rainfall) in this region has increased substantially in the last 10 years, at the same time that mass balance shows a positive trend. This increase of precipitation could be ascribed to recent retreat of sea ice cover and increase of winter temperature. We find a significant increasing trend in runoff from the entire glacierized area (6.83×10^6 m^3 a^{-1} with $p<0.09$) as well as from the north (3.47×10^6 m^3 a^{-1} with $p<0.1$) and east region (6.83×10^6 m^3 a^{-1} with $p<0.08$) over the simulation period. Area-averaged runoff is highest for the southern region, while the eastern region contributes the maximum freshwater to the fjord. Runoff from the non-glacierized area due to snowmelt adds substantial freshwater to the fjord in early and peak melt season and amounts to 16% of the total runoff from the entire basin.

We used observational data at different spatial scales to get a robust estimate of the evolution of mass balance of the glaciers and the runoff for the entire Kongsfjord basin. Calibration of parameters for radiation fluxes (Van Pelt and Kohler, 2015) and temperature with the observational data helped to minimize the uncertainty of model parameters. The major uncertainty in the result comes from precipitation forcing, which often is not able to capture small-scale variability. Wide accumulation variability has been observed in this region through in-situ measurements. The snowpack controls the cold content and thereby refreezing. Mass balance has non-linear response to snow accumulation, and ignoring small-scale accumulation variability will induce a bias in area-averaged mass balance estimates.

Another source of uncertainty is that we used fixed topography and ice extent, which adds uncertainty to extrapolation of elevation dependent parameters, and to runoff due to glacier length fluctuations. The low resolution DEM (250x250 m) cannot resolve the surrounding topography of the smaller glaciers, leading to inappropriate shading, and thus to uncertainty in radiation budget of these glaciers. Extrapolation of stake data to glacier-wide grid and using time-invariant temperature lapse rate, which in reality varies with cloud conditions (Van Tricht et al., 2016), are other sources of model uncertainty. Finally, observations used for model calibration and validation do not include any glaciers in the north region, which increases uncertainty of the results in this region. More observational data from this region will help to constrain uncertainties.

5.3 Paper III

The main aim of this paper is to estimate the spatial and temporal variation of the freshwater influx to the Kongsfjord in recent years. Freshwater from tidewaters rises buoyantly to form plumes; this water mixes with the fjord water at different vertical depths, affecting fjord circulation. Plumes bring nutrients to the fjord surface, creating a feeding ground for marine animals. Hence it is of interest to biologists and oceanographers to know the freshwater influx to the fjord. Most of the freshwater in Kongsfjord comes from snow and ice melt from the glaciers (84%), whereas freshwater from the non-glacierized area produced by seasonal snowmelt contributes 16% of freshwater to the fjord. In paper II, we simulated distributed runoff from the entire glacierized and non-glacierized area of Kongsfjord basin. There can be substantial delays between the location where meltwater is produced and the exit point where runoff enters the fjord, involving flow in the hydrological system in and beneath the glacier. Meltwater produced at the glacier surface travels supraglacially, englacially, and subglacially before reappearing at the glacier front, the fjord. Estimating the freshwater influx into the fjord requires proper routing scheme. Detailed hydrological models are available to accurately estimate the transport of freshwater to the fjord, models that consider the formation of distributed or channelized systems underneath the glacier (Hewitt et al., 2012, Schoof et al., 2012, Werder et al., 2013). Such detailed hydrological models have a large number of adjustable parameters and different setup possibilities. Simpler routing models, which just treat the transport of water from the bottom of the energy balance-subsurface layer model as a simple delay process, are also able to estimate discharge at the glacier outlet points which often serves the interest of glaciologists, oceanographers and biologists.

In this study, we analyzed subglacial hydrology of tidewater glaciers considering steady-state behavior (Shreve, 1972). We calculated the hydraulic potential of the water underneath the tidewater glaciers using surface elevation and ice thickness data. We considered different ice overburden pressure (k) (Lindbäck et al., 2015, Everett et al., 2016) to calculate subglacial drainage basins for all of the tidewater glaciers. We compare a simple routing model to a more physically based model (HydroFlow) to derive discharge at the glacier outlets around Kongsfjord. For tidewater glaciers, water is routed according to the hydraulic head gradient, whereas for land-terminating glaciers, water is routed according to the surface topography. For the simple routing model, we considered different uniform wave speeds and calculated discharge hydrographs at the outlet points of each glacier. For tidewater glaciers, we use the plume area-extent derived from time-lapse im-

agery to calibrate the model parameters, treating the size of the plume as a proxy for subglacial discharge. The proglacial discharge record is used to calibrate parameters for runoff routing of land-terminating glaciers.

The subglacial hydrological analysis shows that there is a strong possibility that there is subglacial water piracy between Isachsenfonna and Holtedahlfonna. Isachsenfonna is connected to the glacier Kongsbreen, while Holtedahlfonna is connected to the outlet glacier Kronebreen. Subglacial hydrological analysis shows that substantial area of Isachsenfonna will drain to Holtedahlfonna and then to Kronebreen when pressure in the basal drainage system is not completely at ice overburden pressure (k<0.97), which is a most likely scenario for summer. Other tidewater glacier drainage basins remain mostly unaltered for different basal water pressures. Observations show a substantial plume at the Kronebreen front and hardly any plume at Kongsbreen North front, although the drainage area according to the surface flow of these two glaciers are not very different.

We found Kronebreen outlet contributes the most freshwater to the fjord, of all the tidewater outlet points. Discharge at the outlet points varies owing to different k values. The discharge amount from the Kronebreen outlet increases by 1.5 times when the k value is below 1, owing to water piracy from Isachsenfonna.

We derived discharge hydrographs from all the drainage basins around Kongsfjord with the simple routing model and with the HydroFlow model. We find good agreement between both the model derived discharge hydrographs for both tidewater and land-terminating glaciers in all the years, which suggests that the simple routing model is able to produce the timings of the discharge quite accurately. The five tidewater glaciers of the Kongsfjord basin contribute most of the freshwater flux to the fjord. This has significant importance, as mixing of freshwater from glaciers and non-glacierized area with the seawater of the fjord enhances primary and secondary production, and plays an important role in fjord ecosystem (Lydersen et al., 2014) and circulation (Sundfjord et al., 2017). The average runoff period from all the five tidewater glacier outlets over the 2014-2016 period was 105±10 days, with some late discharge events in 2016 mostly due to rain. The duration of the runoff period was high in 2015, but total runoff volume increased by 46% from 2014 to 2015 and by 12% from 2015 to 2016.

Glaciers on the south side of the fjord are all land-terminating. The discharge hydrographs derived for these glaciers are about one order less in magnitude than that of tidewater glaciers. The south region contributes around 10% of the total freshwater to the fjord over a year. Discharge from land-terminating glaciers mixes with the fjord at the

surface. River discharge is important for glacier geochemistry study and plays a crucial role in controlling the physical and chemical environment of the fjord.

Time delays for runoff, in general, increase with the discharge, as more runoff comes from the upper part of glaciers during high discharge events. Delays between peak melt and peak discharge reach up to a day. Detailed hydrological analysis is required to understand the evolution of subglacial hydrology of these two glaciers throughout the season, which, if incorporated with a physically based routing model, would provide better estimate of freshwater discharge at the outlet points. Nevertheless, more observational data would be required to constrain the models and understand the hydrological behavior of tidewater glaciers.

6 Discussions and Outlook

6.1 Synthesis: Objectives to outcomes

This thesis consists of three different studies, which establish potential links of glaciology (Paper II) with atmospheric research (Paper I), and with biology/ecology and oceanography (Paper III). The output and analyses of our third paper are useful for different communities (e.g. Paper IV, Paper V, and paper VI) and open for further understanding of the subglacial hydrology of this area.

The main aim of this thesis was to quantify spatial and temporal influx of freshwater to Kongsfjorden from the glacierized and non-glacierized area of the basin. I needed to answer some antecedent questions to finally address it. I tried to answer them through analysis of observational data and modeling approach, and that resulted in Paper I and Paper II.

I use a coupled energy balance-snow model (Van Pelt et al., 2012) to simulate spatial production of runoff which serves as input to the routing model. Mass balance models require climate forcing, the most important of which is precipitation as it is the major source of mass gain for glaciers. Accurate estimates of mass balance require well-constrained precipitation fields. Precipitation data were available from ERA-Interim reanalysis and also from the nearby meteorological station at Ny-Ålesund. Both datasets have their limitations, however, this lead to an investigation of the long-term snow depth data measured at two weather stations on two different glaciers in the Kongsfjord basin, which are compared with the ERA-Interim reanalysis and with Ny-Ålesund precipitation datasets (Paper I). My further aim was to detect and quantify snowfall events and find variability in snowfall between these two glacier sites. I analyze the glacier snow depth data together with temperature and wind speed to categorize different accumulation events. I am able to detect accumulation events at two sites, but the effect of wind limits quantification of precipitation events to a large extent. However, through this analysis, I show that there is significant difference in accumulation between two nearby glacier sites, and I explain the underlying cause. I find that ERA-Interim captures more number of precipitation and

accumulation events at the glacier sites compared to Ny-Ålesund, thus, help us to choose one precipitation forcing over the other.

The coupled energy balance-snow/firn model (Paper II) simulates spatial production of meltwater and runoff. With the further inclusion of a soil model (Westermann et al., 2011), runoff from the seasonal snow of the non-glacierized area is also simulated. With this study, I investigate the long-term mass balance trend of the glacierized area of Kongsfjord basin in changing climate.

Finally, the spatial runoff distribution served as input to a routing model, which calculates the discharge hydrograph at all glacier outlet points. These results and data will be important for oceanographers, who are doing ocean modelling in the area, and for biologists or ecologists, who are studying the fjord ecosystem at the front of the tidewater glaciers.

6.2 Main outcomes

I used an energy balance model to simulate mass balance and runoff evolution over 1980-2016 from the entire Kongsfjord basin (Paper II). Mass balance model requires climate forcing which often comes from either nearby meteorological stations or from climate models. Precipitation is one important variable which varies substantially with topography and wind, and even climate models are often unable to predict synoptic precipitation events. Precipitation is the source of major mass gain for glaciers, and therefore, needed to be constrained well, else it will result in bias with actual mass balance measurement. I analyzed automatic weather stations data from two glaciers to infer information about the spatial and temporal variability of accumulation and precipitation (Paper I). I used a simple routing model along with subglacial hydrological analysis to quantify discharge hydrograph at different outlet points in Kongsfjord (Paper III).

Analyses of Paper I show that geographic location, surrounding topography and wind pattern control the occurrence of precipitation and accumulation, which, I found, varies even between two nearby glacier sites KNG6 and HDF4.5 in Kongsfjord basin. Comparing accumulation and precipitation from these two sites with ERA-Interim reanalysis and Ny-Ålesund precipitation, I found that ERA-Interim reanalysis better captures the occurrence of the accumulation and precipitation at the glacier sites, however, ERA-Interim could not capture all the events, especially the synoptic events. Accumulation and precipitation variability could be even higher for glaciers on the north side of Kongsfjord. ERA-Interim reanalysis shows higher precipitation occurrence for this region. More observational data

is required to understand accumulation and precipitation variability which will eventually help in constraining precipitation field to certain extent when used in mass balance models.

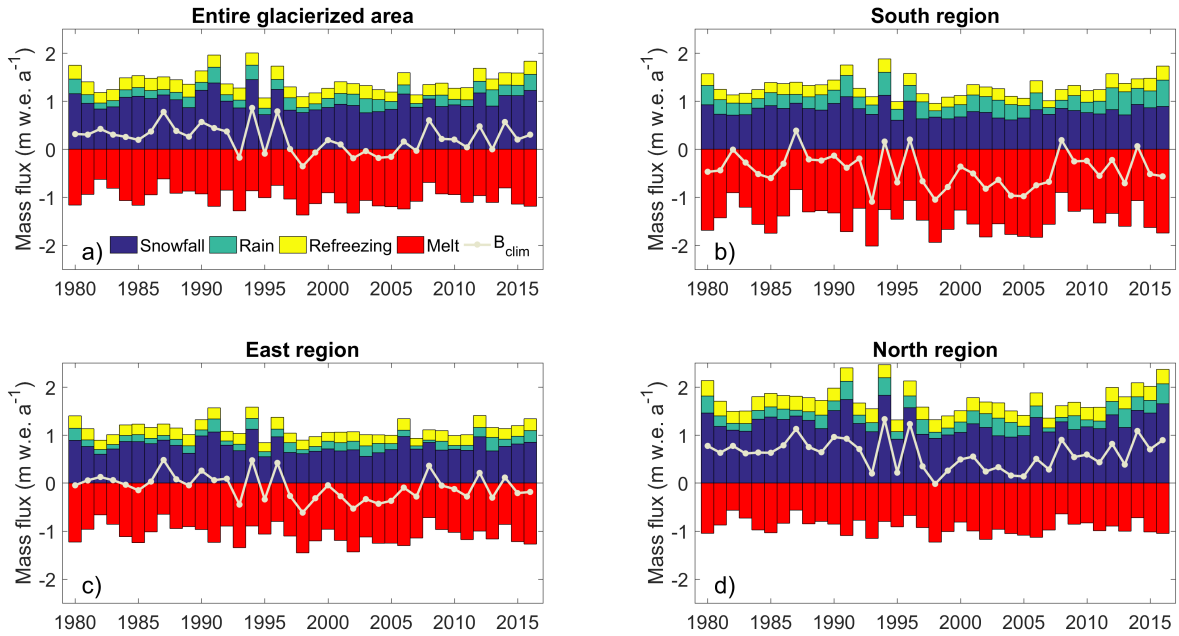

Figure 6.1: Simulated climatic mass balance and its components over the simulation period 1980-2016 for a) entire glacierized area, b) south region, c) east region and d) north region.

I find that average climatic mass balance of the entire glacierized area of Kongsfjord basin over 1980-2016 is +0.23 m w.e. a^{-1}, with a substantial variability in mass balance in three different subregions: south, east and north region of the fjord. Glaciers in the north region have more positive mass balance than those in the south and the east region, with on average 56% more snowfall and 59% less melt. In spite of the significant increase in summer temperature, no significant trend is observed in net climatic mass balance for the entire glacierized area, nor for the subregions; however, the summer balance has a significant negative trend for the entire glacierized area and for two subregions (east and north). Net mass balance is significantly correlated to annual snowfall in the south ($r = +0.63$, $p<0.01$), east ($r = +0.68$, $p<0.03$), and north ($r = +0.85$, $p<0.01$) region, with the best correlation observed in the latter region. The anti-correlation of net mass balance with mean summer temperature is weakest in the north region ($r = -0.24$, $p<0.15$), and stronger in the east ($r = -0.37$, $p<0.03$) and south ($r = -0.42$, $p<0.01$) regions; this indicates that the mass balance of glaciers of south and east is more sensitive to temperature than in the north.

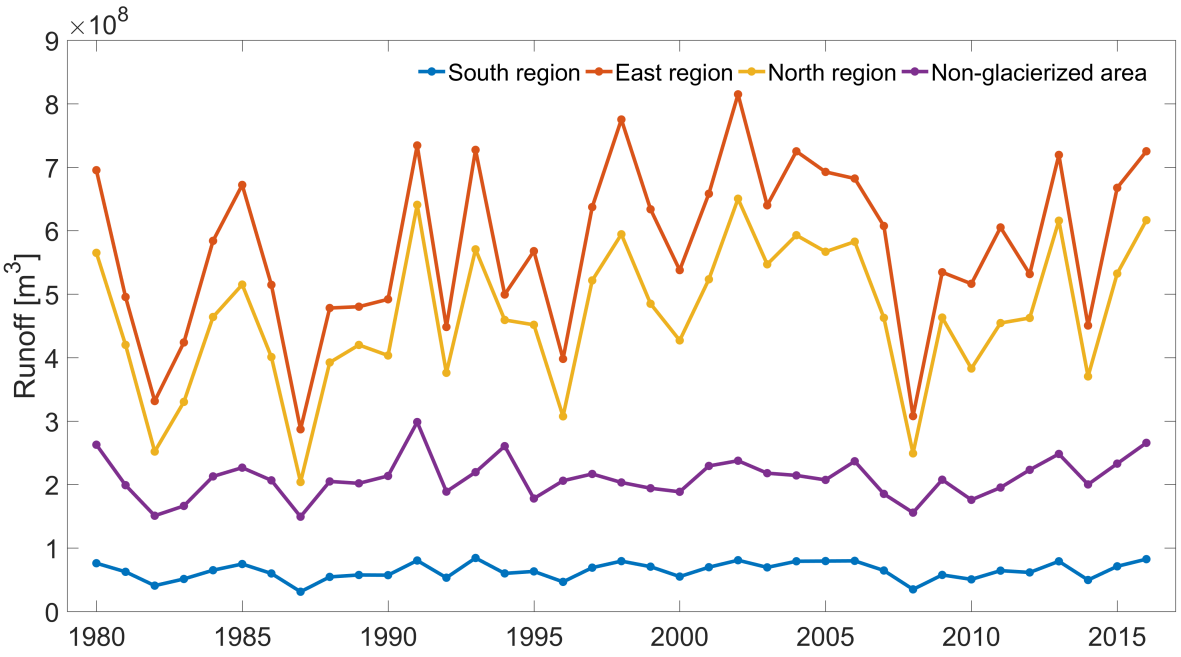

Figure 6.2: Total annual runoff from glacierized and non-glacierized areas over the simulation period 1980-2016. Total runoff from non-glacierized area contributes 16% of total freshwater flux to the fjord.

Runoff time-series show a significant increasing trend for the entire glacierized area (6.83×10^6 m^3 a^{-1}, with $p<0.09$), the east (3.47×10^6 m^3 a^{-1}, with $p<0.1$) and north (3.1×10^6 m^3 a^{-1}, with $p<0.08$) region over the simulation period 1980-2016. The non-glacierized area contributes 16% of the total runoff from the entire basin, and east region contributes maximum freshwater to the fjord over a year. In future warming scenario, runoff from all the glaciers will increase substantially. The increased runoff will potentially lead to more rapid vertical mixing of freshwater at the tidewater glacier fronts, which would impact the fjord circulation (Sundfjord et al., 2017) and promote more foraging of marine mammals (Lydersen et al., 2014).

Steady-state subglacial hydrological analysis of tidewater glaciers show the possibility of substantial water piracy underneath two big ice cap: Holtedahlfonna and Isachsenfonna of Kongsfjord basin. These two ice caps along with their outlet glaciers contribute maximum freshwater to the fjord. I found that substantial area of Isachsenfonna drains to Holtedahlfonna when subglacial water is not at or very close to ice overburden pressure ($k<0.97$), which is the most likely scenario during summer. The other tidewater glaciers are well constrained by topography and do not show any changes in subglacial hydrology when varying ice overburden pressure.

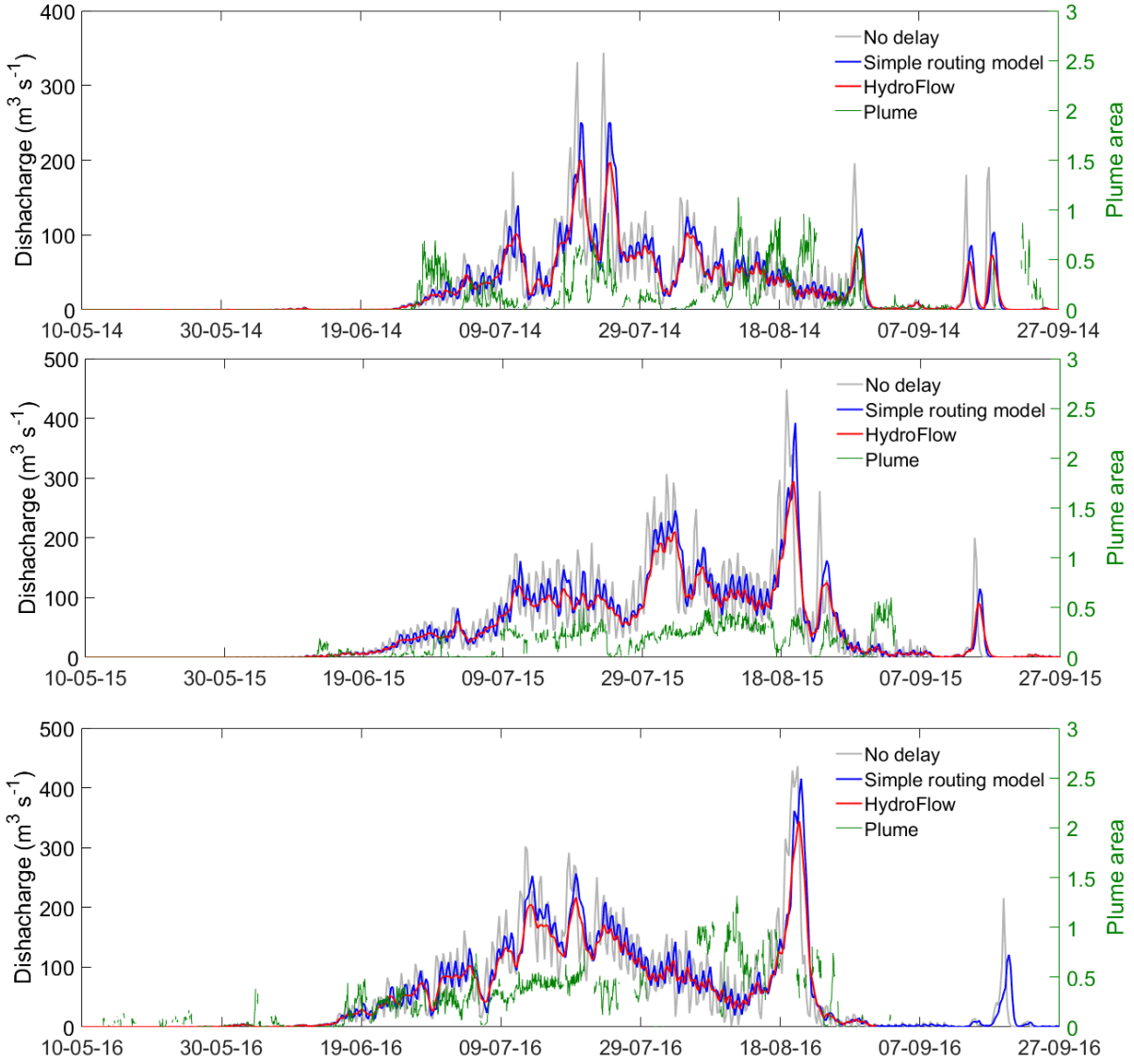

Figure 6.3: Discharge hydrograph at Kronebreen outlet for 2014, 2015, and 2016, derived by simple routing model, Hydroflow. Plume area extent is shown with green color.

I constrain the parameter of our routing model with the observational plume data. Plume observations are useful for investigating subglacial hydrology. While plume intensity and extent are dependent on several factors such as buoyancy, wind direction and speed, fjord depth and outlet shape, the most important controlling factor is the runoff. Therefore, plume data could be used as a proxy for discharge. Given the difficulty in measuring discharge at the tidewater glacier front, hydrological modeling is really the only way to estimate accurate discharge time-series. Several hydrological models of different degree of complexity have been used to simulate flow in and beneath glaciers, but while

more model complexity may yield apparently more accurate simulations, it comes at the cost of a large number of parameters that need to be specified (Fountain and Walder, 1998, Fountain et al., 2005, Hewitt, 2011, Werder et al., 2013). There has been a debate among hydrological modelers whether a higher degree of complexity improves model accuracy especially in predicting freshwater discharge at outlet points of glaciers. I use a simple routing model and a more physically based model (HydroFlow) to estimate freshwater flux on sub-daily scales.

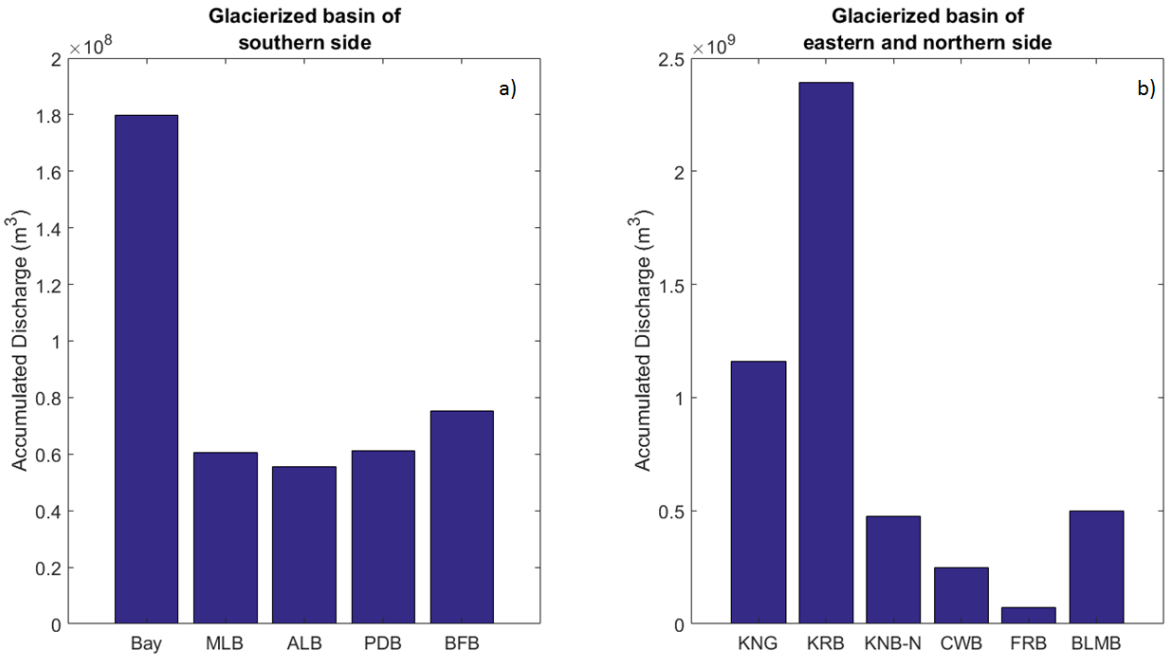

Figure 6.4: Total runoff from the glacierized basin (>10 km^2) in a) south, and b) east and north region of the fjord in 2015. Glaciers in the south are all land-terminating glaciers, whereas glaciers in east and north are mostly tidewater glaciers. Bay = Bayaelva, MLB = Midtre Lov 'enbreen, ALB = Austre Lov 'enbreen, PDB = Pedersenbreen, BFB = Botnfjellbreen, KNG = Kongsvegen, KRB = Kronebreen-Holtedahlfonna, KNB-N = Kongsbreen north, CWB = Conwaybreen, BLMB = Blomstrandbreen

Comparison of discharge hydrographs from the two models shows a good agreement for all the drainage basins. The time-delay for big discharge events on the tidewater glaciers can reach up to one day. Discharge from glaciers on the east and north sides of the fjord are about one order of magnitude higher than those in the south. On the south side of the fjord, the Bayelva river basin contributes the most freshwater to the fjord.

With the difficulties in measuring discharge at the tidewater glaciers front, uncertainties of any hydrological model used for a tidewater glacier system is difficult to estimate. With improved technology, by using the time-lapse camera, CTD measurement by seal

(Everett et al., 2018), along with plume modeling, information about freshwater discharge at tidewater glacier front can be inferred to a greater detail.

6.3 Limitations and future work

It is an ongoing challenge to develop an accurate automated precipitation measurement device, whether liquid (rain) or solid (snow). Sonic rangers can provide valuable information about snow accumulation and precipitation at a remote site, but there are limitations, which, if eliminated, would improve measurement significantly. Wind plays a complex role on snow deposition, and can affect the mass budget of glaciers and ice sheets. For example, wind distributed snow has a significant effect on the mass balance of East Antarctica ice sheet (Davis et al., 2005, Boening et al., 2012). The effect of wind on snow accumulation is important for glaciers in Kongsfjord basin and varies spatially, but it is difficult to quantify the variability over the entire basin with the data available. Although temperature and wind data allow one to distinguish wind-affected events from calm snowfall events, major uncertainty remains when precipitation occurs with high wind, which can lead to deposition as well as erosion. In this study, I found KNG6 is prone to high wind and therefore we were able to detect limited snowfall events, whereas HDF4.5 is less wind affected site which allows detection of a higher number of snowfall events. A recent study in Greenland summit by Castellani et al. (2015) shows that even with a sophisticated measurement device and continuous monitoring, wind effects could not be removed completely from precipitation measurements. In spite of the difficulties of automatic snow measurements, a distributed network of sonic rangers in a region will improve our understanding and help to better constrain precipitation with climate model data.

A major source of inaccuracy in glacier mass balance models is the precipitation forcing. Global climate model generated precipitation fields are generally too coarsely represented to capture all the spatial variability of synoptic precipitation events. Other uncertainties come from topographic representation, parameter estimation, initialization etc. Through calibration, model performance improves significantly, as seen in this study (paper II), but, the amount (spatial and temporal coverage) and quality of data often restrict the capability of model calibration. The model results show good agreement with the measured variables, especially for the glaciers on the south and east sides of Kongsfjord. Lack of observational data leads to limitation in validating the model for the glaciers on the north side of Kongsfjord, where significantly more positive mass balance is simulated,

compared to the other regions. More observational data needs to be acquired from this region, by installing AWSs and mass balance stakes. Instead of using a fixed DEM in the model, a dynamic DEM would better reflect changes in the actual topography, although this will improve model accuracy to only a slight extent. Through this study, I found the possibility of significant water piracy beneath two ice caps of Kongsfjord basin, which is supported by the relative plume sizes in front of the respective glaciers. Detailed understanding of subglacial behavior throughout the season requires detailed analysis and more physically based model. I used a simple routing model and a physically based model (HydroFlow) of a lesser degree of complexity to transport the water from respective grid cells to the outlet points. I considered observational plume data as a proxy to runoff and used that to calibrate the wave speed of simple routing model, however, wave speed varies over time. Furthermore, plume visibility and plume area extent are dependent on several factors, such as wind, outlet shape, fjord depth, etc. A plume model would be useful to infer important information about plume dynamics in this regard. Considering all this in a model framework will undoubtedly increase the model accuracy. A physically based hydrological model coupled with the plume model would lead to improved understanding, better prediction of meltwater routing, and discharge at the outlets of tidewater glaciers.

7 References

Bibliography

Aas, K. S., Berntsen, T. K., Boike, J., Etzelmüller, B., Kristjánsson, J. E., Maturilli, M., Schuler, T. V., Stordal, F., and Westermann, S. 2015. A Comparison between Simulated and Observed Surface Energy Balance at the Svalbard Archipelago. *Journal of Applied Meteorology and Climatology*, 54(5):1102–1119.

Arnold, N. S., Rees, W. G., Hodson, A. J., and Kohler, J. 2006. Topographic controls on the surface energy balance of a high Arctic valley glacier. *Journal of Geophysical Research*, 111(F2).

Arthern, R. J., Vaughan, D. G., Rankin, A. M., Mulvaney, R., and Thomas, E. R. 2010. In situ measurements of Antarctic snow compaction compared with predictions of models. *Journal of Geophysical Research-Earth Surface*, 115.

Banwell, A., Hewitt, I., Willis, I., and Arnold, N. 2016. Moulin density controls drainage development beneath the Greenland ice sheet. *Journal of Geophysical Research: Earth Surface*, 121(12):2248–2269.

Barstad, I. and Smith, R. B. 2005. Evaluation of an orographic precipitation model. *Journal of Hydrometeorology*, 6(1):85–99.

Bartholomaus, T. C., Larsen, C. F., West, M. E., O'Neel, S., Pettit, E. C., and Truffer, M. 2015. Tidal and seasonal variations in calving flux observed with passive seismology. *Journal of Geophysical Research-Earth Surface*, 120(11):2318–2337.

Bartholomew, I., Nienow, P., Sole, A., Mair, D., Cowton, T., and King, M. A. 2012. Short-term variability in Greenland Ice Sheet motion forced by time-varying meltwater drainage: Implications for the relationship between subglacial drainage system behavior and ice velocity. *Journal of Geophysical Research-Earth Surface*, 117.

Björk, G., Gustafsson, B. G., and Stigebrandt, A. 2001. Upper layer circulation of the Nordic seas as inferred from the spatial distribution of heat and freshwater content and potential energy. *Polar Research*, 20(2):161–168.

Błaszczyk, M., Jania, J. A., and Hagen, J. O. 2009. Tidewater glaciers of Svalbard: Recent changes and estimates of calving fluxes. *Polish Polar Research*, 30(2):85–142.

Boening, C., Lebsock, M., Landerer, F., and Stephens, G. 2012. Snowfall-driven mass change on the East Antarctic ice sheet. *Geophysical Research Letters*, 39.

Bolch, T., Kulkarni, A., Kääb, A., Huggel, C., Paul, F., Cogley, J. G., Frey, H., Kargel, J. S., Fujita, K., Scheel, M., Bajracharya, S., and Stoffel, M. 2012. The State and Fate of Himalayan Glaciers. *Science*, 336(6079):310–314.

Box, J. E., Bromwich, D. H., and Bai, L. S. 2004. Greenland ice sheet surface mass balance 1991-2000: Application of Polar MM5 mesoscale model and in situ data. *Journal of Geophysical Research-Atmospheres*, 109(D16).

Braaten, D. A. 2000. Direct measurements of episodic snow accumulation on the Antarctic polar plateau. *Journal of Geophysical Research: Atmospheres*, 105(D8):10119–10128.

Brandt, O., Kohler, J., and Lüthje, M. 2008. Spatial mapping of multi-year superimposed ice on the glacier Kongsvegen, Svalbard. *Journal of Glaciology*, 54(184):73–80.

Bruland, O. and Hagen, J. O. 2002. Glacial mass balance of Austre Brøggerbreen (Spitsbergen), 1971-1999, modelled with a precipitation-run-off model. *Polar Research*, 21(1):109–121.

Burton, D. J., Dowdeswell, J. A., Hogan, K. A., and Noormets, R. 2016. Marginal fluctuations of a Svalbard surge-type tidewater glacier, Blomstrandbreen, since the Little Ice Age: a record of three surges. *Arctic Antarctic and Alpine Research*, 48(2):411–426.

Carroll, D., Sutherland, D. A., Shroyer, E. L., Nash, J. D., Catania, G. A., and Stearns, L. A. 2015. Modeling Turbulent Subglacial Meltwater Plumes: Implications for Fjord-Scale Buoyancy-Driven Circulation, journal = Journal of Physical Oceanography. 45(8):2169–2185.

Castellani, B. B., Shupe, M. D., Hudak, D. R., and Sheppard, B. E. 2015. The annual cycle of snowfall at Summit, Greenland. *Journal of Geophysical Research: Atmospheres*, 120(13):6654–6668.

Chandler, D. M., Wadham, J. L., Lis, G. P., Cowton, T., Sole, A., Bartholomew, I., Telling, J., Nienow, P., Bagshaw, E. B., Mair, D., Vinen, S., and Hubbard, A. 2013.

Evolution of the subglacial drainage system beneath the Greenland Ice Sheet revealed by tracers. *Nature Geoscience*, 6(3):195–198.

Chu, V. W. 2013. Greenland ice sheet hydrology: A review. *Progress in Physical Geography*, 38(1):19–54.

Church, J. A., White, N. J., Konikow, L. F., Domingues, C. M., Cogley, J. G., Rignot, E., Gregory, J. M., van den Broeke, M. R., Monaghan, A. J., and Velicogna, I. 2011. Revisiting the Earth's sea-level and energy budgets from 1961 to 2008. *Geophysical Research Letters*, 38(18).

Cogley, J. G. and Adams, W. P. 1998. Mass balance of glaciers other than the ice sheets. *Journal of Glaciology*, 44(147):315–325.

Cogley, J. G., Hock, R., Rasmussen, L. A., Arendt, A. A., Bauder, A., Braithwaite, R. J., Jansson, P., Kaser, G., Möller, M., Nicholson, L., and Zemp, M. 2011. *Glossary of Glacier Mass Balance and Related Terms* , volume 86. IHP-VII Technical Documents in Hydrology, UNESCO-IHP,Paris.

Cohen, L. and Dean, S. 2013. Snow on the Ross Ice Shelf: comparison of reanalyses and observations from automatic weather stations. *The Cryosphere*, 7(5):1399–1410.

Cottier, F., Tverberg, V., Inall, M., Svendsen, H., Nilsen, F., and Griffiths, C. 2005. Water mass modification in an Arctic fjord through cross-shelf exchange: The seasonal hydrography of Kongsfjorden, Svalbard. *Journal of Geophysical Research-Oceans*, 110(C12).

Cowton, T., Nienow, P., Sole, A., Wadham, J., Lis, G., Bartholomew, I., Mair, D., and Chandler, D. 2013. Evolution of drainage system morphology at a land-terminating Greenlandic outlet glacier. *Journal of Geophysical Research-Earth Surface*, 118(1):29–41.

Cowton, T., Slater, D., Sole, A., Goldberg, D., and Nienow, P. 2015. Modeling the impact of glacial runoff on fjord circulation and submarine melt rate using a new subgrid-scale parameterization for glacial plumes. *Journal of Geophysical Research-Oceans*, 120(2):796–812.

Cox, L. H. and March, R. S. 2004. Comparison of geodetic and glaciological mass-balance techniques, Gulkana Glacier, Alaska, USA. *Journal of Glaciology*, 50(170):363–370.

Cuffey, K. and Paterson, W. 2010. *The Physics of Glaciers*. Elsevier, Amsterdam, 4th edition.

Davis, C. H., Li, Y. H., McConnell, J. R., Frey, M. M., and Hanna, E. 2005. Snowfall-driven growth in East Antarctic ice sheet mitigates recent sea-level rise. *Science*, 308(5730):1898–1901.

Dee, D. P., Uppala, S. M., Simmons, A. J., Berrisford, P., Poli, P., Kobayashi, S., Andrae, U., Balmaseda, M. A., Balsamo, G., Bauer, P., Bechtold, P., Beljaars, A. C. M., van de Berg, L., Bidlot, J., Bormann, N., Delsol, C., Dragani, R., Fuentes, M., Geer, A. J., Haimberger, L., Healy, S. B., Hersbach, H., Hólm, E. V., Isaksen, L., Kållberg, P., Köhler, M., Matricardi, M., McNally, A. P., Monge-Sanz, B. M., Morcrette, J. J., Park, B. K., Peubey, C., de Rosnay, P., Tavolato, C., Thepaut, J. N., and Vitart, F. 2011. The ERA-Interim reanalysis: configuration and performance of the data assimilation system. *Quarterly Journal of the Royal Meteorological Society*, 137(656):553–597.

Depoorter, M. A., Bamber, J. L., Griggs, J. A., Lenaerts, J. T. M., Ligtenberg, S. R. M., van den Broeke, M. R., and Moholdt, G. 2013. Calving fluxes and basal melt rates of Antarctic ice shelves. *Nature*, 502(7469):89–+.

Dery, S. J. and Yau, M. K. 2001. Simulation of blowing snow in the Canadian Arctic using a double-moment model. *Boundary-Layer Meteorology*, 99(2):297–316.

Dowdeswell, J. A., Hamilton, G. S., and Hagen, J. O.

Dunse, T., Schellenberger, T., Hagen, J. O., Kääb, A., Schuler, T. V., and Reijmer, C. H. 2015. Glacier-surge mechanisms promoted by a hydro-thermodynamic feedback to summer melt. *Cryosphere*, 9(1):197–215.

Essery, R., Li, L., and Pomeroy, J. 1999. A distributed model of blowing snow over complex terrain. *Hydrological Processes*, 13(14-15):2423–2438.

Everett, A., Kohler, J., Sundfjord, A., Kovacs, K. M., Torsvik, T., Pramanik, A., Boehme, L., and Lydersen, C. 2018. Subglacial discharge plume behaviour revealed by CTD-instrumented ringed seals. *Scientific Reports*, 8(1):13467.

Everett, A., Murray, T., Selmes, N., Rutt, I. C., Luckman, A., James, T. D., Clason, C., O'Leary, M., Karunarathna, H., Moloney, V., and Reeve, D. E. 2016. Annual down-glacier drainage of lakes and water-filled crevasses at Helheim Glacier, southeast Greenland. *Journal of Geophysical Research-Earth Surface*, 121(10).

Fettweis, X., Box, J. E., Agosta, C., Amory, C., Kittel, C., Lang, C., van As, D., Machguth, H., and Gallée, H. 2017. Reconstructions of the 1900-2015 Greenland ice sheet surface mass balance using the regional climate MAR model. *Cryosphere*, 11(2):1015–1033.

Flowers, G. E., Roux, N., Pimentel, S., and Schoof, C. G. 2011. Present dynamics and future prognosis of a slowly surging glacier. *Cryosphere*, 5(1):299–313.

Foken, T. 2006. 50 years of the monin-obukhov similarity theory. *Boundary-Layer Meteorology*, 119(3):431–447.

Førland, E. J., Benestad, R., Hanssen-Bauer, I., Haugen, J. E., and Skaugen, T. E. 2011. Temperature and Precipitation Development at Svalbard 1900-2100. *Advances in Meteorology*.

Førland, E. J. and Hanssen-Bauer, I. 2000. Increased precipitation in the Norwegian Arctic: True or false? *Climatic Change*, 46(4):485–509.

Førland, E. J. and Hanssen-Bauer, I. 2003. Past and future climate variations in the Norwegian Arctic: overview and novel analyses. *Polar Research*, 22(2):113–124.

Fountain, A. G., Jacobel, R. W., Schlichting, R., and Jansson, P. 2005. Fractures as the main pathways of water flow in temperate glaciers. *Nature*, 433(7026):618–621.

Fountain, A. G., Nylen, T. H., Monaghan, A., Basagic, H. J., and Bromwich, D. 2010. Snow in the mcmurdo dry valleys, antarctica. *International Journal of Climatology*, 30(5):633–642.

Fountain, A. G. and Vecchia, A. 1999. How many stakes are required to measure the mass balance of a glacier? *Geografiska Annaler Series a-Physical Geography*, 81A(4):563–573.

Fountain, A. G. and Walder, J. S. 1998. Water flow through temperate glaciers. *Reviews of Geophysics*, 36(3):299–328.

Fowler, A. C., Murray, T., and Ng, F. S. L. 2001. Thermally controlled glacier surging. *Journal of Glaciology*, 47(159):527–538.

Gleick, P. H. and White, G. F. 1993. *Water in crisis: a guide to the world's fresh water resources*. Oxford University, New York.

Greuell, W. and Konzelmann, T. 1994. Numerical modelling of the energy-balance and the englacial temperature of the Greenland ice-sheet- Calculations for the ETH-camp location (West Greenland, 1155 masl). *Global and Planetary Change*, 9(1-2):91–114.

Hagen, J. O., Kohler, J., Melvold, K., and Winther, J. G. 2003a. Glaciers in Svalbard: mass balance, runoff and freshwater flux. *Polar Research*, 22(2):145–159.

Hagen, J. O., Liestøl, O., Roland, E., and Jørgensen, T. 1993. *Glacier atlas of Svalbard and Jan Mayen*. Norsk Polarinstitutt, Oslo.

Hagen, J. O., Melvold, K., Pinglot, F., and Dowdeswell, J. A. 2003b. On the net mass balance of the glaciers and ice caps in Svalbard, Norwegian Arctic. *Arctic Antarctic and Alpine Research*, 35(2):264–270.

Hanssen-Bauer, I. and Førland, E. J. 1998. Long-term trends in precipitation and temperature in the Norwegian Arctic: can they be explained by changes in atmospheric circulation patterns? *Climate Research*, 10(2):143–153.

Hewitt, I. J. 2011. Modelling distributed and channelized subglacial drainage: the spacing of channels. *Journal of Glaciology*, 57(202):302–314.

Hewitt, I. J., Schoof, C., and Werder, M. A. 2012. Flotation and free surface flow in a model for subglacial drainage. Part 2. Channel flow. *Journal of Fluid Mechanics*, 702:157–187.

Hisdal, V. 1998. *Svalbard: nature and history*. Oslo.

Hock, R. 2003. Temperature index melt modelling in mountain areas. *Journal of Hydrology*, 282(1-4):104–115.

Hock, R. and Jensen, H. 1999. Application of kriging interpolation for glacier mass balance computations. *Geografiska Annaler Series a-Physical Geography*, 81A(4):611–619.

Houghton, H. G. 1954. ON THE ANNUAL HEAT BALANCE OF THE NORTHERN HEMISPHERE. *Journal of Meteorology*, 11(1):1–9.

How, P., Benn, D. I., Hulton, N. R. J., Hubbard, B., Luckman, A., Sevestre, H., van Pelt, W. J. J., Lindbäck, K., Kohler, J., and Boot, W. 2017. Rapidly changing subglacial hydrological pathways at a tidewater glacier revealed through simultaneous observations of water pressure, supraglacial lakes,meltwater plumes and surface velocities. *Cryosphere*, 11(6):2691–2710.

Huss, M. and Farinotti, D. 2012. Distributed ice thickness and volume of all glaciers around the globe. *Journal of Geophysical Research-Earth Surface*, 117.

Immerzeel, W. W., Pellicciotti, F., and Bierkens, M. F. P. 2013. Rising river flows throughout the twenty-first century in two Himalayan glacierized watersheds. *Nature Geoscience*, 6(9):742–745.

IPCC 2007. Climate change 2007: working group III contribution to the Fourth Assessment Report of the IPCC. Report.

Isaksson, E., Pohjola, V., Jauhiainen, T., Moore, J., Pinglot, J. M., Vaikmäe, R., van de Wal, R. S. W., Hagen, J. O., Ivask, J., Karlöf, L., Martma, T., Meijer, H. A. J., Mulvaney, R., Thomassen, M., and van den Broeke, M. 2001. A new ice-core record from Lomonosovfonna, Svalbard: viewing the 1920-97 data in relation to present climate and environmental conditions. *Journal of Glaciology*, 47(157):335–345.

James, T. D., Murray, T., Barrand, N. E., Sykes, H. J., Fox, A. J., and King, M. A. 2012. Observations of enhanced thinning in the upper reaches of Svalbard glaciers. *Cryosphere*, 6(6):1369–1381.

Jansson, P. 1999. Effect of uncertainties in measured variables on the calculated mass balance of Storglaciären. *Geografiska Annaler Series a-Physical Geography*, 81A(4):633–642.

Jansson, P. and Pettersson, R. 2007. Spatial and temporal characteristics of a long mass balance record, Storglaciären, Sweden. *Arctic Antarctic and Alpine Research*, 39(3):432–437.

Jiskoot, H., Boyle, P., and Murray, T. 1998. The incidence of glacier surging in Svalbard: Evidence from multivariate statistics. *Computers & Geosciences*, 24(4):387–399.

Jones, J. A. A. 1999. Climate change and sustainable water resources: placing the threat of global warming in perspective. *Hydrological Sciences Journal-Journal Des Sciences Hydrologiques*, 44(4):541–557.

Kääb, A., Lefauconnier, B., and Melvold, K. 2005. *Flow field of Kronebreen, Svalbard, using repeated Landsat 7 and ASTER data*, volume 42 of *Annals of Glaciology*, pages 7–13.

Käsmacher, O. and Schneider, C. 2011. An objective circulation pattern classification for the region of Svalbard. *Geografiska Annaler Series a-Physical Geography*, 93A(4):259–271.

Knuth, S. L., Tripoli, G. J., Thom, J. E., and Weidner, G. A. 2010. The Influence of Blowing Snow and Precipitation on Snow Depth Change across the Ross Ice Shelf and Ross Sea Regions of Antarctica. *Journal of Applied Meteorology and Climatology*, 49(6):1306–1321.

Kohler, J., James, T. D., Murray, T., Nuth, C., Brandt, O., Barrand, N. E., Aas, H. F., and Luckman, A. 2007. Acceleration in thinning rate on western Svalbard glaciers. *Geophysical Research Letters*, 34(18).

Kondratyev, K. Y. 1972. *Radiation processes in the atmosphere*. World meteorological organization. Geneva.

König, M., Nuth, C., Kohler, J., Moholdt, G., and Pettersen, R. 2014. *Global Land Ice Measurements from Space*. A digital glacier database for svalbard. Springer, Berlin, Heidelberg.

König, M., Wadham, J., Winther, J. G., Kohler, J., and Nuttall, A. M. 2002. *Detection of superimposed ice on the glaciers Kongsvegen and midre Lovenbreen, Svalbard, using SAR satellite imagery*, volume 34 of *Annals of Glaciology*, pages 335–342.

Krimmel, R. M. 1999. Analysis of difference between direct and geodetic mass balance measurements at South Cascade Glacier, Washington. *Geografiska Annaler Series a-Physical Geography*, 81A(4):653–658.

Lang, C., Fettweis, X., and Erpicum, M. 2014. Stable climate and surface mass balance in Svalbard over 1979-2013 despite the Arctic warming. *The Cryosphere Discussions*, 8(4):4497–4543.

Lang, C., Fettweis, X., and Erpicum, M. 2015. Future climate and surface mass balance of Svalbard glaciers in an RCP8.5 climate scenario: a study with the regional climate model MAR forced by MIROC5. *Cryosphere*, 9(3):945–956.

Leclercq, P. W. and Oerlemans, J. 2012. Global and hemispheric temperature reconstruction from glacier length fluctuations. *Climate Dynamics*, 38(5-6):1065–1079.

Leclercq, P. W., Oerlemans, J., and Cogley, J. G. 2011. Estimating the Glacier Contribution to Sea-Level Rise for the Period 1800-2005. *Surveys in Geophysics*, 32(4-5):519–535.

Lefauconnier, B. and Hagen, J. O. 1992. *Surging and calving glaciers in eastern Svalbard*, volume 116. Meddelelser / Norsk polarinstitutt, Oslo.

Lefauconnier, B., Hagen, J. O., Pinglot, J. F., and Pourchet, M. 1994. Mass balance estimates on the glacier complex Kongsvegen and Sveabreen, Spitsbergen, Svalbard, using radioactive layers . *Journal of Glaciology*, 40(135):368–376.

Lenaerts, J. T. M., Smeets, C., Nishimura, K., Eijkelboom, M., Boot, W., van den Broeke, M. R., and van de Berg, W. J. 2014. Drifting snow measurements on the Greenland Ice Sheet and their application for model evaluation. *Cryosphere*, 8(2):801–814.

Li, L. and Pomeroy, J. W. 1997. Probability of occurrence of blowing snow. *Journal of Geophysical Research: Atmospheres*, 102(D18):21955–21964.

Ligtenberg, S. R. M., Helsen, M. M., and van den Broeke, M. R. 2011. An improved semi-empirical model for the densification of Antarctic firn. *The Cryosphere*, 5(4):809–819.

Lindbäck, K., Kohler, J., Pettersen, R., Nuth, C., Langley, K., Messerli, A., Vallot, D., Matsuoka, K., and Brandt, O. 2018. Subglacial topography, ice thickness, and bathymetry of kongsfjorden, northwestern svalbard. *Earth Syst. Sci. Data Discuss.*

Lindbäck, K., Pettersson, R., Hubbard, A. L., Doyle, S. H., van As, D., Mikkelsen, A. B., and Fitzpatrick, A. A. 2015. Subglacial water drainage, storage, and piracy beneath the Greenland ice sheet. *Geophysical Research Letters*, 42(18):7606–7614.

Liston, G. E. and Mernild, S. H. 2012. Greenland Freshwater Runoff. Part I: A Runoff Routing Model for Glaciated and Nonglaciated Landscapes (HydroFlow). *Journal of Climate*, 25(17):5997–6014.

Loeng, H. 1991. Features of the physical oceanographic conditions of the Barents Sea. *Polar Research*, 10(1):5–18.

Lüthi, M. P., Bauder, A., and Funk, M. 2010. Volume change reconstruction of Swiss glaciers from length change data. *Journal of Geophysical Research-Earth Surface*, 115.

Lydersen, C., Assmy, P., Falk-Petersen, S., Kohler, J., Kovacs, K. M., Reigstad, M., Steen, H., Strøm, H., Sundfjord, A., Varpe, Ø., Walczowski, W., Weslawski, J. M., and

Zajaczkowski, M. 2014. The importance of tidewater glaciers for marine mammals and seabirds in Svalbard, Norway. *Journal of Marine Systems*, 129:452–471.

Machguth, H., Purves, R. S., Oerlemans, J., Hoelzle, M., and Paul, F. 2008. Exploring uncertainty in glacier mass balance modelling with Monte Carlo simulation. *Cryosphere*, 2(2):191–204.

Mankoff, K. D., Straneo, F., Cenedese, C., Das, S. B., Richards, C. G., and Singh, H. 2016. Structure and dynamics of a subglacial discharge plume in a Greenlandic fjord. *Journal of Geophysical Research-Oceans*, 121(12):8670–8688.

Mansell, D., Luckman, A., and Murray, T. 2012. Dynamics of tidewater surge-type glaciers in northwest svalbard. *Journal of Glaciology*, 58(207):110–118.

Martín-Español, A., Navarro, F. J., Otero, J., Lapazaran, J. J., and Błaszczyk, M. 2015. Estimate of the total volume of Svalbard glaciers, and their potential contribution to sea-level rise, using new regionally based scaling relationships. *Journal of Glaciology*, 61(225):29–41.

McDonald, J. E. 1960. DIRECT ABSORPTION OF SOLAR RADIATION BY ATMOSPHERIC WATER VAPOR. *Journal of Meteorology*, 17(3):319–328.

McNabb, R. W., Womble, J. N., Prakash, A., Gens, R., and Haselwimmer, C. E. 2016. Quantification and Analysis of Icebergs in a Tidewater Glacier Fjord Using an Object-Based Approach. *Plos One*, 11(11).

Medrzycka, D., Benn, D. I., Box, J. E., Copland, L., and Balog, J. 2016. Calving behavior at Rink Isbræ,West Greenland, from time-lapse photos. *Arctic Antarctic and Alpine Research*, 48(2):263–277.

Melvold, K. and Hagen, J. O. 1998. Evolution of a surge-type glacier in its quiescent phase: Kongsvegen, Spitsbergen, 1964-95. *Journal of Glaciology*, 44(147):394–404.

Mernild, S. H., Liston, G. E., Hiemstra, C., and Wilson, R. 2017. The Andes Cordillera. Part III: glacier surface mass balance and contribution to sea level rise (1979-2014). *International Journal of Climatology*, 37(7):3154–3174.

Moholdt, G., Hagen, J. O., Eiken, T., and Schuler, T. V. 2010a. Geometric changes and mass balance of the Austfonna ice cap, Svalbard. *Cryosphere*, 4(1):21–34.

Moholdt, G., Nuth, C., Hagen, J. O., and Kohler, J. 2010b. Recent elevation changes of Svalbard glaciers derived from ICESat laser altimetry. *Remote Sensing of Environment*, 114(11):2756–2767.

Murray, T., Strozzi, T., Luckman, A., Jiskoot, H., and Christakos, P. 2003. Is there a single surge mechanism? Contrasts in dynamics between glacier surges in Svalbard and other regions. *Journal of Geophysical Research-Solid Earth*, 108(B5).

Murray, T., Stuart, G. W., Miller, P. J., Woodward, J., Smith, A. M., Porter, P. R., and Jiskoot, H. 2000. Glacier surge propagation by thermal evolution at the bed. *Journal of Geophysical Research-Solid Earth*, 105(B6):13491–13507.

Nakićenović, N. 2000. Special report on emissions scenarios a special report of Working Group III of the Intergovernmental Panel on Climate Change. Report, IPCC.

Nash, J. D. and Moum, J. N. 2005. River plumes as a source of large-amplitude internal waves in the coastal ocean. *Nature*, 437(7057):400–403.

Nordli, Ø., Przybylak, R., Ogilvie, A. E. J., and Isaksen, K. 2014. Long-term temperature trends and variability on Spitsbergen: the extended Svalbard Airport temperature series, 1898-2012. *Polar Research*, 33.

Nowak, A. and Hodson, A. 2013. Hydrological response of a High-Arctic catchment to changing climate over the past 35 years: a case study of Bayelva watershed, Svalbard. *Polar Research*, 32(1):19691.

Nowak, A. and Hodson, A. 2014. Changes in meltwater chemistry over a 20-year period following a thermal regime switch from polythermal to cold-based glaciation at Austre BrÃÿggerbreen, Svalbard. *Polar Research*, 33(1):22779.

Nowak, A. and Hodson, A. 2015. On the biogeochemical response of a glacierized High Arctic watershed to climate change: revealing patterns, processes and heterogeneity among micro-catchments. *Hydrological Processes*, 29(6):1588–1603.

Nuth, C. 2011. *Quantification and interpretation of glacier elevation changes*. Thesis.

Nuth, C., Kohler, J., König, M., von Deschwanden, A., Hagen, J. O., Kääb, A., Moholdt, G., and Pettersson, R. 2013. Decadal changes from a multi-temporal glacier inventory of Svalbard. *Cryosphere*, 7(5):1603–1621.

Nuth, C., Moholdt, G., Kohler, J., Hagen, J. O., and Kääb, A. 2010. Svalbard glacier elevation changes and contribution to sea level rise. *Journal of Geophysical Research-Earth Surface*, 115.

Nuth, C., Schuler, T. V., Kohler, J., Altena, B., and Hagen, J. O. 2012. Estimating the long-term calving flux of Kronebreen, Svalbard, from geodetic elevation changes and mass-balance modelling. *Journal of Glaciology*, 58(207):119–133.

Nye, J. F. 1960. The response of glaciers and ice-sheets to seasonal and climatic changes. *Proceedings of the Royal Society of London Series a-Mathematical and Physical Sciences*, 256(1287):559–584.

Oerlemans, J. 2005. Extracting a climate signal from 169 glacier records. *Science*, 308(5722):675–677.

Oerlemans, J. and Grisogono, B. 2002. Glacier winds and parameterisation of the related surface heat fluxes. *Tellus Series a-Dynamic Meteorology and Oceanography*, 54(5):440–452.

Østby, T. I., Schuler, T. V., Hagen, J. O., Hock, R., Kohler, J., and Reijmer, C. H. 2017. Diagnosing the decline in climatic mass balance of glaciers in Svalbard over 1957-2014. *The Cryosphere*, 11(1):191–215.

Østrem, G. and Brugman, M. M. 1991. *Glacier mass-balance measurements: A manual for field and office work*. National Hydrology Research Institute, Inland Waters Directorate, Conservation and Protection, Environment Canada. Saskatoon, Canada.

Parkinson, C. L. 2006. Earth's cryosphere: Current state and recent changes. *Annual Review of Environment and Resources*, 31:33–60.

Paterson, W. 1993. *The physics of glaciers*. Pergamon Press, Oxford.

Pelliccioni, A., Monti, P., Gariazzo, C., and Leuzzi, G. 2012. Some characteristics of the urban boundary layer above rome, italy, and applicability of monin-obukhov similarity. *Environmental Fluid Mechanics*, 12(5):405–428.

Pinglot, J. F., Pourchet, M., Lefauconnier, B., Hagen, J. O., Isaksson, E., Vaikmäe, R., and Kamiyama, K. 1999. Accumulation in Svalbard glaciers deduced from ice cores with nuclear tests and Chernobyl reference layers, journal = Polar Research. 18(2):315–321.

Pohjola, V. A., Moore, J. C., Isaksson, E., Jauhiainen, T., van de Wal, R. S. W., Martma, T., Meijer, H. A. J., and Vaikmäe, R. 2002. Effect of periodic melting on geochemical and isotopic signals in an ice core from Lomonosovfonna, Svalbard, journal = Journal of Geophysical Research-Atmospheres. 107(D4).

Pramanik, A., Van Pelt, W., Kohler, J., and T.V., S. 2018. Simulating climatic mass balance, seasonal snow development and associated freshwater runoff in the Kongsfjord basin,Svalbard (1980-2016). *Journal of Glaciology*, 64(248):943–956.

Prandtl, L. 1942. *Führer durch die Strömungslehre*. Braunschweig, Vieweg.

Radić, V. and Hock, R. 2010. Regional and global volumes of glaciers derived from statistical upscaling of glacier inventory data. *Journal of Geophysical Research-Earth Surface*, 115.

Reijmer, C. H. and Hock, R. 2008. Internal accumulation on Storglaciären, Sweden, in a multi-layer snow model coupled to a distributed energy- and mass-balance model. *Journal of Glaciology*, 54(184):61–72.

Rignot, E. 2002. *Mass balance of East Antarctic glaciers and ice shelves from satellite data*, volume 34 of *Annals of Glaciology*, pages 217–227.

Rodrigues, J. 2008. The rapid decline of the sea ice in the Russian Arctic. *Cold Regions Science and Technology*, 54(2):124–142.

Sand, K., Winther, J. G., Marechal, D., Bruland, O., and Melvold, K. 2003. Regional variations of snow accumulation on Spitsbergen, Svalbard, 1997-99. *Nordic Hydrology*, 34(1-2):17–32.

Schellenberger, T., Dunse, T., Kääb, A., Kohler, J., and Reijmer, C. H. 2015. Surface speed and frontal ablation of Kronebreen and Kongsbreen, NW Svalbard, from SAR offset tracking. *The Cryosphere*, 9(6):2339–2355.

Schild, K. M., Hawley, R. L., and Morriss, B. F. 2016. Subglacial hydrology at Rink Isbræ, West Greenland inferred from sediment plume appearance. *Annals of Glaciology*, 57(72):118–127.

Schneider, T. and Jansson, P. 2004. Internal accumulation in firn and its significance for the mass balance of Storglaciären, Sweden. *Journal of Glaciology*, 50(168):25–34.

Schoof, C., Hewitt, I. J., and Werder, M. A. 2012. Flotation and free surface flow in a model for subglacial drainage. Part 1. Distributed drainage. *Journal of Fluid Mechanics*, 702:126–156.

Schoof, C., Rada, C. A., Wilson, N. J., Flowers, G. E., and Haseloff, M. 2014. Oscillatory subglacial drainage in the absence of surface melt. *The Cryosphere*, 8(3):959–976.

Schuler, T. V., Crochet, P., Hock, R., Jackson, M., Barstad, I., and Jóhannesson, T. 2008. Distribution of snow accumulation on the Svartisen ice cap, Norway, assessed by a model of orographic precipitation. *Hydrological Processes*, 22(19):3998–4008.

Schutz, B. E., Zwally, H. J., Shuman, C. A., Hancock, D., and DiMarzio, J. P. 2005. Overview of the ICESat Mission. *Geophysical Research Letters*, 32(21).

Schwanghart, W. and Scherler, D. 2014. Short Communication: TopoToolbox 2-MATLAB-based software for topographic analysis and modeling in Earth surface sciences. *Earth Surface Dynamics*, 2(1):1–7.

Serreze, M. C., Barrett, A. P., Stroeve, J. C., Kindig, D. N., and Holland, M. M. 2009. The emergence of surface-based Arctic amplification. *Cryosphere*, 3(1):11–19.

Serreze, M. C. and Francis, J. A. 2006. The arctic amplification debate. *Climatic Change*, 76(3-4):241–264.

Sevestre, H., Benn, D. I., Hulton, N. R. J., and Bælum, K. 2015. Thermal structure of Svalbard glaciers and implications for thermal switch models of glacier surging. *Journal of Geophysical Research-Earth Surface*, 120(10):2220–2236.

Sharma, K. P., Vorosmarty, C. J., and Moore, B. 2000. Sensitivity of the Himalayan hydrology to land-use and climatic changes. *Climatic Change*, 47(1-2):117–139.

Shchepetkin, A. F. and McWilliams, J. C. 2005. The regional oceanic modeling system (ROMS): a split-explicit, free-surface, topography-following-coordinate oceanic model. *Ocean Modelling*, 9(4):347–404.

Shekhar, M., Bhardwaj, A., Singh, S., Ranhotra, P. S., Bhattacharyya, A., Pal, A. K., Roy, I., Martín-Torres, F. J., and Zorzano, M. P. 2017. Himalayan glaciers experienced significant mass loss during later phases of little ice age. *Scientific Reports*, 7.

Shreve, R. L. 1972. Movement of Water in Glaciers. *Journal of Glaciology*, 11(62):205–214.

Sicart, J. E., Hock, R., and Six, D. 2008. Glacier melt, air temperature, and energy balance in different climates: The Bolivian Tropics, the French Alps, and northern Sweden. *Journal of Geophysical Research-Atmospheres*, 113.

Sjögren, B., Brandt, O., Nuth, C., Isaksson, E., Pohjola, V., Kohler, J., and Van De Wal, R. S. W. 2007. Instruments and methods - Determination of firn density in ice cores using image analysis. *Journal of Glaciology*, 53(182):413–419.

Slater, D., Nienow, P., Sole, A., Cowton, T. O. M., Mottram, R., Langen, P., and Mair, D. 2017. Spatially distributed runoff at the grounding line of a large Greenlandic tidewater glacier inferred from plume modelling, journal = Journal of Glaciology. 63(238):309–323.

Sturm, M., Holmgren, J., König, M., and Morris, K. 1997. The thermal conductivity of seasonal snow. *Journal of Glaciology*, 43(143):26–41.

Sund, M. and Eiken, T. 2010. Recent surges on blomstrandbreen, comfortlessbreen and nathorstbreen, svalbard. *Journal of Glaciology*, 56(195):182–184.

Sund, M., Eiken, T., Hagen, J. O., and Kääb, A. 2009. Svalbard surge dynamics derived from geometric changes. *Annals of Glaciology*, 50(52):50–60.

Sundfjord, A., Albretsen, J., Kasajima, Y., Skogseth, R., Kohler, J., Nuth, C., Skarðhamar, J., Cottier, F., Nilsen, F., Asplin, L., Gerland, S., and Torsvik, T. 2017. Effects of glacier runoff and wind on surface layer dynamics and Atlantic Water exchange in Kongsfjorden, Svalbard; a model study. *Estuarine Coastal and Shelf Science*, 187:260–272.

Thibert, E., Blanc, R., Vincent, C., and Eckert, N. 2008. Glaciological and volumetric mass-balance measurements: error analysis over 51 years for Glacier de Sarennes, French Alps. *Journal of Glaciology*, 54(186):522–532.

Urbanski, J. A., Stempniewicz, L., Węsławski, J. M., Dragañska-Deja, K., Wochna, A., Goc, M., and Iliszko, L. 2017. Subglacial discharges create fluctuating foraging hotspots for sea birds in tidewater glacier bays. *Scientific Reports*, 7.

van As, D., Mikkelsen, A. B., Nielsen, M. H., Box, J. E., Liljedahl, L. C., Lindbäck, K., Pitcher, L., and Hasholt, B. 2017. Hypsometric amplification and routing moderation of Greenland ice sheet meltwater release. *Cryosphere*, 11(3):1371–1386.

van de Berg, W. J., van den Broeke, M. R., Reijmer, C. H., and van Meijgaard, E. 2006. Reassessment of the Antarctic surface mass balance using calibrated output of a regional atmospheric climate model. *Journal of Geophysical Research-Atmospheres*, 111(D11).

Van den Broeke, M. R., Duynkerke, P. G., and Henneken, E. A. C. 1994. Heat, momentum and moisture budgets of the katabatic layer over the melting zone of the west Greenland ice sheet in summer. *Boundary-Layer Meteorology*, 71(4):393–413.

Van Pelt, W. and Kohler, J. 2015. Modelling the long-term mass balance and firn evolution of glaciers around Kongsfjorden, Svalbard. *Journal of Glaciology*, 61(228):731–744.

Van Pelt, W. J. J., Oerlemans, J., Reijmer, C. H., Pettersson, R., Pohjola, V. A., Isaksson, E., and Divine, D. 2013. An iterative inverse method to estimate basal topography and initialize ice flow models. *Cryosphere*, 7(3):987–1006.

Van Pelt, W. J. J., Oerlemans, J., Reijmer, C. H., Pohjola, V. A., Pettersson, R., and van Angelen, J. H. 2012. Simulating melt, runoff and refreezing on Nordenskiöldbreen, Svalbard, using a coupled snow and energy balance model. *Cryosphere*, 6(3):641–659.

Van Tricht, K., Lhermitte, S., Lenaerts, J. T. M., Gorodetskaya, I. V., L'Ecuyer, T. S., Noel, B., van den Broeke, M. R., Turner, D. D., and van Lipzig, N. P. M. 2016. Clouds enhance Greenland ice sheet meltwater runoff. *Nature Communications*, 7.

Walczowski, W. and Piechura, J. 2011. Influence of the West Spitsbergen Current on the local climate. *International Journal of Climatology*, 31(7):1088–1093.

Walder, J. S. and Fowler, A. 1994. Channelized subglacial drainage over a deformable bed. *Journal of Glaciology*, 40(134):3–15.

Werder, M. A., Hewitt, I. J., Schoof, C. G., and Flowers, G. E. 2013. Modeling channelized and distributed subglacial drainage in two dimensions. *Journal of Geophysical Research-Earth Surface*, 118(4):2140–2158.

Westermann, S., Boike, J., Langer, M., Schuler, T. V., and Etzelmüller, B. 2011. Modeling the impact of wintertime rain events on the thermal regime of permafrost. *Cryosphere*, 5(4):945–959.

WGMS 2017. *Global Glacier Change Bulletin No. 2 (2014-2015)*, page 244. WGMS, Zurich, Switzerland.

Winther, J. G., Bruland, O., Sand, K., Gerland, S., Marechal, D., Ivanov, B., Gøowacki, P., and König, M. 2003. Snow research in Svalbard - an overview. *Polar Research*, 22(2):125–144.

Yen, Y.-C. 1981. Review of thermal properties of snow, ice and sea ice. Report, Cold Regions Research and Engineering Laboratory.

Zemp, M., Jansson, P., Holmlund, P., Gärtner-Roer, I., Koblet, T., Thee, P., and Haeberli, W. 2010. Reanalysis of multi-temporal aerial images of Storglaciären, Sweden (1959-99) - Part 2: Comparison of glaciological and volumetric mass balances. *Cryosphere*, 4(3):345–357.

Zuo, Z. and Oerlemans, J. 1996. Modelling albedo and specific balance of the Greenland ice sheet: Calculations for the Sondre Stromfjord transect. *Journal of Glaciology*, 42(141):305–317.

Zwally, H. J., Abdalati, W., Herring, T., Larson, K., Saba, J., and Steffen, K. 2002. Surface melt-induced acceleration of Greenland ice-sheet flow. *Science*, 297(5579):218–222.

Part II

List of Papers

Paper II:

Pramanik, A., **Van Pelt, W., Kohler, J., and Schuler, T.V. (2018). Simulating climatic mass balance, seasonal snow development and associated freshwater runoff in the Kongsfjord basin, Svalbard (1980-2016).** ***Journal of Glaciology*****, doi: 10.1017/jog.2018.80**

Journal of Glaciology (2018), **64**(248) 943–956 doi: 10.1017/jog.2018.80

Simulating climatic mass balance, seasonal snow development and associated freshwater runoff in the Kongsfjord basin, Svalbard (1980–2016)

ANKIT PRAMANIK,[1,2,3] WARD VAN PELT,[4] JACK KOHLER,[1] THOMAS V. SCHULER[2,5]

[1]*Norwegian Polar Institute; Fram Centre, Tromsø, Norway*
[2]*Department of Geosciences, University of Oslo, Oslo, Norway*
[3]*ESSO-National Centre for Antarctic and Ocean Research, Ministry of Earth Sciences, Goa, India*
[4]*Department of Earth Sciences, Uppsala University, Uppsala, Sweden*
[5]*Department of Arctic Geophysics, University Center in Svalbard, Longyearbyen, Norway*
Correspondence: Ankit Pramanik<ankit@ncaor.gov.in>

ABSTRACT. The Kongsfjord basin in northwest Svalbard is the site of a number of interdisciplinary studies concerned with the effect of fresh water from seasonal snow and glacier melt on the physical and biological environment. We use an energy-balance model coupled with a subsurface snow model to simulate the long-term climatic mass-balance evolution of the glaciers and the seasonal snow development of nonglacierized parts of the Kongsfjord basin. Runoff from both glacierized and nonglacierized parts of the basin is simulated to quantify the fresh water flux to the fjord. The model is calibrated with long-term mass-balance data measured at four glaciers, and with automatic weather station data. The simulated area-averaged climatic mass balance for the whole basin is positive (+0.23 m w.e. a^{-1}) over the period 1980–2016; however, the trend for net mass balance is not statistically significant over the simulation period, despite the observed ongoing summer warming. Refreezing equals 0.24 m w.e. a^{-1}, which is equivalent to 17% of the total mass gain from precipitation and moisture deposition. Total runoff comprises contributions from seasonal snow in the nonglacierized area (16%) and glacier discharge (84%). Model time series shows a significant increasing trend for annual glacier runoff (6.83 × 10^6 m^3 a^{-1}) over the simulation period.

KEYWORDS: energy balance, glacier discharge, glacier mass balance, glacier modelling

1. INTRODUCTION

In the currently warming climate, meltwater runoff from glaciers and ice caps, especially in the Arctic, is a major contributor to sea-level rise (Church and others, 2011; Jacob and others, 2012; Machguth and others, 2013; Mernild and others, 2014; Moon and others, 2018). It is expected that glaciers and ice caps will lead to 81 ± 43 mm of sea-level rise by 2050, assuming current acceleration (Meier and others, 2007; Radić and Hock, 2011; IPCC, 2013). The Arctic is experiencing greater warming than the global average through feedbacks caused by changes in sea-ice extent, surface reflectivity and air temperature, a process known as the 'Arctic amplification' (Manabe and Stouffer, 1980; Serreze and Francis, 2006; Serreze and others, 2009).

The High Arctic archipelago Svalbard has a glacierized area of ~34 000 km^2 (Nuth and others, 2013), equivalent to 5% of the world's land-ice mass outside of Greenland and Antarctica (Pfeffer and others, 2014; Aas and others, 2016). Glaciers cover ~60% of the land area of Svalbard (Hagen and others, 2003) and, if melted, could potentially contribute 14–26 mm to global sea-level rise (Radić and Hock, 2010; Huss and Farinotti, 2012; Martín-Español and others, 2015). Mean annual temperature in Longyearbyen has increased by 0.25 K $decade^{-1}$ over the past 100 years (Førland and others, 2011), with most of the warming in the more recent period, since 1975 (~1.0 K $decade^{-1}$); the strongest recorded warming in Europe (Førland and others, 2011; Nordli and others, 2014). The recent warming is most pronounced in winter and spring and temperatures are expected to continue to increase in the 21st century (IPCC, 2013). Simultaneously, over the period 1964–97, precipitation in Longyearbyen has increased by 1.7% $decade^{-1}$ (Førland and Hanssen-Bauer, 2000). In terms of glacier mass balance, however, this weak increase is not enough to compensate for effects of the warming. Svalbard glaciers show a declining mass-balance trend since 1967, when the first glaciological measurements were started (WGMS, 2017; Østby and others, 2017).

In northwest Svalbard, the Kongsfjord basin near Ny-Ålesund plays a crucial role in scientific research in oceanography, meteorology, biology, ecology and land surface processes (hydrology, glaciology). In Kongsfjord, there are glaciers of different shapes and sizes and with different dynamic behaviour (Liestøl, 1988; Hagen and others, 1993). Studying mass balance of these glaciers is important for understanding the present trend of glacier retreat as well as to quantify fresh water discharge to the fjord. Apart from glacier runoff, another significant source of fresh water to the fjord in this region is meltwater from seasonal snow in the nonglacierized area. Freshwater runoff at the base of tidewater glaciers creates a buoyant plume when entering the fjord (Cowton and others, 2015; How and others, 2017) and mixes with the fjord water at different vertical depth affecting the fjord's circulation (Sundfjord and others,

2017). Plumes bring nutrients and plankton to the fjord surface, propagating their impact through the food chain to a wide range of species, and thus plays a crucial role in the fjord ecosystem (Lydersen and others, 2014). Accurately quantifying the spatial and temporal distributions of meltwater runoff is, therefore, crucial for understanding the fjord system. Insight into runoff can only be gained through distributed modelling; Kongsfjord is particularly well suited for this task since long-term records (the longest in Svalbard) of glacier data exist for model calibration and validation.

Models have been widely used to simulate mass balance of glaciers from regional to global scales ranging in complexity from conceptual degree day models (Hock, 2003; Nuth and others, 2012) to physically-based energy-balance models (Hock, 2005; Arnold and others, 2006). Energy-balance models consider all the energy fluxes interacting with the glacier surface to compute surface temperatures T_S; the energy equivalent of $T_S > 0$ °C is used to calculate melt at the glacier surface. Meltwater percolates through the snowpack and may refreeze, depending on the subsurface temperature; any excess meltwater contributes to runoff. Refreezing plays a crucial role in the mass budget of Arctic glaciers as it increases the temperature and density of the snowpack, and reduces and delays mass loss through runoff (Wright and others, 2007; Reijmer and others, 2012). Furthermore, heat released by refreezing has a major impact on the thermal structure of a glacier (Poinar and others, 2017). Refreezing below the previous year's summer surface in the firn area is known as internal accumulation (Schneider and Jansson, 2004), which is not captured by conventional mass-balance monitoring. In contrast to non-polar regions, refreezing strongly affects the mass balance of High Arctic glaciers, mainly due to the strong seasonal temperature cycle (Bliss and others, 2014). Very cold winters with relatively little or no insolation lead to cold snowpacks, increasing the potential for refreezing of percolated meltwater during the melt season and storage of water in the snow or firn after the melt season.

Previous modelling studies of mass balance in the Kongsfjord region mainly focused on four glaciers: Austre Brøggerbreen (BRB), Midtre Lovénbreen (MLB), Kongsvegen (KNG) and Kronebreen-Holtedahlfonna (HDF) (Table 1). All of these studies have focused on either single glaciers (Bruland & Hagen, 2002) or partial areas of Kongsfjord (Lefauconnier and others, 1994a; Kohler and others, 2007; Rasmussen and Kohler, 2007; Nuth and others, 2012; Van Pelt and Kohler, 2015). In this study, meltwater production is simulated considering all glaciers in the Kongsfjord basin, and additionally, we simulate seasonal snow in the nonglacierized area. This enables us to distinguish runoff contributions to the fjord from glaciers and land. Glacier and seasonal snow runoff modelling over entire catchments is required to estimate the total water budget, as has been done in several glacierized catchments in the world (e.g. Himalaya, Alps, Central Asia, Alaska, Andes) (Verbunt and others, 2003; Jeelani and others, 2012; Duethmann and others, 2015; Bring and others, 2016; Mernild and others, 2016; Valentin and others, 2018). The long-term simulation allows us to detect trends in seasonal snow amounts and the climatic mass balance (CMB) and its components, and relate them to transient climate conditions. We estimate and analyze the long-term CMB evolution of the entire glacierized area of Kongsfjord basin, and quantify runoff into the fjord from glaciers and from the seasonal snow of the nonglacierized area. Simulations are performed with a surface energy balance – firn model (Van Pelt and Kohler, 2015), which has been extended with a soil model (Westermann and others, 2011) to simulate seasonal snow in nonglacierized parts of the domain.

2. STUDY AREA

Kongsfjord is open to the sea to the west and is surrounded by glaciers to the south, east, and north (Fig. 1). The glaciers to the south are small land-terminating glaciers (average area per glacier ~6.5 km^2), whereas the glaciers to the east and north are mainly large tidewater glaciers (>50 km^2). The total nonglacierized area (tundra, hills, and nunataks) amounts to 293 km^2 and accounts for 20% of the Kongsfjord basin (~1440 km^2).

In this study, we divide the glacierized area of Kongsfjord basin into three subregions; south (~42 km^2), east (~ 573 km^2) and north (~533 km^2) (Figs 1, 2). Glaciers in south region are all land-terminating, low-lying and relatively slow moving (Hagen and others, 1993). The east region contains two large tidewater glacier systems; Kongsvegen-Sidevegen and Kronebreen, the latter draining the ice fields of Holtedahlfonna (HDF) and Infantfonna. KNG is a surge-type glacier currently in its quiescent phase, flowing at low velocities (2–8 m a^{-1}) and undergoing surface steepening (Hagen and others, 1999; Kohler and others, 2007; Nuth and others, 2012). Kronebreen (KRB), which shares its terminus with KNG, is a fast-flowing tidewater glacier (300–800 m a^{-1}; Kääb and others, 2005). It has experienced two periods of rapid frontal retreat, ~ 3 km between 1966 and 1980, and ~1 km between 2011 and 2013 (Nuth and others, 2012, 2013); this most recent retreat is still ongoing.

Table 1. Previous mass-balance studies on four glaciers of Kongsfjord basin

Glacier	Study year	CMB (m w.e. a^{-1})	Method	Study
Austre Brøggerbreen (BRB)	1912–88	−0.45	Simple statistical model	Lefauconnier and Hagen (1990)
	1971–99	−0.69	Precipitation-runoff model	Bruland and Hagen (2002)
	1948–2005	−0.41	Upper-air meteorological model	Rasmussen and Kohler (2007)
Midtre Lovénbreen (MLB)	1948–2005	−0.31	Upper-air meteorological model	Rasmussen and Kohler (2007)
Kongsvegen (KNG)	1967–90	−0.11	Ice-coring and radioactive layering	Lefauconnier and others (1994a)
	1948–2005	+0.03	Upper-air meteorological model	Rasmussen and Kohler (2007)
	1969–2007	−0.04	Degree-day model	Nuth and Others (2012)
	1961–2012	+0.01	Coupled energy-balance- snow model	Van Pelt and Kohler (2015)
Holtedahlfonna (HDF)	1969–2007	−0.02	Degree-day model	Nuth and Others (2012)
	1961–2012	+0.13	Coupled energy-balance- snow model	Van Pelt and Kohler (2015)

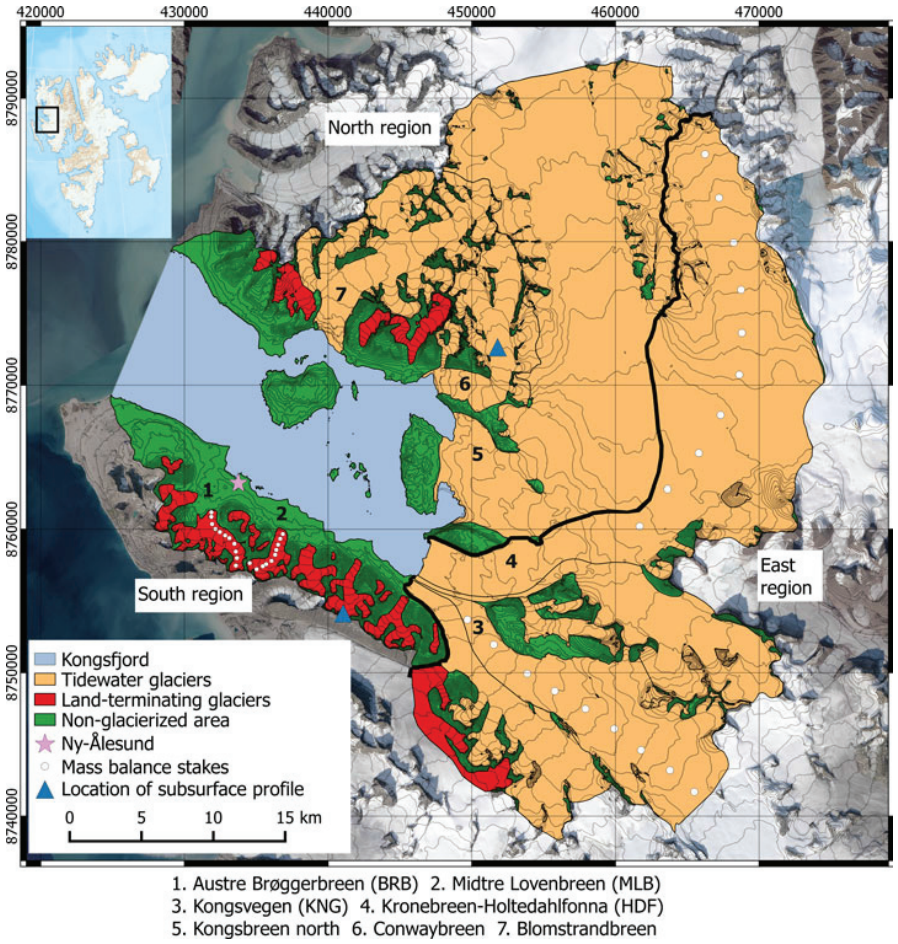

Fig. 1. Kongsfjord basin; Orange colour indicates tidewater glaciers, red colour indicates land-terminating glaciers, and green colour indicates non-glacierized area. Individual glaciers are shown with the thin black line. Thick black lines divide east region from south region and north region from east region. Mass-balance stakes of the four mass balance glaciers are shown with white dots. Ny-Ålesund is shown with magenta star. Blue triangles indicate the locations (elevation 610 m a.s.l.) where subsurface density has been investigated. The background is Landsat mosaic image.

The north region of the basin contains three tidewater glaciers (Blomstrandbreen, Conwaybreen and Kongsbreen, from west to east) and a few smaller land-terminating glaciers (Hagen and others, 1993). The tidewater glaciers in this area vary in their dynamic behaviour and contribute substantial mass to the fjord through calving (Liestøl, 1988; Lefauconnier and others, 1994b). Blomstrandbreen surged in 2007 (Sund and Eiken, 2010; Mansell and others, 2012; Burton and others, 2016). Kongsbreen North was observed to move at ~2.8 m d^{-1} in autumn 2012 (Schellenberger and others, 2015).

A meteorological station is situated on the southwest side of the fjord at Ny-Ålesund (78.92° N, 11.91° E). We use observational data from four glaciers (Fig. 1) (Kohler, 2013) monitored by the Norwegian Polar Institute (NPI) to calibrate and validate the model; two tidewater glaciers, HDF and KNG, and two land-terminating glaciers, BRB and MLB.

3. DATA

3.1. Surface DEM and glacier mask

We use a Digital Elevation Model (DEM) with a 5 m horizontal resolution, constructed by the NPI from aerial surveys in 2009 and 2010 (NPI, 2014), averaging values onto a 250 m × 250 m model grid. A recent model grid and the most recent glacier mask (König and others, 2014) is used throughout the study period. Elevation and glacier outlines are assumed to be constant throughout the simulation period.

3.2. Meteorological input

To force the model, we use 6 hourly weather station data from Ny-Ålesund (air temperature, air pressure, cloud cover and relative humidity), and downscaled precipitation data derived from the ERA-Interim re-analysis of the European Center for Medium-Range Weather Forecast (Dee and others, 2011). Pressure, cloudiness and humidity records from Ny-Ålesund are extrapolated to the model grid using fixed lapse rates, extracted from HIRLAM regional climate model output used in Van Pelt and Kohler (2015). In this work, the temperature lapse rate (TLR) is an adjustable parameter, the calibration of which is discussed in section 4.2. Precipitation from ERA-Interim is available from 1979 at 6-h intervals and at ~80 km horizontal resolution (Dee and others, 2011). Østby and others (2017) downscaled this product to 1 km resolution over Svalbard using the linear theory of orographic precipitation (Smith and Barstad,

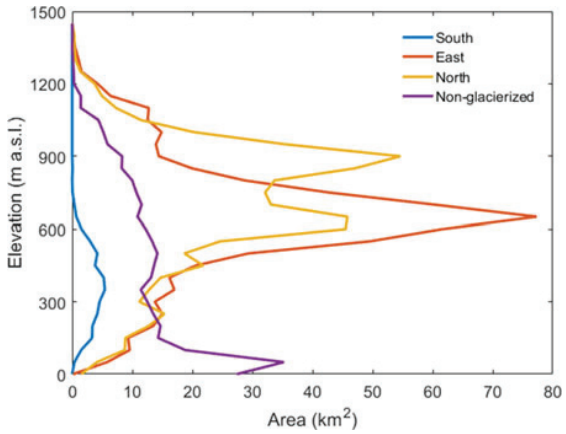

Fig. 2. Regional hypsometries of three regions. Elevation interval is 50 m. Maximum elevation is 1417 m a.s.l.

2004). In this study, we re-grid the 1 km product to our model domain by linear interpolation and apply a spatial linear correction derived from the measured winter mass balance, to reduce the biases of ERA-Interim precipitation.

3.3. Stake and glacier-wide mass balance

Mass-balance measurements of the two land-terminating glaciers BRB and MLB started in 1967 and 1968, respectively, while monitoring of KNG and HDF started in 1987 and 2004, respectively (WGMS, 2017). Seasonal mass balance is measured using stakes drilled into firn/ice along the glacier centrelines (Fig. 1). Stakes are measured twice a year in April and September to yield winter (b_w) and summer (b_s) balances. These point measurements (henceforth referred to as stake balances) are then extrapolated using the glacier hypsometry to calculate glacier-wide winter (B_w), summer (B_s) and net (B_n) mass balances, assuming a functional relationship between mass balance and elevation. We use stake balances (winter and summer) for calibration of climate parameters of the model (section 4.2).

4. MODEL AND SET UP

4.1. Model description

The model employed in this study simulates mass and energy exchange between atmosphere, surface and the underlying snow, firn and /or ice and it has been used previously by Van Pelt and Kohler (2015) for the glacier system KNG and HDF. Here, we use a different precipitation product for forcing and add a separate subsurface scheme for the nonglacierized part of the domain to expand the application to the entire Kongsfjord basin.

The model iteratively solves the energy-balance equation for each time step to calculate the surface temperature. The surface temperature is capped at the melting point and excess energy is used to melt the surface. The meltwater enters the subsurface snow/firn pack and serves as input to the subsurface module.

The subsurface module is an update (Reijmer and Hock, 2008) of the SOMARS model (Simulation Of glacier Mass balance And Related Subsurface processes; Greuell and Konzelmann (1994)), which simulates the evolution of vertical profiles of temperature, density and water content and which has been repeatedly applied on Svalbard (Van Pelt and others, 2012, 2014, 2016b; Østby and others, 2013; Østby and others, 2017). Briefly, percolated meltwater refreezes, depending on the subsurface temperature and density of snowpack in each layer and excess meltwater, if any, is routed vertically according to a tipping-bucket scheme. As percolated meltwater refreezes, it releases latent heat, which increases the temperature of the snowpack. Apart from gravitational densification, refrozen meltwater increases the density of the snowpack. Runoff occurs at the firn/ice transition in case a snowpack is present or at the surface in case of bare-ice exposure. The model does not consider any horizontal transport of water in between grid cells since it requires explicit treatment of surface and subsurface drainage, which is beyond the scope of the study. The subsurface model comprises a vertically adjustable grid of 100 layers, the thickness of which increases with depths by merging the 15th, 30th and 45th layers, and which vary from 0.1 m to 0.8 m. For the nonglacierized area, a subsurface soil model (Westermann and others, 2011) connected with the energy-balance model simulates the heat conduction in the soil below the snowpack.

The CMB is the sum of the mass gain due to precipitation, riming at the surface and mass loss due to runoff, sublimation or evaporation. The winter balance refers to the period between 1 September of the previous year and 15 April of the current year, while summer balance corresponds to the period between 16 April and 31 August. The net balance is calculated as the sum of the winter and summer balances i.e. it covers the period between 1 September of the previous year and 31 August of the present year. Annual melt, refreezing and runoff are also calculated over the same period.

4.2. Calibration of parameters

Van Pelt and Kohler (2015) calibrated parameters determining incoming shortwave and longwave radiation, turbulent exchange coefficient and the albedos of snow and firn. Here, we adopt their parameter values without further refinement but calibrate TLR to achieve optimal agreement between modelled and measured stake summer balances at four glaciers (BRB, MLB, KNG and HDF; Fig. 3) by minimizing the RMSE value. Model calibration experiments are run over the observation period at selected grid points where observational data exist. Table 2 presents the calibrated parameter values used for the model application to the whole domain. We used similar TLRs for glaciers close to their respective calibrating glaciers, i.e. we use the HDF TLR for the glaciers in the north and the MLB TLR for the south side of the fjord. Time series of glacier-wide winter (B_w), summer (B_s) and net balance (B_n) of the four mass-balance glaciers BRB, MLB, KNG and HDF (Figs 4a–d) demonstrate that the model reproduces year to year variability of mass balance very well, thus giving confidence in the interannual variability of precipitation forcing and TLR calibration.

4.3. Initialization

An initialization run is performed to generate suitable subsurface conditions (temperature, density and water content) for the start of the simulation in 1979. At the start of the initialization, the density corresponds to that of ice (900 kg m^{-3}), with a constant temperature of 270 K and zero water content. We perform 40 years of initialization in two steps, first running

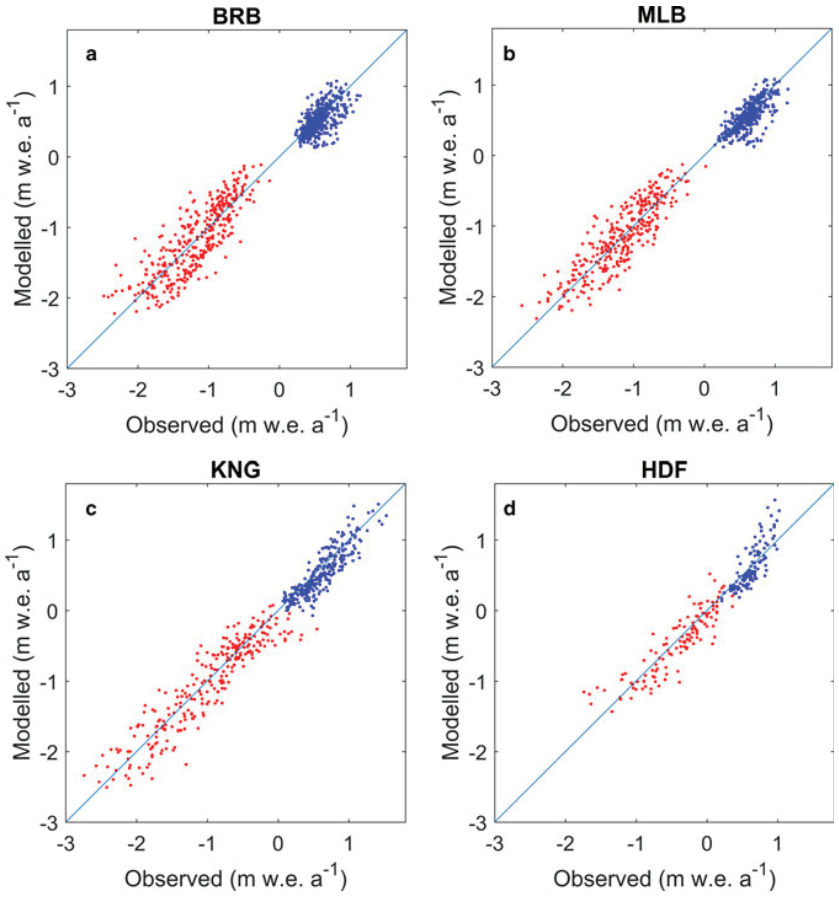

Fig. 3. Best match of modelled and measured stake winter (b_w, blue) and summer (b_s, Red) balance for all four mass balance glaciers (a) Austre Brøggerbreen (BRB), (b) Midtre Lovénbreen (MLB), (c) Kongsvegen (KNG) and (d) Holtedahlfonna (HDF) after calibration.

the model from 1979 to 1999 and then starting the second iteration from the final state of the first iteration over the same period.

5. RESULTS AND DISCUSSION

5.1. Climatic mass balance

The area-averaged climatic mass balance, snowfall, rainfall, melt, refreezing and runoff over the period 1980–2016 for the entire glacierized basin and the three subregions are shown in Table 3. Figure 5 shows spatial distributions of precipitation, melt, refreezing and climatic mass balance. Glaciers on the south and east sides of the fjord receive less snowfall compared with the glaciers in the north, while overall melt rates are highest in the south. The modelled mean CMB of glacierized area of Kongsfjord is positive (+0.23 m w.e. a^{-1}) for the period 1980–2016. The CMB varies considerably between regions, however, with a strongly negative CMB in the south (−0.43 m w.e. a^{-1}), a weakly negative mass balance in the east (−0.08 m w.e. a^{-1}) and positive mass balance in the north (+0.61 m w.e. a^{-1}). We found glacier-wide mass losses for the (land-terminating) glaciers on the south side, in agreement with the observed retreat (Rippin and others, 2003; Kohler and others, 2018). Glaciers in the north are at higher elevations, and experience on average 56% more snowfall and 59% less melt compared with glaciers in the south region. Glaciers in the north and east are mostly tidewater glaciers and lose mass due to calving. For HDF, calving rates at its tidewater terminus KRB have previously been estimated at -0.42 ± 0.10 m w.e. a^{-1} for 1966–2007 (Nuth and others, 2012), which suggests that the total

Table 2. Calibrated temperature lapse rates for mass-balance glaciers. Bias is defined as mean difference between modelled and measured mass balance

Glacier	Temperature lapse rate (km^{-1})	Summer Balance (m w.e. a^{-1})		Winter balance (m w.e. a^{-1})	
		RMSE	Bias	RMSE	Bias
Austre Brøggerbreen	3.2	0.29	0.00	0.17	−0.04
Midtre Lovénbreen	3.2	0.25	0.02	0.17	−0.07
Kongsvegen	3.8	0.26	−0.04	0.17	−0.08
Holtedahlfonna	4.2	0.22	−0.04	0.18	−0.01

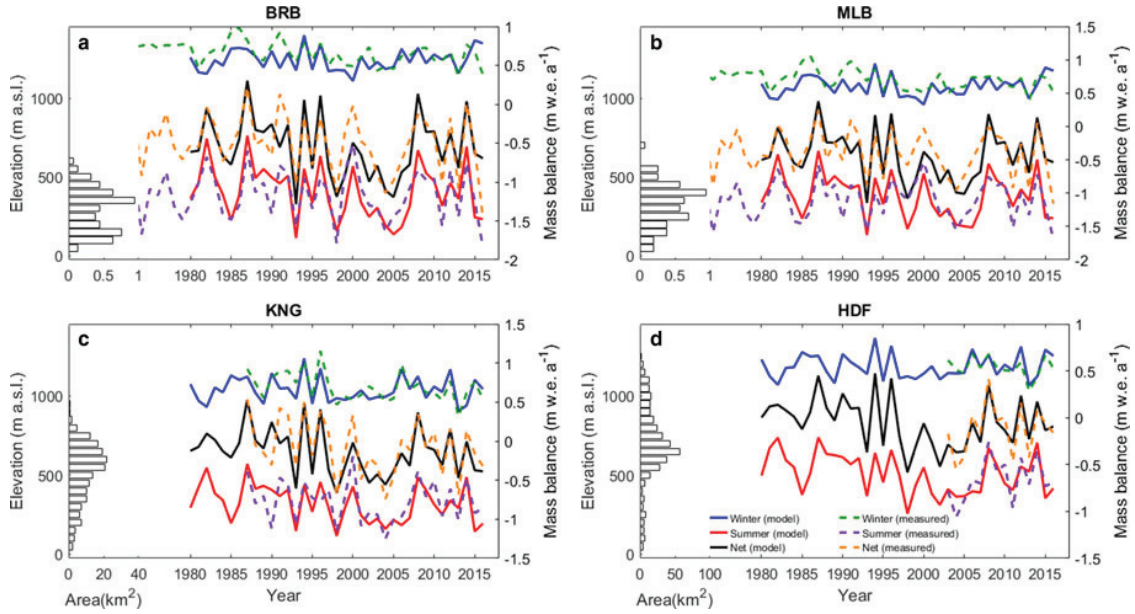

Fig. 4. Modelled (solid line) and measured (dashed line) winter (B_w), summer (B_s) and net (B_n) mass balances of (a) Austre Brøggerbreen (BRB), (b) Midtre Lovénbreen (MLB), (c) Kongsvegen (KNG) and (d) Holtedahlfonna (HDF) (right axis). The left-hand side of each panel shows the hypsometry of the respective glacier (left axis).

mass balance is much more negative than the simulated CMB of -0.05 ± 0.26 m w.e. a^{-1} for 1980–2016.

Overall, refreezing comprises 17% of the total accumulation from precipitation and moisture deposition for the entire glacierized part of the basin. Average refreezing amounts to 0.24 m w.e. a^{-1} and consists of similar contributions of refreezing of percolating water (0.12 m w.e. a^{-1}) in spring/summer and refreezing of stored irreducible and slush water (0.12 m w.e. a^{-1}) in winter. For comparison, a mean value for total refreezing of 0.30 m w.e. a^{-1} was found on HDF and KNG by Van Pelt and Kohler (2015). Refreezing varies spatially, with lower values in the south (0.21 m w.e. a^{-1}) than the north region (0.27 m w.e. a^{-1}). The higher refreezing rates in the north region are most likely due to the relatively larger accumulation zones that allow deeper water storage in firn and refreezing in the winter season. Substantial refreezing also occurs in seasonal snow on soil (0.21 m w.e. a^{-1}), most of which is related to rainfall events during the cold season. Major refreezing events after heavy rainfall during the core winter season can cause the formation of basal ice in the snowpack (Hansen and others, 2014; Van Pelt and others, 2016a, 2016b), which can dramatically impact food supplies of grazing herbivores in Svalbard (Kohler and Aanes, 2004).

Time series of annual climatic mass balance, snowfall, rain, melt and refreezing are shown in Fig. 6 for the entire glacierized area and for the three subregions. The area-averaged net balance has a weakly negative but nonsignificant trend for the entire glacierized basin and the south and north regions over the simulation period, whereas the trend is significant for the east region (Table 4). Summer balance has a weakly negative but significant trend for the entire glacierized area, east and north region, while the trend in the south region is nonsignificant over the simulation period 1980–2016 (Table 4).

We find an increasing trend of 0.12 K a^{-1}, 0.04 K a^{-1} and 0.09 K a^{-1} (with $p < 0.005$ for all) for mean winter, summer and annual temperatures respectively (Fig. 7) over the simulation period 1980–2016. We find correlations of -0.32 ($p < 0.06$) and 0.77 ($p < 0.01$) between net mass balance and mean summer temperature, and between net mass balance and annual snowfall, respectively, for the entire glacierized area. Net mass balance has a significant correlation to the annual snowfall for the south, east and north regions, with the strongest correlation observed in the latter region (Table 5). The anticorrelation of net mass balance with mean summer temperature is weakest and nonsignificant for north region, however, the anticorrelation is stronger in the east and south regions (Table 5), which indicates that mass balance of glaciers in the south and east is more sensitive to temperature than in the north. Winter precipitation shows a positive but nonsignificant trend for the entire

Table 3. Area-averaged glacier wide climatic mass balance (B_w, B_s, B_n), melt, refreezing and runoff for three regions and entire glacierized area, 1980–2016

	Area averaged (1980–2016): m w.e. a^{-1}							
	B_w	B_s	B_n	Snowfall	Rain	Melt	Refreezing	Runoff
All Glaciers	0.73	−0.50	0.23	0.99	0.19	1.01	0.24	0.97
South	0.58	−1.01	−0.43	0.80	0.30	1.46	0.21	1.55
East	0.58	−0.66	−0.08	0.77	0.15	1.07	0.22	1.00
North	0.89	−0.28	0.61	1.25	0.23	0.92	0.27	0.88

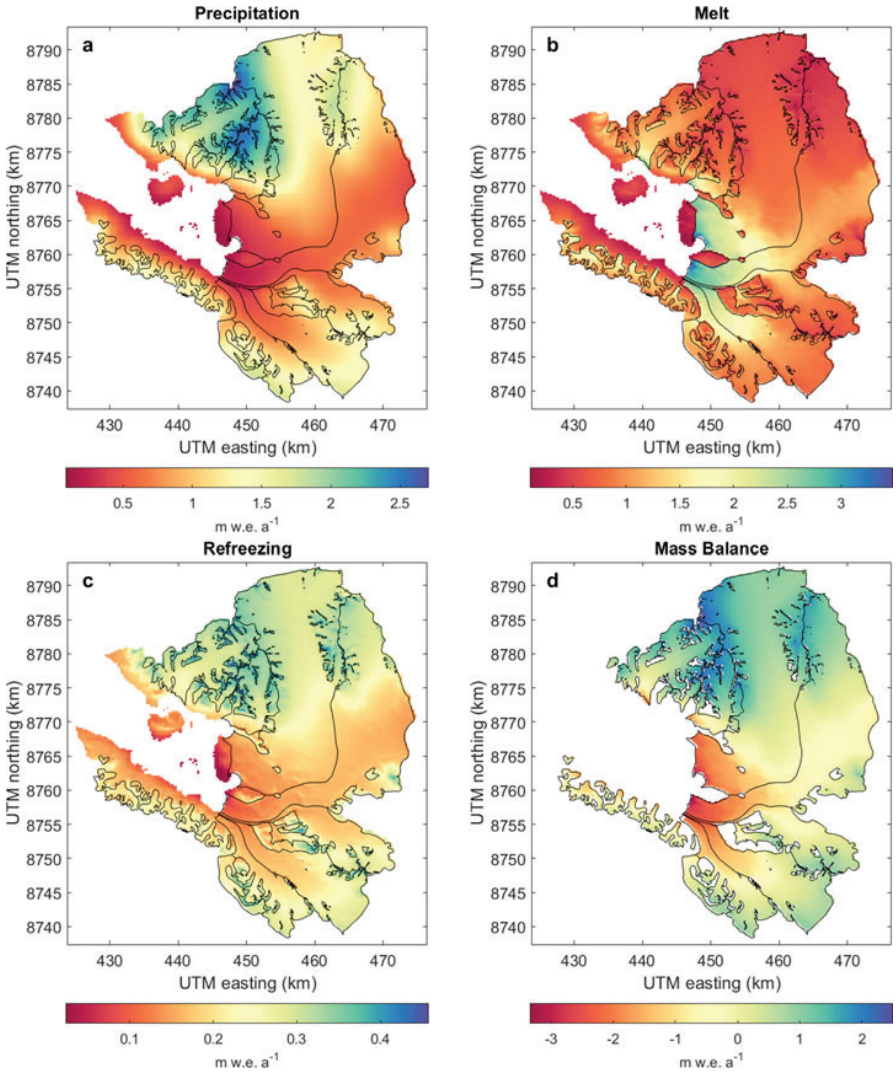

Fig. 5. Long-term spatially distributed pattern of (a) precipitation, (b) melt, (c) refreezing and (d) climatic mass balance averaged over the simulation period 1980-2016. (a–c) are for the entire Kongsfjord basin while (d) shows only the glacierized area.

glacierized basin (+0.0023 m w.e. a^{-2}, $p < 0.4$) as well as the south (+0.0024 m w.e. a^{-2}, $p < 0.3$), east ($+8.9 \times 10^{-4}$ m w.e. a^{-2}, $p < 0.7$) and north (+0.0038 m w.e. a^{-2}, $p < 0.3$) regions over the simulation period 1980–2016. There is a significant increasing trend in summer temperature, which induces a negative and significant trend in summer balance for the entire glacierized basin as well as in two of the subregions (east and north). However, the summer balance is compensated to a certain extent by the slightly increasing winter precipitation for the entire glacierized area as well as all subregions, thereby yielding a nonsignificant trend in the net climatic mass balance.

5.2. Runoff

Figure 8 shows time series of total annual runoff from the glacierized subregions and nonglacierized areas. Runoff from the nonglacierized area is mainly due to snowmelt and comprises ~16% of the total runoff from the whole basin over the simulation period. Runoff from seasonal snow is limited by the amount of cumulative snowfall in the cold season. Area-averaged runoff from glaciers is largest in the south, followed by the east and north regions (Table 3). Nevertheless, total glacier runoff is smallest in the south due to the small glacier area; the east region contributes the most fresh water to the fjord (Fig. 8). Differences in runoff between glacierized and nonglacierized areas are largest in years with warm summers due to high rates of glacier ice melt after the disappearance of the seasonal snow.

We find an increasing and statistically significant trend in annual runoff from the glacierized area (6.83×10^6 m^3 a^{-1} with $p < 0.09$), and the east (3.47×10^6 m^3 a^{-1} with $p < 0.1$) and north (3.1×10^6 m^3 a^{-1} with $p < 0.08$) regions over the simulation period, while a positive but nonsignificant trend is observed in runoff from the south region (2.51×10^5 m^3 a^{-1}, $p < 0.24$). With future warming, runoff from all the glaciers will increase substantially (see section 5.5). Increased runoff volume will potentially lead to more rapid vertical mixing of fresh water at the tidewater glacier front, which would impact the fjord circulation (Sundfjord and others, 2017) and promote more foraging of marine mammals (Lydersen and others, 2014). Increased runoff from land-terminating glaciers would lead to greater stratification and affect the physical and chemical environment of the fjord (Nowak and Hodson, 2013, 2015).

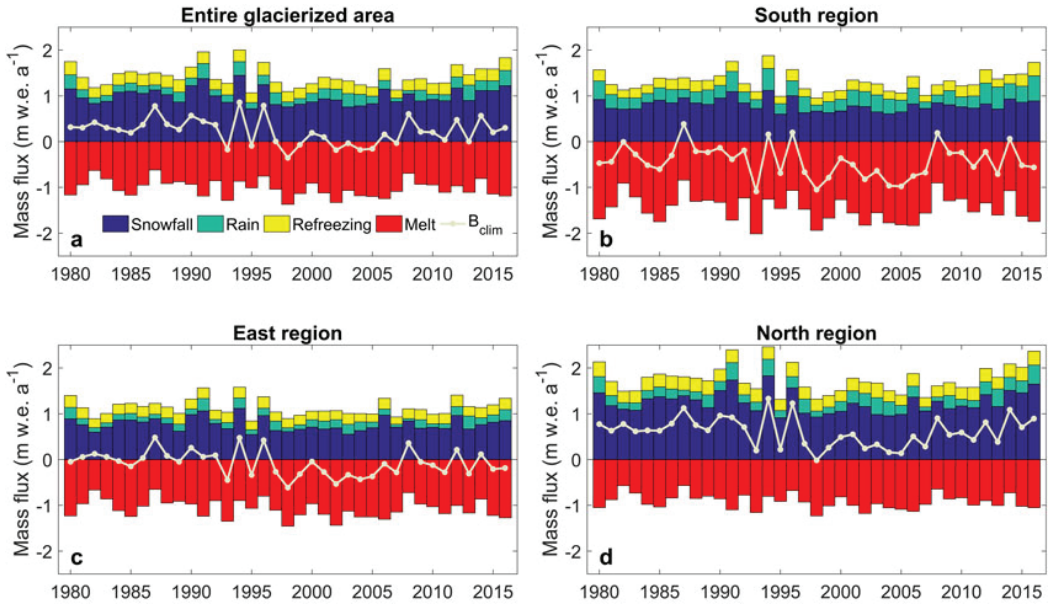

Fig. 6. Glacier area-averaged climatic mass balance and its components over the simulation period 1980–2016 for the (a) entire glacierized area, (b) south region, (c) east region and (d) north region. The climatic mass balance of a year is calculated between 1 September of the previous year and 31 August of the present year.

5.3. Decadal changes

Figure 9 shows averages of climatic mass balance, snowfall and rainfall as a function of elevation for the glacierized area of Kongsfjord basin during four periods; 1980–89, 1990–99, 2000–09 and 2010–16 (7 years). The overall positive mass-balance gradient is especially pronounced for the period 2010–16 (Fig. 9a), mainly driven by an increase in snowfall at high elevations (Fig. 9b). On average, mass balance is positive above 600 m a.s.l., with the major contribution coming from glaciers on the north and northeast side of the fjord. We find substantial increases in precipitation (both snowfall and rainfall) at higher elevations of the basin in the most recent period. However, there is no significant change in snowfall at lower elevations, although rainfall has increased substantially at all elevations. Average rainfall during the last three decades was 0.15 m w.e. a^{-1} and has increased by 27% in 2010–16 compared with 1980–2009. In a warmer and wetter future Svalbard climate (Førland and others, 2011), rainfall is likely to further increase; with most pronounced warming in winter, more rainfall is likely to occur also during the cold season (Van Pelt and others, 2016a).

The mass balance of the entire glacierized area of Kongsfjord has decreased over the last three periods (1990–99, 2000–09, 2010–16) compared with the 1980–89 period, with 2000–09 having the lowest mass balance (+ 0.08 m w.e. a^{-1}) (Fig. 6). Melt and runoff in the 1990–99 and 2000–09 periods increased substantially compared with the 1980–89 period and decreased in 2010–16. However, melt and runoff in 2010–16 has increased by 12 and 17%, respectively compared with 1980–89 (Fig. 6). The average Equilibrium Line Altitude (ELA) of the glacierized area has increased from 437 ± 75 m a.s.l. in 1980–89 to 509 ± 153 m a.s.l. and 572 ± 110 m a.s.l. in 1990–99 and 2000–09, respectively, decreasing to 517 ± 74 m a.s.l. in 2010–16.

5.4. Subsurface variables

Figures 10a, b show the time-depth evolution of subsurface density for the period 1990–2015 at two sites; one on a glacier in the south region and the other on a glacier in the north region (locations are shown in Fig. 1). The elevation of both sites is ~610 m a.s.l., within the accumulation zone of the respective glaciers. In spite of being at similar elevations, we find significant differences in the firn density evolution at these locations. The glacier in the south region has a small accumulation area, and the proximity of the ELA inhibits the formation of a thick firn layer. Firn almost disappears at this location over the period 1998–2006, due to low snowfall and high melting. At a similar elevation in the glacier in the north region, the significantly thicker firn started depleting between 1998 and 2006, caused by low snowfall in this period, when all glaciers show most negative mass balance. The site in the north region is higher above its local ELA than the site in the south, thus leading to the

Table 4. Climatic mass-balance trend of three subregions and entire glacierized area with their corresponding p values

Region	Winter Balance (B_w)	Summer Balance (B_s)	Annual Balance (B_n)
South	0.0013 ($p < 0.6$)	−0.007 ($p < 0.15$)	−0.006 ($p < 0.28$)
East	0.0001 ($p < 0.9$)	−0.0076 ($p < 0.03$)	−0.0074 ($p < 0.09$)
North	0.0028 ($p < 0.4$)	−0.0081 ($p < 0.03$)	−0.053 ($p < 0.28$)
Entire glacierized area	0.0014 ($p < 0.6$)	−0.0078 ($p < 0.03$)	−0.0064 ($p < 0.16$)

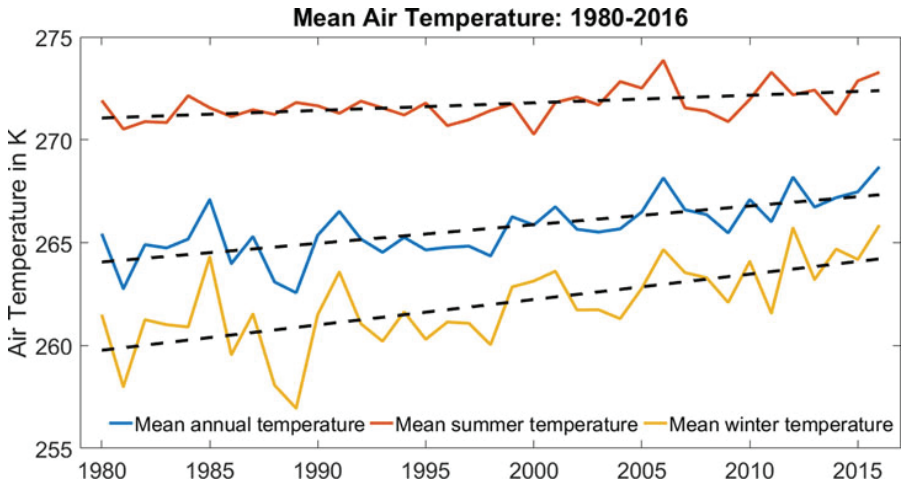

Fig. 7. Temperature (winter, summer and annual) for the period 1980–2016. Mean winter temperature increased around 2 K between 1980 and 2016. The trends for winter, summer and annual temperature are 0.12 K a^{-1}, 0.03 K a^{-1} and 0.09 K a^{-1}, respectively, shown with black dashed line.

formation of a thicker snow and firn pack. Due to higher snowfall in the post-2006 period, firn thickness starts to increase, especially after 2011, at both locations.

5.5. Climate sensitivity

To reduce computational cost, sensitivity tests were conducted at the mass-balance stake locations of the four NPI study glaciers over the period 1979–2016. We performed multiple runs perturbing air temperature (T), precipitation (P) and cloud cover (C) uniformly over the simulation period, without considering any seasonal variability. Table 6 provides the sensitivities of net mass balance, refreezing and runoff to perturbations in T, P and C in terms of anomalies to the long-term mean of the unperturbed state for three glaciers (MLB, KNG and HDF). Altitudinal profiles of sensitivities of mass balance, refreezing and runoff for six changing climate scenarios for KNG are shown in Figure 11. Mass balance and runoff are generally more sensitive to temperature than precipitation; runoff in the accumulation zone is nearly insensitive to precipitation changes. Refreezing has a complex response to changes in precipitation and temperature (Fig. 11b). Increases in precipitation lead to increased refreezing as a thicker snowpack has a higher cold content and a larger pore volume. This promotes both refreezing of meltwater in the early melt season and refreezing of stored irreducible water after the melt season. Similarly, reduced temperatures will increase snow depth and the extent of the accumulation zone and will simultaneously enhance winter cooling, all of which contribute to enhance refreezing. With the upward migration of the ELA in a warming climate refreezing rates drop and runoff amplifies. This explains the strong nonlinearity in the mass balance and runoff sensitivity to temperature change at sites just above the present ELA (Fig. 11). Table 6 shows that an increase in cloud cover increases runoff and decreases refreezing substantially.

Table 5. Correlation between winter snowfall and CMB and temperature and CMB for three subregions and entire glacierized area

Region	Winter snowfall-CMB correlation	Temperature-CMB correlation
South	+0.63 ($p < 0.01$)	−0.42 ($p < 0.01$)
East	+0.68 ($p < 0.01$)	−0.37 ($p < 0.03$)
North	+0.85 ($p < 0.01$)	−0.24 ($p < 0.15$)
Entire glacierized area	+0.77 ($p < 0.01$)	−0.32 ($p < 0.06$)

5.6. Uncertainties

A substantial source of uncertainty in the presented results comes from the small-scale variability of spatial snow distribution that is not accounted for by the orographic precipitation model. Local topography, wind speed and direction influence snow deposition and distribution in mountainous terrain like Kongsfjord basin (Hodgkins and others, 2005; Lehning and others, 2008; Dadic and others, 2010). Ignoring the small-scale variability of accumulation leads to biases in the area-averaged mass balance as the mass balance has a nonlinear response to snow accumulation (Van Pelt and others, 2014). Another source of uncertainty is that we used a fixed topography and ice extent throughout the entire simulation, which adds uncertainty to the extrapolation of elevation-dependent meteorological parameters, such as temperature and precipitation, and to runoff due to glacier length fluctuations. A 250 m × 250 m DEM would not properly resolve the topography around smaller glaciers leading to inappropriate shading, which would lead to uncertainty in radiation budget for those glaciers.

We used fixed start and end dates to calculate the mass balance of each year. Although in a warming climate the mass-balance year may need to be redefined eventually, it is convenient for comparison and to detect trends to have fixed dates define the mass-balance year.

Extrapolation of stake data to a glacier-wide grid also leads to uncertainty. In particular, the extrapolation of winter balance may contain significant uncertainty due to potential snow accumulation variability in our study region.

We used a fixed time-invariant TLR for different glaciers over the simulation period which is another source of uncertainty in the model, as cloud condition substantially affects the TLR (Petersen and others, 2013; Matuszko and Węglarczyk, 2014; Van Tricht and others, 2016).

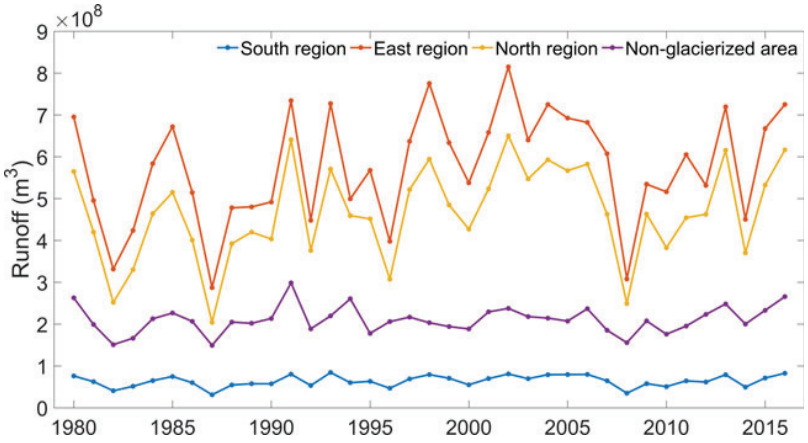

Fig. 8. Total annual runoff from the glacierized and non-glacierized areas over the simulation period 1980–2016. Total runoff from non-glacierized area contributes 16% of the total freshwater to the fjord. Runoff from seasonal snow is limited by the winter snowfall whereas runoff from the glacierized area is from both snow and ice melt from glaciers.

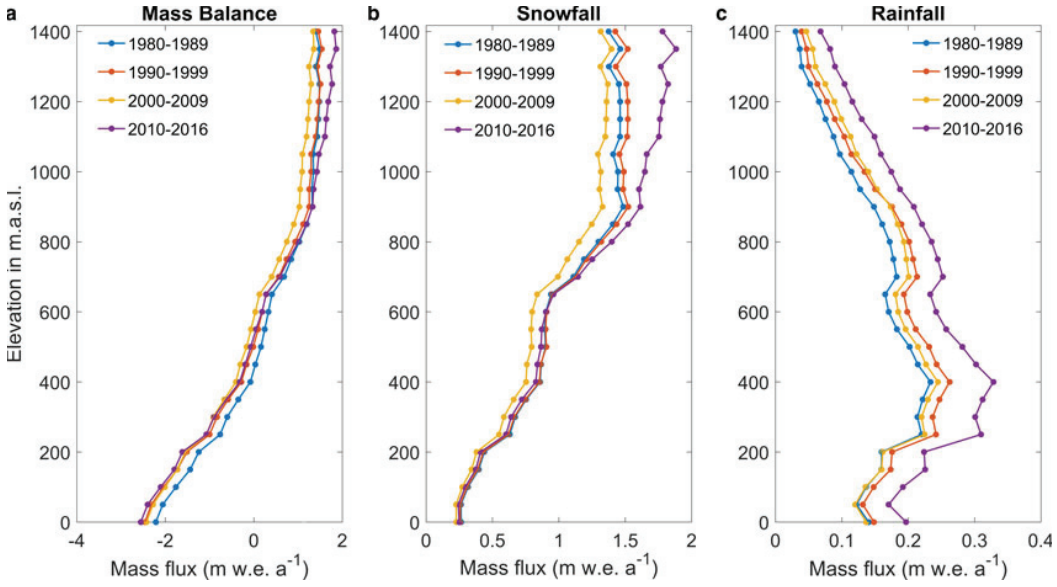

Fig. 9. Evolution of (a) climatic mass balance, (b) snowfall and (c) rainfall for four different periods as a function of elevations. CMB, snowfall and rainfall are averaged over the periods and spatially integrated within 50 m elevation bins for the glacierized area of the whole Kongsfjord basin.

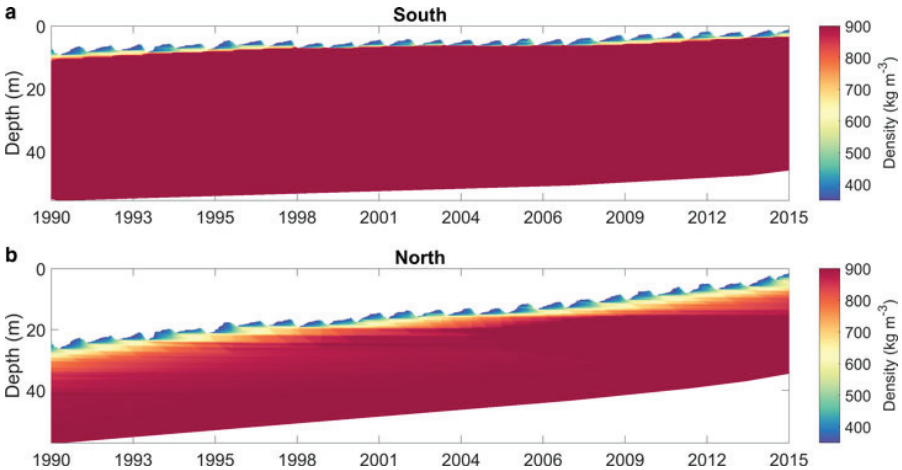

Fig. 10. Time series of simulated subsurface density at a location in the accumulation area of (a) a glacier in the south region and (b) a glacier in the north region. Locations are shown in Fig. 1; both are at an elevation of 610 m a.s.l.

Table 6. Overview of mass-balance sensitivity (δB), refreezing sensitivity (δRE) and runoff sensitivity (δRU) to changing temperature (*T*), precipitation (*P*) and cloud cover (*C*) of three glaciers along their central line. Units are in m w.e. a^{-1}.

	MLB			KNG			HDF		
Run	δB	δRE	δRU	δB	δRE	δRU	δB	δRE	δRU
T + 3 K	−2.72	0.051	2.79	−2.41	0.028	2.46	−1.9	−0.011	1.93
T + 2 K	−1.73	0.039	1.77	−1.50	0.015	1.53	−1.16	−0.019	1.18
T + 1 K	−0.83	0.018	0.85	−0.69	0.003	0.71	−0.55	−0.014	0.55
T−1 K	0.70	0.014	−0.71	0.56	0.022	−0.57	0.41	0.032	−0.42
T−2 K	1.18	0.049	−1.20	0.99	0.054	−1.01	0.61	0.043	−0.62
T−3 K	1.51	0.087	−1.53	1.29	0.071	−1.31	0.70	0.002	−0.71
P + 30%	0.36	0.034	−0.02	0.33	0.032	−0.06	0.36	0.033	−0.10
P + 20%	0.25	0.024	−0.02	0.23	0.023	−0.05	0.25	0.023	−0.07
P + 10%	0.13	0.013	−0.02	0.12	0.015	−0.03	0.13	0.013	−0.04
P−10%	−0.12	−0.009	0.01	−0.12	−0.007	0.04	−0.13	−0.006	0.04
P−20%	−0.28	−0.02	0.05	−0.26	−0.019	0.08	−0.26	−0.016	0.09
P−30%	−0.45	−0.031	0.11	−0.40	−0.031	0.14	−0.40	−0.027	0.14
C + 15%	−0.16	−0.007	0.15	−0.13	−0.006	0.12	−0.11	−0.011	0.1
C + 10%	−0.12	−0.004	0.12	−0.09	−0.002	0.09	−0.07	−0.006	0.07
C + 5%	−0.07	−0.002	0.07	−0.05	0.002	0.05	−0.03	−0.001	0.03
C−5%	0.2	0.006	−0.19	0.18	0.011	−0.17	0.19	0.016	−0.19
C−10%	0.36	0.014	−0.34	0.33	0.019	−0.31	0.33	0.027	−0.31
C−15%	0.48	0.023	−0.46	0.45	0.028	−0.43	0.42	0.037	−0.4

Sensitivity values of BRB are similar to MLB and therefore not shown here.

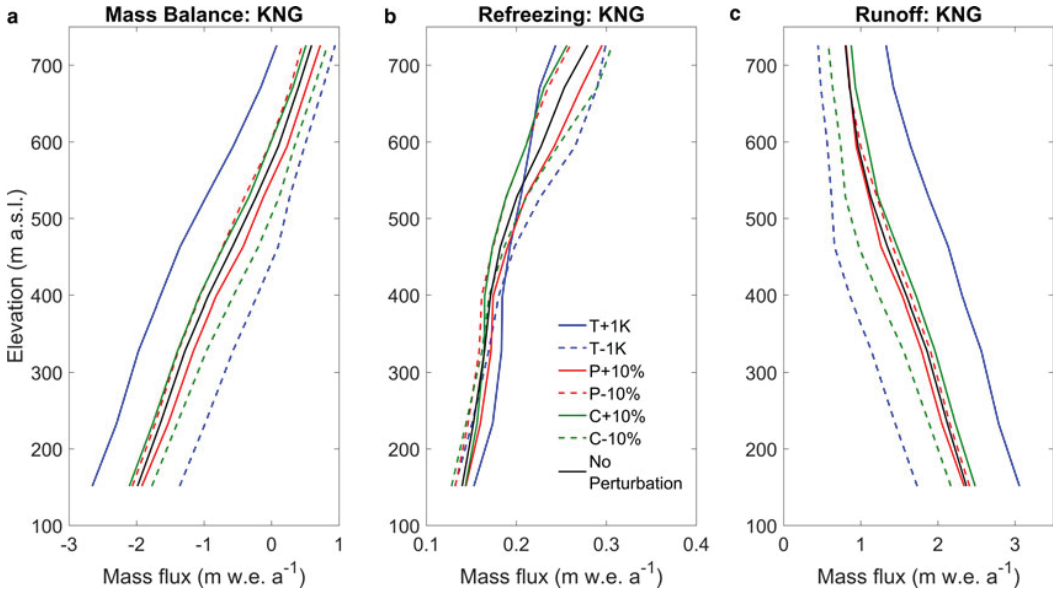

Fig. 11. Sensitivities to perturbations in temperature (*T*), precipitation (*P*) and cloud cover (*C*) of (a) mass balance, (b) refreezing and (c) runoff along the centreline of Kongsvegen (KNG).

Finally, observations used for model calibration and validation do not include any glaciers in the north region, which increases the uncertainty of the results in this region. More observational data from this region will help to constrain uncertainties.

6. CONCLUSIONS

We use a surface energy-balance model coupled with a subsurface snow/firn model (Van Pelt and others, 2012) to simulate the long-term (1980–2016) evolution of the CMB of glaciers and the associated fresh water flux into the Kongsfjord basin. The model is forced with downscaled ERA-Interim precipitation and climate data extrapolated from the nearby meteorological station in Ny-Ålesund, on a 250 m × 250 m grid. Calibration is performed by adjusting the TLR to match the measured summer balance data.

Results indicate that glaciers of Kongsfjord basin show wide variability in mass balance from south to north and from west to east. The CMB of the entire Kongsfjord basin is estimated to an average of + 0.23 m w.e. a^{-1} over the simulation period. Glaciers in the north region of Kongsfjord show overall positive CMB and are least sensitive to temperature perturbations, whereas glaciers in the south and east regions show overall negative CMB and are more sensitive. The net CMB of the entire glacierized basin shows a weakly negative but nonsignificant trend, although summer balance has a negative and significant trend over the simulation period 1980–2016.

Comparison of mass-balance components during the periods 1980–89, 1990–99, 2000–09 and 2010–16 shows a lowest CMB (+0.08 m w.e. a^{-1}) in the 2000–09 period. The most recent period (2010–16) had above-average precipitation, which could be related to recent retreat of Arctic sea-ice cover and increasing winter temperatures. Increase in snowfall is observed only at higher elevation but rainfall increases throughout the domain.

Refreezing accounts for 17% of the total mass gain and is higher in the north (0.27 m w.e. a^{-1}) than in the south (0.21 m w.e. a^{-1}). Snowmelt from nonglacierized areas in early summer contributes 16% of the total runoff to the fjord, while the remaining 84% is from glacier runoff. The largest contribution to total runoff comes from the east region. We find a significant increase in runoff trend over the simulation period from the entire glacierized area.

ACKNOWLEDGEMENTS

The first author received Ph.D. studentship support from ESSO-National Centre for Antarctic and Ocean Research (NCAOR), financed by the Ministry of Earth Sciences, Government of India; Grant/Award number: MoES/16/22/12-RDEAS (PhD fellowship-NPI). Additional funding came from the Polish-Norwegian Research Programme GLAERE, the Norwegian Research Council project TIGRIF, and the Norwegian Polar Institute's TW-ICE project. We thank the editor, H. Jiskoot and one anonymous referee for their insightful comments that helped to improve the manuscript. This article is NCAOR contribution no. 46/2018.

REFERENCES

Aas KS and 6 others (2016) The climatic mass balance of Svalbard glaciers: a 10-year simulation with a coupled atmosphere–glacier mass balance model. *Cryosphere*, **10**(3), 1089–1104

Arnold NS, Rees WG, Hodson AJ and Kohler J (2006) Topographic controls on the surface energy balance of a high Arctic valley glacier. *J. Geophys. Res.*, **111**(F2), F02011 (doi: 10.1029/2005jf000426)

Bliss A, Hock R and Radić V (2014) Global response of glacier runoff to twenty-first century climate change. *J. Geophys. Res.- Earth Surf.*, **119**(4), 717–730

Bring A and 9 others (2016) Arctic terrestrial hydrology: a synthesis of processes, regional effects, and research challenges. *J. Geophys. Res.: Biogeo.*, **121**(3), 621–649

Bruland O and Hagen JO (2002) Glacial mass balance of Austre Brøggerbreen (Spitsbergen), 1971–1999, modelled with a precipitation-run-off model. *Polar Res.*, **21**(1), 109–121

Burton DJ, Dowdeswell JA, Hogan KA and Noormets R (2016) Marginal fluctuations of a Svalbard surge-type tidewater glacier, Blomstrandbreen, since the Little Ice Age: a record of three surges. *Arct. Antarct. Alp. Res.*, **48**(2), 411–426

Church JA and 9 others (2011) Revisiting the Earth's sea-level and energy budgets from 1961 to 2008. *Geophys. Res. Lett.*, **38** (18), L18601 (doi: 10.1029/2011gl048794)

Cowton T, Slater D, Sole A, Goldberg D and Nienow P (2015) Modeling the impact of glacial runoff on fjord circulation and submarine melt rate using a new subgrid-scale parameterization for glacial plumes. *J. Geophys. Res.- Oceans*, **120**(2), 796–812

Dadic R, Mott R, Lehning M and Burlando P (2010) Wind influence on snow depth distribution and accumulation over glaciers. *J. Geophys. Res.- Earth Surf.*, **115**, F01012 (doi: 10.1029/2009jf001261)

Dee DP and 35 others (2011) The ERA-interim reanalysis: configuration and performance of the data assimilation system. *Q. J. Roy. Meteor. Soc.*, **137**(656), 553–597

Duethmann D and 9 others (2015) Attribution of streamflow trends in snow and glacier melt-dominated catchments of the Tarim river, Central Asia. *Water Resour. Res.*, **51**(6), 4727–4750

Førland EJ and Hanssen-Bauer I (2000) Increased precipitation in the Norwegian Arctic: true or false? *Climate Change*, **46**(4), 485–509

Førland EJ, Benestad R, Hanssen-Bauer I, Haugen JE and Skaugen TE (2011) Temperature and precipitation development at Svalbard 1900-2100. *Adv. Meteorol.*, **2011**, 893790 (doi: 10.1155/2011/893790)

Greuell W and Konzelmann T (1994) Numerical modelling of the energy-balance and the englacial temperature of the Greenland ice-sheet- calculations for the ETH-camp location (West Greenland, 1155 masl). *Global Planet. Change*, **9**(1–2), 91–114

Hagen JO, Liestøl O, Roland E and Jørgensen T (1993). *Glacier atlas of Svalbard and Jan Mayen*. Norsk Polarinstitutt, Oslo.

Hagen JO, Melvold K, Eiken T, Isaksson E and Lefauconnier B (1999) Mass balance methods on Kongsvegen, Svalbard. *Geogr. Ann. A.*, **81A**(4), 593–601

Hagen JO, Kohler J, Melvold K and Winther JG (2003) Glaciers in Svalbard: mass balance, runoff and freshwater flux. *Polar Res.*, **22**(2), 145–159

Hansen BB and 8 others (2014) Warmer and wetter winters: characteristics and implications of an extreme weather event in the high Arctic. *Environ. Res. Lett.*, **9**(11), 114021 (doi: 10.1088/1748-9326/9/11/114021)

Hock R (2003) Temperature index melt modelling in mountain areas. *J. Hydro.*, **282**(1–4), 104–115

Hock R (2005) Glacier melt: a review of processes and their modelling. *Prog. Phys. Geog.*, **29**(3), 362–391

Hodgkins R, Cooper R, Wadham J and Tranter M (2005). Interannual variability in the spatial distribution of winter accumulation at a high-Arctic glacier (Finsterwalderbreen, Svalbard), and its relationship with topography. *Ann. Glaciol* **42**, 243–248

How P and 9 others (2017) Rapidly changing subglacial hydrological pathways at a tidewater glacier revealed through simultaneous observations of water pressure, supraglacial lakes, meltwater plumes and surface velocities. *Cryosphere*, **11** (6), 2691–2710

Huss M and Farinotti D (2012) Distributed ice thickness and volume of all glaciers around the globe. *J. Geophys. Res.- Earth Surf.*, **117**, F04010 (doi: 10.1029/2012jf002523)

IPCC (2013). Summary for Policymakers. In Stocker TF, Qin D, Plattner G-K, Tignor M, Allen SK, Boschung J, Nauels A, Xia Y, Bex V and Midgley PM, eds. Climate Change 2013: The Physical Science Basis. Contribution of Working Group I to the Fifth Assessment Report of the Intergovernmental Panel on Climate Change. Cambridge, United Kingdom and New York, NY, USA. 9–23

Jacob T, Wahr J, Pfeffer WT and Swenson S (2012) Recent contributions of glaciers and ice caps to sea level rise. *Nature*, **482**(7386), 514–518

Jeelani G, Feddema JJ, van der Veen CJ and Stearns L (2012) Role of snow and glacier melt in controlling river hydrology in Liddar watershed (western Himalaya) under current and future climate. *Water Resour. Res.*, **48**, W12508 (doi: 10.1029/2011wr011590)

Kääb A, Lefauconnier B and Melvold K (2005) Flow field of Kronebreen, Svalbard, using repeated Landsat 7 and ASTER data. *Ann. Glaciol.*, **42**, 7–13

Kohler J (2013) *Mass balance for glaciers near Ny-Ålesund [Data set]* Norwegian Polar Institute. (doi: 10.21334/npolar.2013.ad6c4c5a)

Kohler J and Aanes R (2004) Effect of winter snow and ground-icing on a Svalbard reindeer population: results of a simple snowpack model. *Arct. Antarct. Alp. Res.*, **36**(3), 333–341

Kohler J and 7 others (2007) Acceleration in thinning rate on western Svalbard glaciers. *Geophys. Res. Lett.*, **34**(18), L18502 (doi: 10.1029/2007gl030681)

Kohler J, König M, Nuth C and Villaflor G (2018). *Svalbard tidewater glacier front database [Data set]* Norwegian Polar Institute. (doi: 10.21334/npolar.2018. 7cd67b1a)

König M, Nuth C, Kohler J, Moholdt G and Pettersen R (2014). *Global land Ice measurements from space*, Springer, Berlin, Heidelberg.

Lefauconnier B and Hagen JO (1990) Glaciers and Climate in Svalbard: Statistical Analysis and Reconstruction of the Brøggerbreen Mass Balance for the Last 77 Years. *Ann. Glaciol.*, **14**, 148–152

Lefauconnier B, Hagen JO, Pinglot JF and Pourchet M (1994a) Mass balance estimates on the glacier complex Kongsvegen and Sveabreen, Spitsbergen, Svalbard, using radioactive layers *J. Glaciol.*, **40**(135), 368–376

Lefauconnier B, Hagen JO and Rudant JP (1994b) Flow speed and calving rate of Kongsbreen glacier, Svalbard, using SPOT images. *Polar Res.*, **13**(1), 59–65

Lehning M, Löwe H, Ryser M and Raderschall N (2008) Inhomogeneous precipitation distribution and snow transport in steep terrain. *Water Resour. Res.*, **44**(7), W07404 (doi: 10.1029/2007wr006545)

Liestøl O (1988) The glaciers in the Kongsfjorden area, Spitsbergen. *Norsk Geogr. Tidsskr.*, **42** (4), 231–238

Lydersen C and 12 others (2014) The importance of tidewater glaciers for marine mammals and seabirds in Svalbard, Norway. *J. Marine Syst.*, **129**, 452–471

Machguth H and 8 others (2013) The future sea-level rise contribution of Greenland's glaciers and ice caps. *Environ. Res. Lett.*, **8**(2), 025005 (doi: 10.1088/1748-9326/8/2/025005)

Manabe S and Stouffer RJ (1980) Sensitivity of a global climate model to an increase of CO_2 concentration in the atmosphere. *J. Geophys. Res.- Oceans*, **85**(C10), 5529–5554

Mansell D, Luckman A and Murray T (2012) Dynamics of tidewater surge-type glaciers in northwest Svalbard. *J. Glaciol.*, **58**(207), 110–118

Martín-Español A, Navarro FJ, Otero J, Lapazaran JJ and Błaszczyk M (2015) Estimate of the total volume of Svalbard glaciers, and their potential contribution to sea-level rise, using new regionally based scaling relationships. *J. Glaciol.*, **61**(225), 29–41

Matuszko D and Węglarczyk S (2014) Effect of cloudiness on long-term variability in air temperature in Krakow. *Int. J. Climatol.*, **34** (1), 145–154

Meier MF and 7 others (2007) Glaciers dominate eustatic sea-level rise in the 21st century. *Science*, **317**(5841), 1064–1067

Mernild SH, Liston GE and Hiemstra CA (2014) Northern hemisphere glacier and ice cap surface mass balance and contribution to sea level rise. *J. Climate*, **27**(15), 6051–6073

Mernild SH and 5 others (2016) The Andes Cordillera. Part IV: spatio-temporal freshwater run-off distribution to adjacent seas (1979-2014). *Int. J. Climatol.*, **37**, 3175–3196 (doi: 10.1002/joc.4922)

Moon T, Ahlstrøm A, Goelzer H, Lipscomb W and Nowicki S (2018) Rising oceans guaranteed: arctic land ice loss and sea level rise. *Curr. Clim. Change Rep.*, **4**(3), 211–222

Nordli Ø, Przybylak R, Ogilvie AEJ and Isaksen K (2014) Long-term temperature trends and variability on Spitsbergen: the extended Svalbard Airport temperature series, 1898–2012. *Polar Res*. **33**, 21349 (doi: 10.3402/polar.v33.21349)

Norwegian Polar Institute (NPI) (2014). *Terrengmodell Svalbard (S0* Terrengmodell*)* [data set]. Norwegian Polar Institute. (doi: 10.21334/npolar.2014.dce53a47)

Nowak A and Hodson A (2013) Hydrological response of a high-Arctic catchment to changing climate over the past 35 years: a case study of Bayelva watershed, Svalbard. *Polar Res.*, **32**(1), 19691

Nowak A and Hodson A (2015) On the biogeochemical response of a glacierized high Arctic watershed to climate change: revealing patterns, processes and heterogeneity among micro-catchments. *Hydrol. Process.*, **29**(6), 1588–1603

Nuth C, Schuler TV, Kohler J, Altena B and Hagen JO (2012) Estimating the long-term calving flux of kronebreen, Svalbard, from geodetic elevation changes and mass-balance modelling. *J. Glaciol.*, **58**(207), 119–133

Nuth C and 7 others (2013) Decadal changes from a multi-temporal glacier inventory of Svalbard. *Cryosphere*, **7**(5), 1603–1621

Østby TI, Schuler TV, Hagen JO, Hock R and Reijmer LH (2013) Parameter uncertainty, refreezing and surface energy balance modelling at Austfonna ice cap, Svalbard, 2004-08. *Ann. Glaciol.*, **54**(63), 229–240

Østby TI and 5 others (2017) Diagnosing the decline in climatic mass balance of glaciers in Svalbard over 1957-2014. *Cryosphere*, **11**(1), 191–215

Petersen L, Pellicciotti F, Juszak I, Carenzo M and Brock B (2013) Suitability of a constant air temperature lapse rate over an Alpine glacier: testing the Greuell and Böhm model as an alternative. *Ann. Glaciol.*, **54**(63), 120–130

Pfeffer WT and 76 others (2014) The Randolph Glacier Inventory: a globally complete inventory of glaciers. *J. Glaciol.*, **60**(221), 537–552

Poinar K, Joughin I, Lenaerts JTM and van den Broeke MR (2017) Englacial latent-heat transfer has limited influence on seaward ice flux in western Greenland. *J. Glaciol.*, **63**(237), 1–16

Radić V and Hock R (2010) Regional and global volumes of glaciers derived from statistical upscaling of glacier inventory data. *J. Geophys. Res.- Earth Surf.*, **115**, F01010 (doi: 10.1029/2009jf001373)

Radić V and Hock R (2011) Regionally differentiated contribution of mountain glaciers and ice caps to future sea-level rise. *Nat. Geosci.*, **4**(2), 91–94

Rasmussen LA and Kohler J (2007) Mass balance of three Svalbard glaciers reconstructed back to 1948. *Polar Res.*, **26**(2), 168–174

Reijmer CH and Hock R (2008) Internal accumulation on Storglaciären, Sweden, in a multi-layer snow model coupled to a distributed energy- and mass-balance model. *J. Glaciol.*, **54** (184), 61–72

Reijmer CH, van den Broeke MR, Fettweis X, Ettema J and Stap LB (2012) Refreezing on the Greenland ice sheet: a comparison of parameterizations. *Cryosphere*, **6**(4), 743–762

Rippin D and 6 others (2003) Changes in geometry and subglacial drainage of Midre Lovénbreen, Svalbard, determined from digital elevation models. *Earth Surf. Proc. Land.*, **28**(3), 273–298

Schellenberger T, Dunse T, Kääb A, Kohler J and Reijmer CH (2015) Surface speed and frontal ablation of Kronebreen and Kongsbreen, NW Svalbard, from SAR offset tracking. *Cryosphere*, **9**(6), 2339–2355

Schneider T and Jansson P (2004) Internal accumulation in firn and its significance for the mass balance of Storglaciären, Sweden. *J. Glaciol.*, **50**(168), 25–34

Serreze MC and Francis JA (2006) The Arctic amplification debate. *Climate Change*, **76**(3–4), 241–264

Serreze MC, Barrett AP, Stroeve JC, Kindig DN and Holland MM (2009) The emergence of surface-based Arctic amplification. *Cryosphere*, **3**(1), 11–19

Smith RB and Barstad I (2004) A linear theory of orographic precipitation. *J. Atmos. Sci.*, **61**(12), 1377–1391

Sund M and Eiken T (2010) Recent surges on Blomstrandbreen, Comfortlessbreen and Nathorstbreen, Svalbard. *J. Glaciol.*, **56** (195), 182–184

Sundfjord A and 11 others (2017) Effects of glacier runoff and wind on surface layer dynamics and Atlantic Water exchange in Kongsfjorden, Svalbard; a model study. *Estuar. Coast. Shelf. S.*, **187**, 260–272

Valentin MM, Hogue TS and Hay LE (2018) Hydrologic regime changes in a high-latitude glacierized watershed under future climate conditions. *Water. (Basel)*, **10**(2), 128 (doi: 10.3390/w10020128)

Van Pelt W and Kohler J (2015) Modelling the long-term mass balance and firn evolution of glaciers around Kongsfjorden, Svalbard. *J. Glaciol.*, **61**(228), 731–744

Van Pelt WJJ and 5 others (2012) Simulating melt, runoff and refreezing on Nordenskiöldbreen, Svalbard, using a coupled snow and energy balance model. *Cryosphere*, **6**(3), 641–659

Van Pelt WJJ and 5 others (2014) Inverse estimation of snow accumulation along a radar transect on Nordenskiöldbreen, Svalbard. *J. Geophys. Res.- Earth Surf.*, **119**(4), 816–835

Van Pelt WJJ and 6 others (2016a) Multidecadal climate and seasonal snow conditions in Svalbard. *J. Geophys. Res.- Earth Surf.*, **121**(11), 2100–2117

Van Pelt WJJ, Pohjola VA and Reijmer CH (2016b) The changing impact of snow conditions and refreezing on the mass balance of an idealized Svalbard Glacier. *Front. Earth. Sci.* **4**, 102 (doi: 10.3389/feart.2016.00102)

Van Tricht K and 8 others (2016) Clouds enhance Greenland ice sheet meltwater runoff. *Nat. Commun*. **7**, 10266 (doi: 10.1038/ncomms10266)

Verbunt M and 5 others (2003) The hydrological role of snow and glaciers in alpine river basins and their distributed modeling. *J. Hydro.*, **282**(1–4), 36–55

Westermann S, Boike J, Langer M, Schuler TV and Etzelmüller B (2011) Modeling the impact of wintertime rain events on the thermal regime of permafrost. *Cryosphere*, **5**(4), 945–959

World Glacier Monitoring Service (WGMS) (2017). Global glacier change bulletin No. 2 (2014–2015). In Zemp M, Nussbaumer SU, Gärtner-Roer I, Huber J, Machguth H, Paul F and Hoelzle M, eds. ICSU(WDS)/IUGG(IACS)/UNEP/ UNESCO/WMO, World Glacier Monitoring Service, Zurich, Switzerland, 28–29, 244 pp., (doi: 10.5904/wgms-fog-2017-10).

Wright AP and 5 others (2007) Modeling the refreezing of meltwater as superimposed ice on a high Arctic glacier: a comparison of approaches. *J. Geophys. Res.*, **112**(F4) (doi: 10.1029/2007jf000818)

MS received 3 June 2018 and accepted in revised form 25 September 2018; first published online 31 October 2018

Additional Papers

Paper IV:

Everett, A., Kohler, J., Sundfjord, A., Kovacs, K.M., Torsvik, T., Pramanik, A., Boehme, L., and Lydersen, C. (2018). Subglacial discharge plume behaviour revealed by CTD-instrumented ringed seals. *Scientific Reports*, 8(1), doi: 10.1038/s41598-018-31875-8

Subglacial discharge plume behaviour revealed by CTD-instrumented ringed seals

Alistair Everett[1, *], Arild Sundfjord[1], Kit M. Kovacs[1], Jack Kohler[1], Tomas Torsvik[1], Ankit Pramanik[1], Lars Boehme[2], and Christian Lydersen[1]

1. Norwegian Polar Institute, Fram Centre, N-9296 Tromsø, Norway
2. NERC Sea Mammal Research Unit, Scottish Oceans Institute, University of St Andrews, UK
*Contact author: alistair.everett@npolar.no

ABSTRACT

Subglacial discharge plumes increase submarine melting of marine-terminating glaciers significantly; however, in-situ data on their properties and behaviour are limited. We present oceanographic data collected by ringed seals (Pusa hispida) instrumented with GPS-equipped conductivity-temperature-depth satellite relay data loggers (GPS-CTD-SRDLs) in Kongsfjorden, Svalbard during 2012. The seals foraged just outside the plumes and collected hydrographic data from within the plumes' upwelling cores as they returned to the surface. The seals encountered water with fractions of subglacial discharge as high as 27% at 60 metres below the ocean surface. The ringed seals responded rapidly to spatial and temporal variations in subglacial discharge at the glacier terminus, suggesting that prey is quickly available after the appearance of a plume. The seals' dive locations were used to monitor the presence of plumes over a four-month period. High surface runoff from Kronebreen catchment drove strong plumes, but weak plumes were present even during periods of low surface runoff. The continued retreat of Kronebreen, and other tidewater glaciers, will lead to the loss of these marine-termini as the glaciers retreat onto land. This technique presented here improve our understanding of the drivers of glacial retreat and the implications of future habitat loss for glacier-associated birds and mammals.

Paper V:

Schild, M.K., Renshaw, C.E., Benn, D.I., Luckman, A., Hawley, R.L., How, P., Trusel, P., Pramanik, A., and Hulton, N.R.J. (2018). Calving Rates due to Subglacial Discharge, Fjord Circulation, and Free Convection. ***Journal of Geophysical Research: Earth Surface*****, 123., doi:10.1029/2017JF004520**

Glacier Calving Rates Due to Subglacial Discharge, Fjord Circulation, and Free Convection

K. M. Schild[1,2] , C. E. Renshaw[1] , D. I. Benn[3] , A. Luckman[4,5] , R. L. Hawley[1], P. How[6,7] , L. Trusels[8] , F. R. Cottier[9,10], A. Pramanik[11], and N. R. J. Hulton[7]

[1]Department of Earth Sciences, Dartmouth College, Hanover, NH, USA,
[2]Department of Earth Sciences, Now at University of Oregon, Eugene, OR, USA,
[3]School of Geography and Geosciences, University of St Andrews, Saint Andrews, UK,
[4]Department of Geography, Swansea University, Swansea, UK,
[5]Arctic Geophysics, University Centre in Svalbard, Longyearbyen, Svalbard,
[6]School of GeoSciences, University of Edinburgh, Edinburgh, UK,
7Arctic Geology, University Centre in Svalbard, Longyearbyen, Svalbard,
[8]Department of Geology, Rowan University, Glassboro, NJ, USA,
[9]Scottish Association for Marine Science, Oban, UK,
[10]Department of Arctic and Marine Biology, UiT The Arctic University of Norway, Tromsø, Norway,
[11]Norwegian Polar Institute, Tromsø, Norway

Abstract:

Tidewater glacier calving provides the most direct mechanism of ice transfer from land to the ocean. However, the physical melt processes influencing calving remain challenging to constrain. In this study we focus on calving rates at Kongsbreen, a tidewater glacier in Svalbard, due to three mechanisms of submarine melt: (1) free convection, (2) horizontal fjord circulation, and (3) meltwater discharge. To calculate an overall calving rate, we measure glacier velocity and terminus change using Sentinel imagery. We calculate free convection, fjord circulation, and meltwater discharge calving using mooring data for mid-fjord ocean temperature (30–80 m depth), reanalysis results for meltwater runoff, and georectified time-lapse imagery to track icebergs and infer surface circulation. Results show that the total glacier calving rate is highly correlated with ocean temperature during the 2016 melt season. When runoff was present, we found that subglacial discharge accounted for calving rates an order of magnitude greater than the maximum calving rates assigned to the other two melting mechanisms combined. Further, subglacial discharge at Kongsbreen was more efficient in inducing calving later in the season than earlier in the season, implying that the increase in ocean temperatures, the timing of meltwater discharge within a melt season, and/or the development of discrete meltwater exit channels are critical components to calving rates. As the recent atmospheric warming trend and subsequent increase in meltwater discharge is expected to continue, it is essential to understand the processes contributing to an increase in glacier calving and incorporate these processes into predictive models.

Paper VI:

Halbach, L., Assmy, P., Vihtakari, M., Hop, H., Duarte, P., Wold, A., Kauko, H.M., Kristiansen, S., Everett, A., Myhre, P.I., Wulff, A., Pramanik, A., Pavlov, A.K., Granskog, M.A., Torsvik, T., Steen, H., Tatarek, A., Wiktor, J.M. (In review). Subglacial discharge-induced nutrient upwelling at tidewater glacier fronts fuels primary production in Kongsfjorden, Svalbard. ***Frontiers in Marine Science***

Subglacial discharge-induced nutrient upwelling at tidewater glacier fronts fuels primary production in Kongsfjorden, Svalbard

Laura Halbach[1,2], Philipp Assmy[1], Mikko Vihtakari[1], Haakon Hop[1,3], Pedro Duarte[1], Anette Wold[1], Hanna M. Kauko[1], Svein Kristiansen[3], Alistair Everett[1], Per I. Myhre[1], Angela Wulff[2], Ankit Pramanik[1,4], Alexey K. Pavlov[1,5,6], Mats A. Granskog[1], Tomas Torsvik[1], Harald Steen[1], Agnieszka Tatarek[5], Józef M. Wiktor[5]

[1]Norwegian Polar Institute, Fram Centre, N-9296 Tromsø, Norway
[2]Department of Biological and Environmental Sciences, University of Gothenburg, Box 100, S-405 30 Gothenburg, Sweden
[3]Department of Arctic and Marine Biology, Faculty of Biosciences, Fisheries and Economics, UiT The Arctic University of Norway, N-9037 Tromsø, Norway
[4] ESSO-National Centre for Antarctic and Ocean Research, Vasco-da-Gama, 403804, Goa, India
[5]Institute of Oceanology Polish Academy of Sciences, Powstańców Warszawy 55, 81-712 Sopot, Poland
[6]Akvaplan-niva, Fram Centre, N-9296 Tromsø, Norway

Abstract

Freshwater discharge from tidewater glaciers impacts primary production in fjords. Due to global warming these glaciers are retreating, leading to increased glacial meltwater inflow. Yet, the mechanisms through which meltwater runoff and subglacial discharge from tidewater glaciers influence marine primary production remain poorly understood as data in close proximity to glacier fronts are scarce. Here, we show that subglacial meltwater discharge from tidewater glaciers and the bedrock characteristics of the catchments control primary production in Kongsfjorden, Svalbard. In the southern part of the inner fjord, glacial melt water from subglacial discharge was rich in fine sediments derived from erosion of Devonian Old Red Sandstone and carbonate rock deposits, limiting light availability for phytoplankton (0.6 mg m^{-3} Chl a on average, range 0.2-1.9 mg m^{-3} 43). In contrast, coarser sediments derived from gneiss and granite bedrock and lower subglacial discharge rates were associated with more favourable light conditions facilitating a local phytoplankton bloom in the northern part of the inner fjord with mean Chl a concentration of 2.8 mg m^{-3} (range 1.3-7.4 mg m^{-3}). In the northern part, glacier meltwater was a direct source of silicic acid through weathering of the silica-rich gneiss and granite bedrock. Upwelling of the subglacial freshwater discharge plume at the Kronebreen glacier front in the southern part entrained large volumes of ambient, deeper nutrient-rich fjord waters which led to elevated surface concentrations of ammonium, nitrate and partly silicic acid. Total dissolved inorganic nitrogen transported to the surface with the upwelling of the subglacial plume can sustain up to 24% of the mean summer primary production in Kongsfjorden with ammonium released from the seafloor being of particular importance. Our analysis reveals that subglacial discharge at the tidewater glaciers in Kongsfjorden, overall, fuels primary production in an extended part of the fjord by inducing nutrient upwelling of deeper waters to the euphotic layer during the melt season.